HARDEN, P M

THE SOLID STATE CHEMISTRY OF SOME TITANIA- AND TIN PIGMENTS

DPhil (Chemistry) UP 1998

The solid state chemistry of some titania- and tin pigments

by

Peter Michael HARDEN

Presented in part fulfilment of the requirements for the degree

Doctor of Philosophy
Chemistry

in the Faculty of Science

University of Pretoria

Pretoria

DECEMBER 1998

ACKNOWLEDGEMENTS

I would like to express my sincere gratitude to the following people, departments, companies and institutions for their support throughout my studies.

- My supervisor, Professor Anton M. Heyns for his guidance and encouragement throughout this project.
- My parents for their unconditional support for as long as I can remember. A special thanks to my father in his capacity as a ceramist, for taking care of some of my more customised calcining requirements, for help in the testing of the pigments from time to time, and for supplying raw materials to various specifications for the synthesis of the various materials.
- My family and friends for their encouragement.
- Fellow students of the Department of Chemistry and the rest of the research group for their friendship, encouragement, and for being a part of a very pleasant working environment.
- Various people of the Department of Geology, for XRD analysis, for the use of various instruments, and for valuable discussions.
- The Department of Electron Microscopy for the scanning electron microscopy analysis and SEM photographs.
- Various people of the R&D department at Iscor Refractories for allowing me access to their high temperature ovens.
- Various people at the CSIR (MATEK) for valuable discussions and access to their literature.
- *and Erla ....*

Thank You - Peter

BSc(HONS) - University of Natal, Pietermaritzburg
MSc(cum) - University of Pretoria

SUMMARY

The solid state chemistry of some titania- and tin pigments

by

Peter Michael HARDEN

Presented for the degree Ph.D. (Chemistry)

Supervisor

Professor Anton M. HEYNS
Institute of Applied Materials
University of Pretoria
Pretoria

Natural inorganic pigments have been known since prehistoric times. Initially they were obtained from natural sources, but later synthetic pigments were produced empirically. The modern ceramic pigment industry began early in the 18^{th} century and since then, ceramic pigments have been the subject of scientific studies to the point where today research makes use of the latest techniques in solid state chemistry and physics to try to understand their properties. Over and above the all important colour properties of any colouring material, ceramic pigments require additional properties including exceptional thermal and chemical stability. It is through a better understanding of the nature of ceramic pigments and their extraordinary properties that new and improved pigments, and related materials will be synthesised.

In the current investigation, a number of titania- and tin materials suitable for colouring ceramic articles were investigated using a two fold approach. Firstly, their synthesis was investigated and optimised, and secondly, they were investigated structurally.

The synthesis focused on their physical and aesthetic properties, and the economic implications of the synthesis techniques.

The structural investigation was two dimensional. Firstly, the macroscopic details of the host materials were investigated using scanning electron microscopy (SEM) and x-ray techniques. This is important since it is the host lattice which provides the extraordinary properties required of a ceramic pigment. Secondly, the microscopic structural details of the interaction of the host lattice with the small quantities of dopant(s) were investigated using SEM, vibrational and electronic spectroscopy. This interaction is of paramount importance since it is the interaction between the host lattice and guest chromophore that results in the all important colour of the pigment.

Pigments investigated include chromium doped malayaite, Cr^{4+}:$CaSnOSiO_4$, and its titanium analogue titanite, Cr^{4+}:$CaTiOSiO_4$. The chemical state of the chromium in both materials was investigated. In both cases, the chromium was found to be in its fourth oxidation state. Other properties investigated include the chromium coordination states, bond lengths, bond orders and force constants. In Cr^{4+}:$CaTiOSiO_4$, the chromium was used as a probe to investigate the paraelectric→antiferroelectric temperature phase transition which titanite undergoes at ~500 K using resonance Raman spectroscopy. This technique was also used to investigate the high pressure phase transition of titanite. This transition was shown to occur at ~27 kbar.

Other pigments investigated include two minerals with the pyrochlore structure, $Y_2Ti_2O_7$ and $Y_2Sn_2O_7$, co-doped with calcium and vanadium. The coordination states and chemical states of the calcium and vanadium in these host lattices were investigated. The vanadium was found to be in its fifth oxidation state. The bond lengths and bond orders of the vanadium were determined for these compounds.

Following the investigation of these doped mixed metal oxides, various other compounds were synthesised which were found to have potential for use as pigments.

OPSOMMING

Die vastetoestandchemie van sommige titaan- en tinpigmente

deur

Peter Michael HARDEN

Voorgelê vir die graad Ph.D. (Chemie)

Promotor

Professor Anton M. HEYNS
Instituut vir Toegepaste Materiale
Universiteit van Pretoria
Pretoria

Natuurlike anorganiese pigmente is bekend vanaf prehistoriese tye. Hulle is aanvanklik verkry van natuurlike bronne, maar later is sintetiese pigmente empiries vervaardig. Die moderne pigmente-keramiekindustrie het vroeg in die 18^{de} eeu ontstaan en sedertdien was keramiese pigmente die onderwerp van wetenskaplike studies tot by die punt vandag dat navorsing op hierdie gebied gebruik maak van die nuutste tegnieke in vastetoestandchemie en fisika om hulle eienskappe beter te kan verstaan. Bo en behalwe die uiters belangrike kleureienskappe van enige gekleurde materiaal, vereis keramiese pigmente bykomende eienskappe soos buitengewone termiese en chemiese stabiliteit. Dit is deur 'n beter begrip van die aard van keramiese pigmente en hulle buitengewone eienskappe dat nuwe en verbeterde pigmente en verwante materiale sintetiseer word.

In die huidige studie word 'n aantal titaan- en tinmateriale ondersoek wat geskik is om keramiekvoorwerpe te kleur deur 'n tweevoudige benadering te gebruik.

Eerstens is hulle sinteties ondersoek en optimiseer en tweedens is hulle struktureel ondersoek. Die sintese het gefokus op hulle fisiese en estetiese eienskappe en die ekonomiese implikasies van die sintese-tegnieke.

Die struktuurondersoek was twee-dimensioneel gewees. Eerstens is die makroskopiese besonderhede van die gasheermateriale ondersoek deur skandeer-elektronmikroskopie en x-straal tegnieke te gebruik. Dit is belangrik aangesien dit die gasheer-rooster is wat die buitengewone eienskappe verskaf wat nodig is vir ŉ keramiekpigment. Tweedens is die mikroskopiese struktuur in besonderhede bestudeer veral die wisselwerking tussen die gasheer-rooster en die klein hoeveelhede van die gedoteerde produk deur skanderende elektronmikroskopie, vibrasie- en elektronspektroskopie te gebruik. Hierdie wisselwerking is van oorheersende belang aangesien dit die kleur van die pigment tot gevolg het.

Die pigmente wat ondersoek is, sluit chroom gedoteerde malaiet Cr^{4+}:$CaSnOSiO_4$ in en sy titaananaloog, Cr^{4+}:$CaTiOSiO_4$. Die chemiese toestand van die chroom is ondersoek in beide materiale. In albei materiale was die bevinding dat dit in oksidasietoestand +4 bestaan. Die ander eienskappe wat ondersoek is, sluit die chroom se koördinasietoestand in, bindingslengtes, bindingsordes en kragkonstantes. In Cr^{4+}:$CaTiOSiO_4$ is die chroom gebruik as ŉ middel om die paraelektriese-antiferroelektriese fase-oorgang te ondersoek wat titanaat ondergaan by ~500 K. Resonans Ramanspektroskopie is hiervoor gebruik. Die tegniek is ook gebruik om die hoë-druk fase-oorgang van titanaat te ondersoek wat by ~27 kbar plaasvind by kamertemperatuur.

Ander pigmente wat ondersoek is, sluit twee minerale in wat die pirochloorstruktuur besit, $Y_2Ti_2O_7$ en $Y_2Sn_2O_7$, wat met kalsium en vanadium gesamentlik doteer is. Die koördinasietoestande en chemiese toestande waarin kalsium en vanadium hulself bevind in hierdie roosters, is ondersoek. Dit is gevind dat vanadium in oksidasietoestand +5 verkeer. Die bindingslengtes en bindingsordes van vanadium is bepaal vir hierdie verbindings.

Voortvloeiend uit hierdie ondersoek van gedoteerde gemengde metaaloksiedes is verskeie ander verbindings berei wat bevind is om ħ potensiaal te hê vir gebruik as pigmente.

CONTENTS

Chapter 1

Introduction

1.1 HISTORICAL BACKGROUND

It is likely that prehistoric caveman's first artificially produced article was a pot used for the storage of food and water and for general use. Such a pot would have been formed of clay that was made hard by burning [1]. Indeed, the art of making pottery by forming and burning clay is the oldest technology of mankind. Proof of this assertion may be found in the discoveries of burned clay fragments dating back to the early Neolithic age (8000 b.c.) [1]. The colour of these fragments varied from reddish through brown to grey. The colour of the ceramic articles was as a result of the impurities in the clay, and initially it was accidental rather that intentional. However, man soon realised how to utilise and combine the different raw materials to achieve decorating effects, and strikingly beautiful pottery resulted from his efforts. Natural inorganic pigments have been known since prehistoric times. For example, over 60 000 years ago natural ocher was used in the Ice Age as a colouring material [2].

Ceramics were the first products to liberate man from his total dependence on natural materials [3]. Since the production of ceramics from clay is one of the oldest human activities, it is not surprising that the deliberate colouring of these materials is so as well [4]. Ancient humans were interested in colouring their paintings and various object they happened to make. To do this they dug the coloured earth from around their environments and used organic materials obtained from berries and wood bark, among other sources [5]. While the organic materials were observed to fade away, the inorganic ones were not. Indeed, it is because of the high stability of inorganic pigments, that their use can be traced back over millennia [4]. As old as the manufacture of ceramic vessels is man's desire to decorate their surfaces [3]. This decoration has constituted an invaluable field of research for prehistorians, archaeologists, and art historians. For example, the decorations provide evidence of an industrial finishing process which points towards a degree of experience and knowledge of raw materials possessed by the ancient cultures [3].

Coloured and uncoloured inorganic pigments have been obtained from natural minerals since prehistoric times, at first empirically, and later by specially developed methods [4]. Cave paintings of the Pleistocene peoples of southern France, northern Spain and northern Africa were made with charcoal, ocher, manganese brown and clays, and must have been produced over 30 000 years ago [2]. The next step was the synthesis of pigments. Pigments were already being made in the city and river cultures of antiquity [3]. As an example, about 2000 b.c., natural ocher was burnt, sometimes in mixtures with manganese ores, to produce red, violet and black pigments for pottery [2].

Early pottery found in Egypt, Asia Minor, Crete and Greece exhibit progressively refined application techniques and ornamentation details [1]. At this time potters started using the naturally occurring earth pigments such as ocher, sienna, umber and black magnetite to colour the clay body of their ware and to use coloured dip-coats for glazing. The effect of the firing atmosphere was also recognised, and used effectively to achieve different shades of colour.

The art of glazing (a technique of colouring only the surface of a ceramic article rather than colouring the clay from which it is made) is almost as old as that of pottery [1].

The ancient Egyptians were partial to the colour blue as a result of their reverence for the sky. Consequently, the mineral azurite was used extensively in ancient Egypt. Initially, natural azurite was used, but, since only a limited supply was available, the Egyptians soon learned how to produce a synthetic crystalline compound even more useful than its natural counterpart [1]. A chunk of such a synthetic blue pigment dating back some 4000 years was excavated in Egypt in 1965. Subsequently, it was shown to be the calcination product of copper oxide (1 mole), calcium oxide (1 mole), and silica (4 moles) that was ground and mixed with some egg yolk and gum.

The modern ceramic pigment industry started in the 18^{th} century with products such as Berlin Blue (1707), cobalt blue (1777), Scheele's green and chrome

yellow (1778). Consequently, since the beginning of the 18th century, ceramic pigments have become the object of scientific studies to the point where today research makes use of the latest techniques in solid state chemistry and physics to try to understand the very sophisticated properties of these ceramic pigments. In the last eighty years or so, based on our ideas of technically and aesthetically important properties, it has become possible to synthesise pigments with properties superior to their natural counterparts. In addition, the volume of production of these synthetic pigments has increased dramatically while maintaining or improving the pigment properties. The range of ceramic pigments available for industrial application has also been increased by the addition of new ceramic pigments.

Today, the manufacture of pigments is an enormous industry. In 1989, world production of pigments amounted to ~5 x 10^6 tons, with inorganic pigments accounting for ~96% of this [2].

The ideal situation for ceramic pigment synthesis would be to have an understanding of ceramic pigments that would enable one to design a ceramic pigment for a specific application, taking into account the aesthetic, technical, economical, and of coarse the all important ecological aspects of ceramic pigment synthesis, and consequently, to synthesis the ceramic pigment, cost effectively, on an industrial scale.

1.2 COLOUR

Pigments imply colour. The range of the electromagnetic spectrum in which we are interested, ranges from around 400 nm to around 700 nm. This is the visible region that occurs between ultra-violet and the infrared. It ranges from violet through blue, green, yellow, and all the other colours of the rainbow, to red. A pigments colour stems from its ability to reflect or absorb light. A white pigment reflects all light while a black pigments reflects none [6]. Coloured pigments absorb and reflect light selectively. For example, a red pigment will reflect all radiation perceived as red light, and absorb all others. If it also reflects yellow

light, the eye will perceive a composite orange, for example. Coloration of ceramic products also makes use of the blending of different colours to achieve different colouring effects. The difference between the additive effect of coloured pigments and coloured lights must however be distinguished. For example, mixing red, blue and yellow pigments produces purple, green, orange and black. On the other hand, mixing yellow, blue and green light produces cyan, magenta, yellow and white [6].

There can be no new colours ..... but colorants,
which impart the property of colour,
are a different matter.

1.3 CERAMIC PIGMENTS

Ceramic products include dinnerware, tiles, porcelain enamels, sanitary ware, some glasses and other structural clay products. Colour is an important characteristic of these products and there are a number of ways in which to obtain colour in a ceramic material [7]. They are listed below.

- Ceramic materials containing transition metal ions will often be coloured, particularly if they are vitreous. Although this method is used to make coloured glass, it is rarely used in other products because adequate tinting strength and purity of colour cannot be obtained in this way.
- Colour might also be obtained in a ceramic by inducing the precipitation of a crystalline phase in a glassy matrix during processing. Certain oxides such as zirconium dioxide and titanium dioxide dissolve to the extent of several weight percent in a vitreous material at high temperatures. When the temperature is reduced, the solubility is also reduced and precipitation occurs. This method is widely used for opacification; the production of opaque white colour in a vitreous matrix. For oxide colours other than white, this method lacks the necessary control for reproducible results and, therefore, is seldom used.
- Another method of colouring ceramic articles is to colour the clay body itself. It may be coloured naturally, by the nature of its being, or it may be coloured by

adding colorants to the clay. The adding of colorants to the clay body is however not very cost effective since very little of the colorant in the clay body actually contributes to the colour on the surface of the article. Consequently, this method is not commonly used.

- The most common method of obtaining colour in a ceramic material, is to disperse in the vitreous coating of that material (the glaze), a coloured crystalline phase which is insoluble in the matrix. This crystalline phase, or pigment, imparts its colour to the matrix.

Colorants may be divided into two main groups. They are as follows:

I	Dyes	:	colorants that are coloured and *transparent* (and often soluble)
II	Pigments	:	colorants that are coloured or uncoloured and *opaque*

Ceramic colorants are pigments. The Dry Color Manufacturers Association of America (DCMA) has prepared the following legally accepted definition of a pigment [5]. Essentially a pigment is a coloured, black, white or fluorescent particulate organic or inorganic solid which is usually insoluble in, and essentially physically and chemically unaffected by, the vehicle or substrate into which it is incorporated. A pigment will alter appearance by selective absorption and/or scattering of light. The pigment is usually dispersed in a vehicle or substrate for application as for example in the manufacture of paints, plastics, or other polymeric materials and inks. The pigment will retain its own unique crystalline or particulate structure throughout the incorporation process.

By contrast, dyestuffs are essentially soluble in the carrying medium and therefore any crystalline features are lost in the solution when a dyestuff is used to impart colour to a material [5].

From the above definition, it is clear that pigments may further be divided into two categories. They are as follows:

I Organic II Inorganic

Ceramic pigments are inorganic in nature. Inorganic pigments significantly change our ambient; they are irreplaceable for the colouring of construction materials. They show good light and weather resistance and they withstand the attack of heat and chemicals. These pigments are not only suitable for colouring ceramics, but also paints, resins, plastics etc. Their applications, besides that of ceramic pigmentation, range from concrete to artist colours, from industrial paints to toners in photocopiers, and from colouring food stuffs to their use as raw materials for catalysis [2].

Since pigments are particulate by definition, their colour is dependent on the refractive index of the binder, the particle size and shape distribution, and the degree of dispersion of the pigment.

1.4 CERAMIC PIGMENT PROPERTIES

Ceramics is the art and science of making and using inorganic non-metallic materials that are subjected to high temperatures during their manufacture [1]. Apart from their colour, colorants have certain physical and chemical characteristics which vary from one to another [6]. These properties are summarised in table 1.1 below.

Table 1.1 Physical and chemical properties of colorants.

Optical Properties	Physical Properties
Colour (hue or chroma)	Heat fastness
Tinting strength (saturation)	Light fastness
Opacity	Chemical resistance
Refractive index	Dispersibility

The inorganic pigments dealt with here consist of a host lattice that is doped with a small amount of a metal element, most often a transition metal element that is responsible for imparting colour to the host lattice. The host lattice is formed at a high temperature and so is in a very stable chemical state and consequently, it is insoluble in the vitreous coating which binds it to the surface of the ceramic article. It is therefore not surprising that the host lattice takes on the structure of a naturally occurring mineral (or minerals as in the case of lapis lazuli) that by the nature of their being are stable since natural minerals are generally formed under conditions of high temperature and pressure.

When a photon of light enters a pigmented film, one of three events may occur:

1. It may be absorbed by a pigment particle.
2. It may be scattered by a pigment particle.
3. It may simply pass through the film unaffected.
   (the binder being assumed to be non-absorbent)

The important physical-optical properties of pigments are therefore their light absorbing and light scattering properties [2]. If absorption is very small compared with scattering, the pigment is white. If absorption is much higher than scattering over the entire visible region, the pigment is black. In a coloured pigment, absorption (and usually scattering) are selective (i.e. dependent on the wave length).

The key feature of ceramic pigments, over and above the all important colour, is that they are thermally stable, and many good pigments are useless to the ceramic industry because they are not sufficiently stable. In addition, they must be of good saturation, since more often than not, they are mixed with opaque white materials or other materials of high refractive index. Saturation cannot be improved upon and so it is vital in a basic colorant. It also determines the amount of pigment which must be used to achieve a certain colouring effect. There are usually good reasons why this should be as little as possible, not least of all freedom of formulation, and of coarse the all important cost factor.

The materials used to colour ceramics are chosen because they possess properties beyond that of the tinctorial strength required of an ordinary pigment. These other properties are required because of the high temperatures and the corrosive environments encountered in the firing of ceramics. Ceramic pigments must have good chemical resistance to acids and alkalis and their rate of solution in the ceramic at high temperature must be very low in spite of the very fine particle size of the pigment because ceramic pigments are subjected to very harsh and corrosive conditions present as a result of the vitrification of the fluid vitrifiable medium (glaze). Almost all pigments used in ceramics are oxides since oxides show a greater stability in oxygen containing ceramic systems. The exceptions are the cadmium pigments [7].

It is important to note that the ceramic pigment is only one of a number of components present during processing. Others may include the body of the ceramic, the glaze, opacifiers, various additives and application media. Therefore any glass, glaze, body, opacifier or other material used should be as transparent, stable and as unaggresive as possible to reduce to a minimum the effect on the pigment.

There are limitations on all existing pigments suitable for application in ceramics. An example of this is the unhappy relationship between chromium containing pigments and zinc containing glazes. Another example may be found in the zircon pigments recommended for use under all glazes, and whose only serious limitation is their lack of strength or saturation.

There have always been conflicting demands on the colour suppliers and in the foreseeable future there will be many more. The potters and transfer makers will be asking for stronger, brighter, cleaner colorants. They will be seeking intermixability because this will minimise stock holdings and reduce the skill and training necessary to achieve a flexible product range. All this will be sought against a background of a need for colorants which are safer to produce and use, safer for the environment, and safer for the consumer. In addition, the pigment must be presented in a form which is easy to apply, safe for the user,

and tolerant of any process, conditions or application technique which may be employed. To achieve this, more needs to be learned of the properties of these pigments.

All of the above properties of pigments (and the properties of all colorants for that matter) are related to the 'molecular' structure of the pigment. There are four basic principles which determine the structures of inorganic solid state materials [7]. They are as follows:

1. The principle component of free energy of an ionic solid material at room temperature is its lattice energy which is determined almost totally by the nearest-neighbour cation-anion distance.
2. The coordination polyhedra of the anions about each cation in ionic solid phases are determined almost unequivocally by the radius ratio of cations to anions.
3. The structures that can be built from any combination of cations and anions are the subject of the rules of electrostatic neutrality. This means that in a stable ionic structure, the valence of each anion, with changed sign, is exactly or nearly equal to the sum of the strengths of the electrostatic bonds to it from adjacent cations.
4. The coordination of the cation must increase as the charge of the anion decreases, and decrease as the field strength increases.

The cumulative effect of these four principles is that a given structure exists at or very near a given stoichiometry, and for a small range of ionic sizes of the ions contained [7].

The host lattice formed at high temperatures will most certainly conform rigorously to all of these principles. They are invariably very stable. The introduction of the dopant must also conform to these principles. Since the chemical and physical properties of the dopant will differ from that of the atoms of the host lattice, they will place strain on their immediate environment. Conversely, strain is also placed on the dopant by the host lattice. It is the

interaction between the host lattice and the dopant that results in the colour of a ceramic pigment. Clearly, the macroscopic details of the host lattice and the microscopic details of its interaction with the dopant are very important.

1.5 THE SOLID STATE CHEMISTRY OF SOME TITANIA- AND TIN PIGMENTS

The chemistry of ceramic pigments is more often than not complicated. To a large extent ceramic pigment synthesis takes place on an empirical basis. Even in the most modern production facilities, pigments are synthesised in batches which tend to have colour properties which vary. The different batches are then blended together to yield a pigment with the desired pigmentation properties. The methods are often not well understood and reproducibility is often poor.

The development of new pigments is also not a trivial matter and it also tends to take place on an empirical basis, as was the case for the development of the very first pigments synthesised in ancient times. This is a very limiting factor since the variables involved are vast. They include the temperature at which the pigments are calcined, the duration of the calcination and the ramp of the temperature. The form in which the raw materials are added (e.g. CaO or $CaCO_3$) and the method in which the various reaction components of the final product are mixed together is important. The ratio of the raw materials added, the type of catalyst used and the amount used are also important. And there are many more.

In short, the vast number of elements that can potentially make up the host lattice, and the vast number of elements that might be used as dopants, and the vast number of compounds that might be useful as mineralisers, and the diverse conditions of synthesis make it an enormous, if not impossible task to synthesise new pigments or optimise pigment synthesis on an empirical basis. Consequently, what is needed for more efficient ceramic pigment synthesis, and the development of new pigments, is a better understanding of these pigments.

In this study, several pigments with different colours and chemical compositions were investigated using a two fold approach. Firstly, their synthesis was investigated and optimised, and secondly, they were investigated structurally.

Optimisation of the synthesis was carried out with two main considerations in mind; the physical and aesthetic properties of the pigments, and the economic implications of the synthesis technique. For example, in addition to other factors, the temperature at which the pigments are calcined should be as low as possible. This results in savings in power, time and equipment. Time is saved since furnaces firing at lower temperatures reach temperature faster and also cool down faster. Equipment costs are reduced since ovens that fire at lower temperatures are substantially cheaper than those that fire at higher temperatures.

The investigation of their complex structural properties was also carried out with two main considerations in mind. The first involved the investigation of the host lattice of the pigments using X-ray techniques, scanning electron microscopy (SEM) and vibrational spectroscopy. The second involved the investigation of the dopant incorporated into the structure of the host lattice using Raman spectroscopy and electronic spectroscopy. Raman spectroscopy is a very powerful tool for the investigation of pigments. This is because it can be used to selectively probe the chromophore which has been incorporated into the host lattice and which is present in very small amounts. This may be done using resonance Raman spectroscopy which selectively enhances the intensity of the Raman bands associated with the chromophore thereby making bands visible which under normal conditions would not be visible, as is the case with infrared spectroscopy. This is not possible with most techniques since the host material tends to obscure or overpower any information about the dopant. The way in which the dopant is incorporated into the host lattice is of paramount importance since it is the interaction between the host lattice and the chromophore that results in the all important colour of the pigment.

Chapter 2

The Malayaite Compounds

2.1 INTRODUCTION

Malayaite (calcium tin silicate) is a naturally occurring mineral (rare tin silicate) with the general chemical formula $CaSnOSiO_4$ or simply $CaSnSiO_5$. Malayaite was first found at Perak on the Malay Peninsula by Ingham and Bradfood in 1960. Subsequently, it was named by Alexander and Flinter in 1965 [8]. Since 1960 naturally occurring malayaite has been found in numerous places around the world, including Namibia. These discoveries of malayaite suggest that malayaite is associated with garnet, clinopyroxene, calcite, quartz and wollastonite.

It has been shown that malayaite belongs to the monoclinic space group C2/c (or A2/a), with four formula units per unit cell [9]. Malayaites structure consists of corner sharing $[SnO_6]$ polyhedra that form chains parallel to *a*. These are linked to sevenfold-coordinated Ca-ions by $[SiO_4]$ tetrahedra [10]. The structural details will be discussed more fully in section 2.3 below.

Synchrotron radiation, high-resolution transmission electron microscopy (HRTEM), X-ray powder diffraction and Raman spectroscopic studies have been undertaken to investigate the structural and thermal properties of malayaite [11]. No deviation from A2/a symmetry and no structural transitions were observed between 100 and 870 K. In addition, the HRTEM measurements showed that the material is free of domains and antiphase boundaries. Synthetic malayaite has been prepared by Takenouchi using various hydrothermal techniques (high temperature and pressure) in order to determine the mechanism under which the mineral is formed naturally [8]. Malayaite shows good properties of thermal stability.

For the bulk synthesis of a malayaite pigment to be feasible a synthesis technique other than hydrothermal techniques, which are expensive, must be used. Malayaite has been synthesised at 1370°C at atmospheric pressure [12]. Malayaite has also been synthesised at atmospheric pressure and at temperatures lower than ~1300°C using a mineraliser mixture (flux or catalyst)

[13]. The effects of the doping of malayaite with various chromophores have also been investigated [12;13;14].

The thermal stability of malayaite, and its receptiveness to dopants makes it a good candidate for use as a host lattice for the synthesis of pigments.

2.2 SYNTHESIS

2.2.1 SYNTHESIS

2.2.1.1 Synthesis of Malayaite

Stoichiometric amounts of calcium, tin and silicon in the form of calcium carbonate ($CaCO_3$), tin dioxide (SnO_2), and silicon dioxide (SiO_2) were intimately wet mixed. The tin dioxide and the silicon dioxide were milled prior to mixing to a particle size of 98% < 5µm, 75% < 2µm. After wet mixing, the reaction mixture was dried and dry mixed with a mortar and pestle, and then calcined. The reaction mixture was heated from room temperature to 1550°C. The temperature was held constant for two hours after which the oven was switched off. The resulting product was allowed to cool slowly to room temperature inside the oven. The reaction product was found to have shrunk considerable and, due to the initial onset of sintering, had formed a solid mass with a shape similar to that of the crucible which could not be broken down into a powder with a mortar and pestle.

The above reaction was repeated at the lower temperature of 1500°C. The product of this reaction had also shrunk considerably, though not to the extent of the previous reaction product. The reaction product was broken down into a powder with a mortar and pestle.

2.2.1.2 Synthesis of Chromium Doped Malayaite

Chromium doped malayaite was prepared in the same way as the undoped malayaite above except that one atom percent[1] of chromium, in the form of potassium dichromate ($K_2Cr_2O_7$), was added to the calcium carbonate, tin dioxide and silicon dioxide before wet mixing. The reaction mixture was heated from room temperature to 1450°C. The temperature was held constant for two hours after which the oven was turned off. The reaction product was allowed to cool to room temperature inside the oven. It was then broken down into a powder with a mortar and pestle and leached in boiling water for one hour and dried. The product was then hot acid leached for 30 minutes.

2.2.1.3 Synthesis of Malayaite Using Mineralisers

Undoped and chromium doped malayaite were prepared in the same way as the reaction products above except that five percent[2] of boric acid (H_3BO_3) and one percent of potassium nitrate (KNO_3) were added to the calcium carbonate, tin dioxide and silicon dioxide before wet mixing. The reaction mixtures were fired at temperatures between 1000 and 1300°C. They were heated from room temperature. The temperature was held constant for two hours after which the oven was turned off. The reaction products were allowed to cool to room temperature inside the oven. They were then broken down into powders with a mortar and pestle and leached in boiling water for one hour and dried. In addition, the powders were hot acid leached for 30 minutes.

2.2.2 RESULTS AND DISCUSSION

2.2.2.1 Malayaite Synthesised at 1550°C and 1500°C

These reaction products were synthesised to be use as undoped reference samples for comparison with the doped reaction products of malayaite using various techniques. The high temperatures at which these reaction mixtures

---

1 1% Cr as a percentage of the total number of calcium, tin and silicon atoms before calcining.

2 5 & 1% of H_3BO_3 and KNO_3, respectively, as a percentage of the total number of calcium, tin and silicon atoms before calcining.

were calcined also gives useful information about the thermal stability of the starting materials and the reaction products.

The product of the reaction mixture calcined at 1550°C was white and showed signs of considerable shrinkage though no significant weight loss was observed[1]. In fact, the product was a solid mass which could not be broken down to powder form with a mortar and pestle. At 1550°C, the reaction product was in the process of sintering. The vibrational spectra of the reaction product were recorded. Though the onset of sintering makes SEM analysis and XRD data collection difficult, it is favourable for the recording of vibrational spectra since the reaction product produced at the higher temperature is substantially more crystalline. The results of the spectroscopic investigation of the malayaite reaction products will be discussed in detail in section 2.4 below.

The product of the reaction calcined at 1500°C was white, as expected, and also showed signs of considerable shrinkage, though not to the extent of the 1550°C reaction product. While the product was also in the form of a solid mass, it could be broken down into a powder with a mortar and pestle. A SEM analysis was carried out and XRD data collected on the product. The SEM analysis showed that the calcium, tin and silicon were present in equal proportions within the experimental margin of error associated with the technique. Consequently, none of the starting materials were lost during the calcining process. The XRD data collected show that the only reaction product was $CaSnOSiO_4$ and that no starting materials remained unreacted. The reaction can therefore be said to have gone to completion at 1500°C, without loss of any of the starting materials.

2.2.2.2 Malayaite Doped with Chromium at 1450°C

The product of the doped reaction mixture calcined at 1450°C was a strong maroon colour and also showed signs of considerable shrinkage. While the product was in the form of a solid mass, it could be broken down into a powder

[1] Weight of product expected, calculated on the basis of number of moles of starting material and assuming malayaite to be the only product formed, correlated with observed product mass.

form with a mortar and pestle. A SEM analysis was carried out and XRD data collected on the product.

The SEM analysis results showed the presence of chromium in the doped malayaite though the technique was not found to be sensitive enough to give reproducible quantitative information about the chromium since it is present in such small quantities. The XRD data of the reaction product calcined at 1450°C and other reaction products calcined at lower temperatures are summarised in table 2.1 below. They show that at 1450°C the only compound formed in the firing process was $CaSnOSiO_4$ and that no starting materials remained unreacted. As was the case with the SEM analysis results, this technique was not sensitive enough to yield information about the dopants.

2.2.2.3 Malayaite Synthesised with Mineralisers

Malayaite, both undoped and chromium doped, can be synthesised at temperatures between 1300 and 1450°C with no raw materials remaining unreacted, or by-products being formed. Below 1300°C, it was found that either the reaction did not go to completion or malayaite was not formed at all. As discussed in chapter 1, from a synthesis point of view, it is desirable to synthesise pigments at as low a temperature as possible. Consequently, the effects that various mineraliser mixtures have on the reaction was investigated. A number of mineraliser mixtures were tested. A mixture of boric acid (H_3BO_3) and potassium nitrate (KNO_3) was found to be effective. Numerous reactions were carried out in order to optimise the amounts of boric acid and potassium nitrate needed for the reaction. It was found that a mixture of five percent boric acid and one percent potassium nitrate produced the best pigment. The results of the reactions carried out between 1000 and 1450°C, with and without mineralisers, are summarised in table 2.1 below.

Table 2.1 X-ray powder diffraction analysis results for malayaite reaction mixtures with and without mineraliser, doped with chromium, and calcined at temperatures ranging between 1000 and 1450°C.

Reaction Number	Temperature °C	Mineraliser	SnO_2	SiO_2	$CaSnO_3$	$CaSiO_3$	$CaSnOSiO_4$
1	1450	✗	✗	✗	✗	✗	✓
2	1300	✔	✗	✗	✗	✗	✔
3	1300	✗	✔	✔	✔	✔	✔
4	1200	✔	✗	✗	✗	✗	✔
5	1200	✗	✔	✗	✔	(✔)	(✔)
6	1150	✔	✗	✔	✗	(✔)	✔
7	1150	✗	✔	✔	✔	(✔)	✗
8	1100	✔	(✔)	✔	✗	✗	✔
9	1100	✗	✔	✔	✗	(✔)	✗
10	1000	✔	✔	✔	✗	✗	✗
11	1000	✗	✔	✔	✗	✗	✗

(✔) - Very little present.

2.2.2.4 Discussion

The most desirable result is that the only product formed is malayaite and that no unreacted raw materials are left after calcining. Consequently, a few conclusions may be drawn from table 2.1 above. They are as follows:

- At 1450°C, the only product formed is malayaite.
- At all temperatures below 1450°C, the best results are achieved in the malayaite reactions containing the mineraliser mixture. Reaction mixtures without mineraliser do produce malayaite at temperatures of as low as 1200°C, but also other by-products. In addition, the lower the temperature, the more starting materials are left unreacted after calcining. No mineraliser is needed at temperatures of 1450°C and above.
- At 1200°C the only product of the reaction with the mineraliser mixture is malayaite. In reaction mixtures with the mineraliser mixture calcined at temperatures below 1200°C, malayaite is still produced, but a fair amount of raw materials are left unreacted, and by-products are formed.
- At temperatures below 1200°C, the intensity of the colour of the pigment synthesised with mineraliser is related to the amount of malayaite formed. This is because the unreacted raw materials and the by-products formed tend to dilute the colour of the pigment. Therefore, the lower the temperature the more by-products are formed and the more unreacted raw materials remain after calcining which results in the intensity of the colour of the pigment being weaker.
- At temperatures of 1200°C and above, the only product of the reactions with mineraliser is malayaite. The colour of the pigment improves in intensity as the temperature increases. Therefore, at temperatures of 1200°C and above, the intensity of the colour of the pigment is a function of the crystallinity of the product, and to a lesser extent, the doping efficiency. The advantage of the greater colour intensity must be weighed up against the disadvantage of having to calcining at higher temperatures, and the fact that the particle size of the product increases as the calcining temperature increases.

- When all factors are taken into account, it appears that the most appropriate temperature for calcining these pigments is ~1200°C.

2.3 STRUCTURE

2.3.1 CRYSTAL STRUCTURE OF MALAYAITE

The crystal structure of malayaite has been published [10]. It belongs to the monoclinic space group A2/a (or C2/c) (No.15). The lattice constants of the crystal are as follows: a = 6.667 Å, b = 8.906 Å, c = 7.149 Å; β = 113.3°; with Z = 4 and two molecules per Bravais unit cell. A portion of malayaites structure is shown schematically in figure 2.1 below.

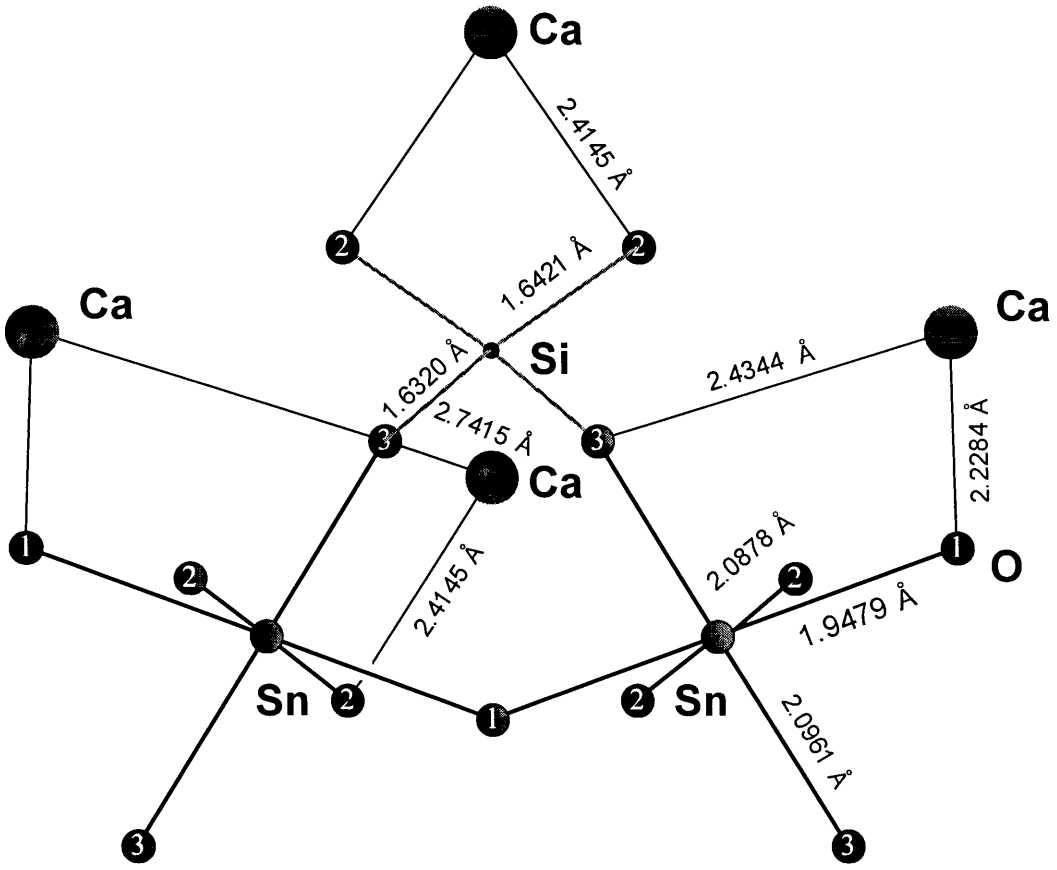

Figure 2.1 Schematic representation of the malayaite structure, adapted from the figure published by Higgens and Ribbe [10].

Malayaite consists of corner sharing (or vertex sharing) $[SnO_6]$ octahedra forming kinked chains which are cross linked by $[SiO_4]$ tetrahedra to form a $[SnOSiO_4]$ framework that accommodates the Ca^{2+}-ions in irregular 7-coordination polyhedra.

The site group symmetries and Wyckoff letters of the atoms in malayaite are listed in table 2.2 below.

Table 2.2 Site group symmetries and Wyckoff letters of the atoms in malayaite.

Ion	Site Group Symmetry	Wyckoff Notation
Ca^{2+}	C_2	4e
Sn^{4+}	C_i	4c
Si^{4+}	C_2	4e
$O_{(1)}^{2-}$	C_1	8f
$O_{(2)}^{2-}$	C_1	8f
$O_{(3)}^{2-}$	C_2	4e

The bond lengths and bond angles found in malayaite are summarised in table 2.3 below.

Table 2.3 Bond lengths and bond angles of malayaite [11].

Atom M	Bond length range, Å M-O	Bond angle range, ° O-M-O
Sn	1.9479 - 2.0961 *mean = 2.0439*	85.24 - 94.76 *mean = 90.0*
Si	1.6421 & 1.6320 *mean = 1.6371*	103.5 - 112.7 *mean = 109.5*
Ca	2.2284 - 2.7415 *mean = 2.483*	irregular

2.4 SPECTROSCOPY

2.4.1 THE SELECTION RULES

It is clear from the discussion above that the crystal structure of malayaite is complex. It is therefore not surprising that the Raman spectrum of malayaite has not yet been fully assigned. A full assignment of the Raman spectrum would be done using various techniques including isotope substitution and single crystal Raman studies.

Isotope substitution is done by substituting one isotope of an element in a complex with another, thereby effectively altering the mass of that element without altering any of its other properties. Consequently, the force constant will remain unchanged. According to equation 2.1 below, the vibrational frequency in the simple case of a diatomic molecule is given by

$$\nu = \frac{1}{2\pi c}\sqrt{\frac{k}{\mu}} \qquad \textbf{equation 2.1}$$

where k is the force constant and μ is the reduced mass [15]. Equation 2.1 shows that ν is proportional to $\sqrt{k}$ (the force constant effect), but inversely proportional to $\sqrt{\mu}$ (the mass effect). Consequently, if the mass changes and the force constant remains the same, the frequency of the band or bands related to bonds between the substituted isotope and the neighbouring atoms to which it is bonded will shift.

Single crystal Raman studies require the synthesis of a reasonably large crystal of reasonably high quality. It is not a trivial matter to obtain crystals of this nature for mixed metal oxide compounds like malayaite, not least of all due to their high thermal stability (malayaite sinters at T > 1550°C). Once suitable single crystals have been synthesised, their polarised Raman spectra are recorded which yield

symmetry properties of normal vibrations and consequently assists in their assignment.

Neither of these two tasks are trivial and constitute a study on their own. It was not the aim of this study to undertake a full assignment of the Raman spectrum of malayaite. A partial assignment was however undertaken. A factor group analysis was performed on malayaite by applying the correlation method (the Halford-Hornig or HH method) which considers the local symmetry of a solid and the number of molecules in the primitive unit cell. If σ is the number of molecules per primitive unit cell and ρ is the number of atoms per molecule then the number of acoustic modes will be 3, and the number of optical modes, N, expected from a solid may be calculated from equation 2.2 below.

$$N = (3\sigma\rho - 3) \qquad \textbf{equation 2.2}$$

As has already been stated, malayaite has two molecules per primitive unit cell (Bravais unit cell), and eight atoms per molecule. Consequently from equation 2.2 above, 45 optical modes are calculated for malayaite. The factor group analysis yielded the following results:

$$\Gamma_{total}^{A2/a} = 9A_g + 12B_g + 12A_u + 15B_u$$
$$\Gamma_{optic}^{A2/a} = 9A_g + 12B_g + 11A_u + 13B_u$$
$$\Gamma_{acoustic}^{A2/a} = 1A_u + 2B_u$$

There are 45 optically active modes as expected, 21 of which are Raman active and 24 of which are infrared active.

The modes can further be divided into internal and external (or lattice) modes. The structure of malayaite can, to an approximation, be described as consisting of $[SiO_4]$ tetrahedra and $[SnO_6]$ octahedra that accommodate the Ca^{2+}-ions. The translatory modes and rotatory modes (or librations) can then be obtained by assuming that the Si-ions and Sn-ions correspond to the centres of gravity of the

$[SiO_4]$ and $[SnO_6]$ 'molecules'. The method is outlined in more detail elsewhere [16;17]. The following results are obtained from this approximation:

$$\Gamma_{internal}^{A2/a} = 4A_g + 5B_g + 7A_u + 8B_u$$

Consequently, the Raman spectrum of malayaite is expected to contain 9 internal modes (4 totally symmetric and 5 antisymmetric modes) and the infrared spectrum of malayaite is expected to contain 15 internal modes (7 symmetric and 8 antisymmetric modes). The Raman spectrum of undoped malayaite can be seen in figure I-2.1 (appendix I). The details of the spectrum are also summarised in table 2.5 below.

In the Raman spectrum of malayaite, the modes of the $[SiO_4]$ tetrahedra are expected to occur as follows [18]:

$\nu'_1(A_1)$ between 830 and 840 cm^{-1}
$\nu'_2(E)$ between 420 and 480 cm^{-1}
$\nu'_3(F_2)$ between 850 and 890 cm^{-1}
$\nu'_4(F_2)$ between 500 and 600 cm^{-1}

Consequently, the following tentative assignments have been made:

ν'_1 at 851 cm^{-1}; ν'_2 at 441 cm^{-1}; components of
ν'_3 at 869, 891 and 960 cm^{-1}; and ν'_4 at 510 cm^{-1}.

The following vibrational modes are predicted for the $[SnO_6]$ polyhedra under O_h symmetry: $\nu'_1(A_{1g})$; $\nu'_2(E_g)$; ν'_3 and $\nu'_4(F_{1u})$; $\nu'_5(F_{2g})$ and $\nu'_6(F_{2u})$. The A_{1g}, E_g and F_{2g} modes are predicted to be Raman active, while the F_{1u} mode is predicted to be infrared active. Under C_i site symmetry, ν'_1, ν'_2, and ν'_5 will remain Raman active while ν'_3 and ν'_4 will remain infrared active only. In addition, ν'_6 will become infrared active. Therefore, the most intense band in the Raman spectrum of malayaite, the band at 570 cm^{-1}, can tentatively be assigned to

ν'_1(Sn-O) and the bands at 321 and 360 cm^{-1} can be assigned to components of ν'_5. The site symmetry approximation, which assumes that each metal oxide polyhedron is separated from the crystalline lattice, was used in the above assignments. While the use of isolated [SiO_4], [SnO_6] and [CaO_7] polyhedra (i.e. the site symmetry approximation) is practical for the tentative assignment of the respective bands of malayaite, it should be stated that it is a simplification since, as it has already been shown, the [SiO_4] tetrahedra bridge the [SnO_6] octahedra and the respective polyhedra share corners or edges (see figure 2.1 above).

2.4.2 SPECTROSCOPY : MALAYAITE THE HOST AND CHROMIUM THE GUEST

2.4.2.1 Resonance Raman Effect of Chromium in Malayaite

In order to produce a pigment stable at high temperatures, the dopant has to be incorporated into the host lattice. There are a number of ways in which this may be achieved. The most likely is a substitution reaction. This occurs when the doping ion substitutes for a host lattice ion. For the incorporation of chromium into malayaite, three possibilities exist for such a substitution reaction. Firstly, the chromium ion can substitute for a silicon ion which, as shown above, is tetrahedrally coordinated with a site symmetry of C_2. Secondly, the chromium ion can substitute for a tin ion which is octahedrally coordinated with a site symmetry of C_i. Thirdly, substitution of the seven coordinated calcium with a site symmetry of C_2 is possible.

The possibility of chromium substituting for calcium in malayaite can be immediately excluded. Seven coordinated Cr^{2+} species are unknown and Cr^{n+} species in general have substantially smaller ionic radii than Ca^{2+}-ions.

In the event that a substitution reaction takes place, involving the substitution of a host lattice ion by a guest chromophore, the laws governing the electro-neutrality of the end product, as discussed in chapter 1, have to be taken into account. A number of different scenarios are possible which will satisfy the laws of electro neutrality in chromium doped malayaite. One possibility might be a co-substitution reaction where chromium enters the host lattice in two oxidation

states. An example of this might be the substitution of one Cr^{6+}-ion and two Cr^{3+}-ion for a three ion combination of Si^{4+} and Sn^{4+} (either two Si^{4+}-ions and one Sn^{4+}-ions or vice versa). However, the simplest case would involve the substitution of chromium in its fourth oxidation state for a tin or silicon cation.

An example of Cr^{4+} doped into a mineral may be found in chromium doped forsterite, Cr^{4+}:Mg_2SiO_4. Forsterite is the magnesium end member of the olivine family of compounds and has an orthorhombic crystalline structure in which the Si^{4+}-ion occupies tetrahedral sites of C_s site symmetry and magnesium occupies two non-equivalent octahedral sites, M_1 and M_2, with site symmetries C_i and C_s, respectively [19]. The [SiO_4] tetrahedra are bridged by Mg^{2+}-ions sharing different oxygen atoms [20]. Chromium can enter the host lattice of forsterite in two oxidation states. Cr^{3+} substitution is favoured by a reducing atmosphere, while Cr^{4+} substitution is favoured by an oxidising atmosphere. The Cr^{3+}-ions substitute for magnesium atoms which are in two distinctly different octahedrally coordinated crystallographic positions, the first of C_i site symmetry, and the second of C_s site symmetry [18]. Cr^{4+} substitutes for tetrahedrally coordinated silicon atoms of C_s site symmetry. The ionic radius of the Cr^{4+}-ion in a fourfold coordination polyhedron is 0.41 Å [21], which is substantially larger than the corresponding ionic radius of for fold coordinated Si^{4+} which is 0.26 Å, but substitution of Si^{4+} in tetrahedral sites by Cr^{4+} is nonetheless well known [19]. It has been found that Cr^{4+} is relatively stable in tetrahedral sites, and the Cr(IV)-O(II) bond is expected to have a high degree of covalency [19;20].

Several other examples of host lattices that accommodate Cr^{4+} in four fold molecular symmetry include Cr^{4+}:Y_2SiO_5 and Cr^{4+}:$LiNdGeO_5$ [18], and Cr^{4+}:$Y_3Al_5O_{12}$ (YAG) [22].

As already stated, methods like XRD and SEM analysis are not sensitive enough to yield information about the chromophore incorporated in the host lattice. Infrared spectroscopy is also not capable of yielding much information about the guest chromophore. Raman spectroscopy is a valuable technique for the

elucidation of molecular structures of complex transition metal oxides. This is because Raman spectroscopy probes directly the structure and bonding of metal oxide complexes by their vibrational spectra. In addition, resonance Raman scattering can be used to selectively enhance Raman modes under investigation and is therefore an ideal tool for the investigation of coloured chromophores in host lattices [23;24].

It is known from the literature that tetrahedral or distorted tetrahedral oxyanions are very polarisable and therefore give rise to strong Raman spectra and even off-resonance [23]. Progressions of $\nu_1(A_1)$ could be expected should CrO_4^{4-}-ions be present in malayaite, together with weaker subsidiary progressions involving one or more of the non-totally symmetric modes $\nu_2(E)$, $\nu_3(F_2)$ and $\nu_4(F_2)$ of the type $\nu_n + v.\nu_1$ (v=1,2) (n=2,3).

The undistorted SiO^{4-}-ion has T_d-symmetry, with nine internal modes.

$$\Gamma_{Td} = A_1+E+2T_2$$

All of these modes are Raman active. Should chromium substitute for silicon, then the undistorted CrO_4^{4-}-ion will have the same symmetry, and consequently, the same number of modes. The correlation between the modes of the free tetrahedron and those under the respective site and factor group symmetries of malayaite are shown in table 2.4 below.

Table 2.4 Modes of the 'free' CrO_4^{4-}-ions of T_d symmetry correlated with those under C_2-site- and C_{2h}-factor group symmetries.

T_d	C_2	C_{2h}
ν_1 - A_1	A	A_g
		A_u
ν_2 - E	A	A_g
		A_u
	A	A_g
		A_u
ν_3,ν_4 - F_2	A	A_g
		A_u
	B	B_g
		B_u
	B	B_g
		B_u

From table 2.4 above it is clear that four symmetric A_g, and two non-symmetric B_g resonance enhanced Raman modes could be expected if chromium ions in their fourth oxidation state substitute for the silicon ions under C_{2h} point group symmetry.

If one considers the electronic transitions of an ideal tetrahedral site of T_d symmetry the lowest free-ion level of the d^2 Cr^{4+}-ion is ^3F and it will split in the following way.

$$^3F \rightarrow {}^3A_2 + {}^3T_2 + {}^3T_1$$

The energy of these levels varies as follows: $^3A_2 < {}^3T_2 < {}^3T_1$. Consequently, the $^3A_2$ state can be considered as the ground state. The $^3A_2 \rightarrow {}^3T_1$ transition is electric dipole allowed (and spin allowed), while the $^3A_2 \rightarrow {}^3T_2$ transition is only magnetic dipole allowed and therefore orders of magnitude less intense than the $^3A_2 \rightarrow {}^3T_1$ transition. Two further states are found in the Tanabe-Sugano diagram for a tetrahedrally coordinated d^2-ion, namely ^1E and ^1A, which result from the ^1D and ^1G free-ion states. It is however very difficult to find absorptions resulting from these states since the transitions are forbidden [22].

The electronic spectrum of Cr^{4+}:YAG shows a visible absorption band between 600 and 700 nm which is assigned to the $^3A_2 \rightarrow {}^3T_1$ transition and an absorption in the near infrared region at 1000 nm which is assigned to the $^3A_2 \rightarrow {}^3T_2$ transition [22]. Several other weaker absorption bands have also been identified in this electronic spectrum which are caused by the lower site symmetry of the Cr^{4+}-ions in the YAG host lattice, namely D_{2d}.

The electronic spectrum of Cr^{4+}:Mg_2SiO_4 shows a visible absorption band at 575 nm which is also assigned to the $^3A_2 \rightarrow {}^3T_1$ transition, or if the distortion of the Cr^{4+}-ion is taken into consideration, a $^3A_2 \rightarrow {}^3B_2$ transition, assuming a site symmetry of C_{2v} for the Cr^{4+}-ions [18].

The electronic spectrum of Cr^{4+}:$CaSnOSiO_4$ between 350 and 800 nm is shown in figure I-2.6 (appendix I). It shows a broad maximum which peaks at around 535 nm. This band is most probably due to the same transition which accounts for the bands of Cr^{4+}:YAG and Cr^{4+}:Mg_2SiO_4 in the same region. Consequently, this band most likely also originates from a $^3A_2 \rightarrow {}^3T_1$ transition of Cr^{4+}-ions under T_d symmetry. If the band does in fact originate from the same transition then resonance enhanced Cr-O bands should be observed using the lines of an Ar^+ laser in the frequency region of this broad band at ~535 nm. Raman spectra were recorded of both the undoped and the chromium doped malayaite (Figures I-2.1, I-2.2, I-2.3 & I-2.4 - appendix I). The bands of the respective spectra are summarised in table 2.5 below.

Table 2.5 Raman band positions and their tentative assignment in undoped and chromium doped malayaite.

$CaSnOSiO_4$ ν/cm^{-1}, 514.5 nm	$Cr^{4+}:CaSnOSiO_4$ ν/cm^{-1}, 514.5 nm	Assignment
133	-	ν_{Lat}
173	-	ν_{Lat}
183 sh	-	ν_{Lat}
292	292	-
321	321	ν_5'(Sn-O)
360	360	ν_5'(Sn-O)
441	-	ν_2'(Si-O)
-	445	ν_4
-	489	ν_2
510	506	ν_4'(Si-O)
570	570	ν_1'(Sn-O)
-	735	ν_1
~740 vw	-	-
-	820 vw	ν_3
851	856	ν_1'(Si-O)
869	-	ν_3'(Si-O)
891	893	ν_3'(Si-O)
-	934	ν_3
960	-	ν_3' (Si-O)
-	974	ν_3
-	1222	$\nu_1+\nu_2$
-	1267	-
-	~1400	$\nu_2+\nu_3$
-	1475	$2\nu_1$
-	1680	$\nu_1+\nu_3$
-	1869	$2\nu_3$
-	1991	$2\nu_1+\nu_2$
-	2220	$3\nu_3$
-	2416	$2\nu_1+\nu_3$
-	~2620	$3\nu_1+\nu_4$

It is immediately evident from a comparison of the Raman spectra of undoped and chromium doped malayaite, and from table 2.5 above, that resonance enhancement of some vibrational modes occurred in the Raman spectrum of chromium doped malayaite using the 514.5 nm excitation laser line. The resonance Raman spectrum is in fact totally dominated by a new band at 735 cm^{-1}. Consequently, this band has been assigned to the totally symmetric Cr-O tetrahedral breathing mode ν_1. The assignment is unambiguous for two reasons. The first is that totally symmetric modes are the ones expected to be most enhanced, and while it has been shown that several totally symmetric modes are predicted in the (Cr-O) stretching mode range, ν_1(Cr-O) is the only totally symmetric mode which originates from a totally symmetric mode under the original T_d symmetry of the free ion. The second is that a progression of overtones of the 735 cm^{-1} band, $2\nu_1$ and $3\nu_1$, can be seen in the Raman spectrum of Chromium doped malayaite (fig. I-2.2 - appendix I). Fourth and higher order progressions of the $\nu_1(A_1)$ and other fundamental modes have not been observed. However, subsidiary progressions of the modes $\nu_n + v.\nu_1$ (v = 1,2)(n = 2,3) are also seen in the Raman spectrum. The overtones and progressions can more easily be seen in figure I-2.5 (appendix I). Long progressions in ν_1 are characterised by a high $I2\nu_1/I\nu_1$ intensity ratio [23]. In chromium doped malayaite $I2\nu_1/I\nu_1$ = 0.17. This relatively low value is in accordance with the short progression observed for $\nu_1(A_1)$

2.4.2.2 Chromium-Oxygen Bond Length in Malayaite

Crystallographically determined chromium oxygen bond lengths were obtained of numerous chromium oxide reference compounds in the solid state, in solution, and in the gas phase by Weckhuysen and Wachs [25]. They were then correlated with their corresponding Raman stretching frequencies. From these results it has been shown that the following simple exponential relationship (eqn. 2.3) exists between the Raman stretching frequency, ν , and the Cr-O bond length, *R*.

$$\nu = 13055\exp(-1.6419 \times R) \qquad \textbf{equation 2.3}$$

Such a direct relationship between these two experimental observables is justified under the assumption of the diatomic approximation. Effectively this approximation assumes that each distinct Cr-O bond is entirely separated from its crystal lattice. Consequently each isolated Cr-O bond exhibits a stretching frequency which is characteristic of its bond length. Within the limits of experimental error, the diatomic approximation provides a good estimate of Cr-O bond distances (±0.030 Å) from observed stretching frequencies [25].

Substituting 735 cm^{-1}, the frequency of the band assigned ν_1 in Cr^{4+}:$CaSnOSiO_4$, for ν in equation 2.3 above, a bond length of R = 1.752 Å is obtained. This can, of course, only represent an average value of the Cr-O bond length since the maximum symmetry that the CrO_4^{4-}-ions can attain in malayaite, substituting for silicon atoms, is C_2 which means that two different bond lengths are expected.

Crystal structure studies of Sr_2CrO_4 show that there are two different types of CrO_4^{4-}-ions in the lattice and in each of the tetrahedra, three Cr-O bond distances are similar (average values of 1.84 and 1.90 Å respectively) while the forth bond is unusually short (1.66 and 1.649 Å respectively) [26;27]. Consequently, a Cr-O bond length of 1.752 Å for Cr in malayaite is not unreasonable.

The Si-O bond lengths in malayaite are equal to 1.6320 and 1.6421 Å respectively. Malayaite thus has a mean Si-O bond distance of 1.6371 Å [11]. Forsterite has three different Si-O bond lengths, two of 1.6370 Å, and one each of 1.6131 and 1.6545 Å, respectively. This yields an average Si-O bond length of 1.6354 Å in forsterite [28;29], which is very close to that of malayaite. Since the SiO_4^{4-} are structurally very similar in forsterite and malayaite, it can be expected that chromium substituting for Si in these compounds will produce similar resonance Raman modes. The band at 764 cm^{-1} in the resonance Raman spectrum of forsterite has been assigned to the tetrahedral breathing mode ν_1 (A_1) [18]. If 764 cm^{-1} is substituted into equation 2.3 above, a bond length of R = 1.729 Å is obtained for the Cr-O bond in Cr^{4+}:Mg_2SiO_4. As expected, this

value is in very good agreement with the bond length of 1.752 Å calculated for Cr-O in Cr^{4+}:$CaSnOSiO_4$.

As stated above, there are two different Si-O bond lengths in malayaite. These correspond to the Si-ion being bonded to two differently coordinated oxygen atoms; $Si\text{-}O_{(2)}$ and $Si\text{-}O_{(3)}$, respectively. From the crystal structure of malayaite [10;11] and figure 2.1 above it can be seen that the oxygen labelled $O_{(2)}$ is coordinated to three metal atoms (Ca,Sn & Si). The oxygen labelled $O_{(3)}$ is coordinated to four metal atoms (2xCa, Sn, & Si). The Si^{4+}-ions are fourfold coordinated, and it therefore follows that the Cr^{4+}-ions will also be fourfold coordinated. Table 2.6 below gives the ionic radii data of the above mentioned ions [11;21].

Table 2.6 Ionic radii data for Si^{4+}, Cr^{4+} and O^{2-}.

Ion	Coordination	Ionic Radii, Å
Si^{4+}	4	0.26
Cr^{4+}	4	0.41
$O^{2-}(O_{(3)})$	4	1.38
$O^{2-}(O_{(2)})$	3	1.36

From table 2.6 above, the following ionic radii sums may be calculated:

$r(Si^{4+}\text{-}O^{2-}_{(2)}) = 0.26 + 1.36 = 1.62$ Å

$r(Si^{4+}\text{-}O^{2-}_{(3)}) = 0.26 + 1.38 = 1.64$ Å

$r(Cr^{4+}\text{-}O^{2-}_{(2)}) = 0.41 + 1.36 = 1.77$ Å

$r(Cr^{4+}\text{-}O^{2-}_{(3)}) = 0.41 + 1.38 = 1.79$ Å

The ionic radii sums of the Si^{4+}- and O^{2-}-ions correlate closely with the Si-O bond lengths found in malayaite. The Cr-O bond lengths are however shorter than predicted by the ionic radii sums of the Cr^{4+}- and O^{2-}-ions and therefore the Cr-O

bonds have strong covalent character in chromium doped malayaite. This is also the case in chromium doped forsterite.

2.4.2.3 Chromium-Oxygen Bond Order in Malayaite

The bond order, or bond valence, reflects the relative strength of a chemical bond and shows the distribution of available valence electrons in the chemical bonding of a molecular species. Hence, the calculated valence state can be compared to the formal oxidation state of the chromium ion in malayaite and thus serves as a book keeping device for the distribution of electrons among the available Cr-O bonds [25].

A general relationship has been developed which relates the cation-oxygen bond valence *s(M-O)* to the corresponding interatomic distance *R* [30]. This empirical relationship, equation 2.4 below, relates a M-O bond length (*R*) to its bond order (*s*).

$$s(M-O) = \left(R/\overline{R}\right)^{-N} \qquad \textbf{equation 2.4}$$

where *N* and $\overline{R}$ are empirical parameters. $\overline{R}$ is the average cation-oxygen bond length for a M-O bond of unit valency. Weckhuysen and Wachs have determined empirically the values of *N* and $\overline{R}$ for chromium-oxygen bonds [25]. Table 2.7 below shows the calculated bond orders for the various possible oxidation states that chromium in $CaSnOSiO_4$ could be in.

Table 2.7 Bond orders for the various chromium species.

M^{n+}	N	$\overline{R}$	Bond Order
Cr^{6+}	5.0	1.787	1.10
Cr^{4+}	5.2	1.770	1.05
Cr^{3+}	5.2	1.733	0.94

These bond orders are calculated from equation 2.4 above, substituting a Cr-O bond length of 1.752 Å for the Cr-O bond, as calculated in section 2.4.2.2 above. From the above table it can be seen that a Cr-O bond order of ~1 is expected for the various chromium species that might be in malayaite. There are a number of ways in which this can be achieved in malayaite.

Firstly, a bond order of around one for chromium in malayaite could be achieved by substituting Cr^{6+} for Sn^{4+}. From ionic radii data, it can be seen that this would require the substitution of $R(Sn^{4+}\text{-}O^{2-})$ = 2.06 Å by $R(Cr^{6+}\text{-}O^{2-})$ = 1.63 Å. This requires a shortening of each of the six M-O bond by ~21%. In the unlikely event of this happening equation 2.3 above shows that the totally symmetric Cr-O stretching vibration would be at ~898 cm^{-1}, ~163 cm^{-1} higher than the position at which it is found. Furthermore, a Cr-O bond length of 1.787 Å is predicted for the perfect $[Cr^{6+}\text{-}O^{2-}]_6$ octahedron which is substantially shorter than the average bond length of the Sn-O bonds in malayaite at 2.0439 Å. Another problem with the substitution of Cr^{6+} for Sn^{4+} is that of electroneutrality. Consequently, the substitution of Sn^{4+} by Cr^{6+} in malayaite can be discounted.

If the bond order calculations are ignored, then the possibility of Cr^{6+} substituting for Si^{4+} needs to be considered for completeness sake. Once again the problem of electroneutrality emerges. A simple way of compensating for the loss of two electrons would be to substitute two Cr^{3+}-ions for two Sn^{4+}-ions. Table 2.8 below shows a comparison of the ionic radii of the respective M-O bonds, the bond length, and the position of the totally symmetric stretching vibration, calculated from equation 2.3 above, should the above mentioned substitutions take place.

Table 2.8 Predicted position of Cr-O Raman bands should Cr^{3+} substitute for Sn^{4+}, and Cr^{6+} substitute for Si^{4+} in malayaite.

Atom, M	$R(M^{n+}-O^{2-})$, Å	Bond Length, Å	ν_{calc} , cm^{-1}
Sn^{4+}	2.06	2.0439[1]	
Cr^{3+}	1.985	-	501.58
Si^{4+}	1.63	1.6371[1]	
Cr^{6+}	1.63	1.648[2]	871

1 Groat et. Al. [11].

2 Value predicted for the perfect four coordinate Cr^{6+} (T_d site symmetry). As the site symmetry is lowered the bond length tends to get shorter [25].

From table 2.8 above it is can be seen that should Cr^{3+} substitute for Sn^{4+} in malayaite, then its totally symmetric stretching vibration would occur at around 500 cm^{-1}, and should Cr^{6+} substitute for Si^{4+} in malayaite, then its totally symmetric stretching vibration would be found at around 870 cm^{-1}. Neither is the case. The totally symmetric stretching vibration in the resonance Raman spectrum of chromium doped malayaite is found at 735 cm^{-1}. Therefore, the possibility of Cr^{6+} substituting for Si^{4+} coupled with Cr^{3+} substituting for Sn^{4+} can also be discounted.

The only other way in which a bond order of ~1 can be achieved for Cr-O bonds in chromium doped malayaite is if Cr^{4+} substitutes for Si^{4+}. The average Si-O bond length in malayaite is 1.6371 Å and the average bond length of Cr-O in malayaite has been calculated as 1.75 Å. $R(Cr^{4+}-O^{2-})$ = 1.78 Å which indicates that the Cr-O bond in malayaite has strong covalent character. It has been shown in section 2.4.2.2 above that bond length considerations support this substitution.

In the molecular orbital configurations of CrO_4^{4-}, all of the bonding orbitals $t_2^6e^4a_1^2t_2^6$ are filled as well as the ligand based non-bonding orbital t_1^6. In CrO_4^{4-} there are also two electrons in the anti-bonding e* orbital and a bond order of ~1 could be expected for Cr^{4+}-O bonds.

The valence state of various Cr-O compounds multiplied by their coordination number are compared with their formal oxidation number in table 2.9 below.

Table 2.9 The site symmetry, bond order(eqn. 2.4), coordination number, valence sum and formal oxidation state of various Cr-O compounds.

Compound	Site symmetry	*s(Cr-O)*	Coord^n Number	Valence Sum	Formal Ox^n State
Cr^{4+}:$CaSnSiO_5$	C_2	1.05	4	(4.20)	+4
Cr^{4+}:Mg_2SiO_4	C_s	1.18	4	(4.72)	+4
K_2CrO_4	T_d	1.49	4	5.96	+6
$K_2Cr_2O_7$	C_{2v}	1.59	4	(6.36)	+6

Strictly speaking, the valence sum rule can only be applied to chromium oxides having four identical Cr-O bonds. From the site symmetry column in the above table, it is readily seen that only K_2CrO_4 has four equivalent Cr-O bonds, and consequently, its valence sum correlates very closely with its formal oxidation state. The others do not correlate as closely since they have two or more different bond lengths but they correlate closely enough to support the assignment of the fourth oxidation state to chromium in malayaite. A bond order of around one can only be achieved in chromium doped malayaite in two ways. The first is if Cr^{4+} substitutes for Si^{4+}, and the second is if Cr^{6+} substitutes for Sn^{4+}, a possibility which has been ruled out for a number of reasons discussed above. Consequently, the bond order of chromium in malayaite supports Cr^{4+} substituting for Si^{4+}.

A bond-order stretching frequency correlation for Cr-O bonds exists, and like the bond-length stretching frequency correlation above (section 2.4.2.2) it is also justified under the diatomic approximation.

The combined use of equations 2.4 and the bond length-stretching frequency correlation, equation 2.3 above, yields the following relationship between the Pauling Cr-O bond strength (*s(Cr-O)* in valence units) and the Raman stretching frequency, ν [25].

$$s(Cr-O) = \left[\left(0.60905/R\right)\ln\left(\frac{13055}{\nu}\right)\right]^{-N} \qquad \textbf{equation 2.5}$$

where *N* and $\overline{R}$ are the same empirical parameters described in equation 2.4 above. Bond order and stretching frequency correlations are useful in the determination of chromate structures since they allow the determination of the Cr-O bond orders from the Cr-O stretching frequencies.

2.4.2.4 Chromium-Oxygen Force Constants in Malayaite

The vibrational frequency, ν, of a diatomic molecule is given by equation 2.6 below,

$$\nu = \frac{1}{2\pi c}\sqrt{\frac{k}{\mu}} \qquad \textbf{equation 2.6}$$

where *k* is the force constant and μ is the reduced mass [15]. This equation shows that ν is proportional to $\sqrt{k}$ (the force constant effect), but inversely proportional to $\sqrt{\mu}$ (the mass effect). To calculate the force constant, it is convenient to rewrite equation 2.6 as

$$k = 4\pi^2\mu c^2(\nu_1)^2 \qquad \textbf{equation 2.7}$$

where μ is the reduced mass, and ν_1 is the wavenumber of totally symmetric stretching mode. The following expressions hold true for the force constant, k_{Td}, of a tetrahedron [31] :

$$k_{Td} = k_1 + 4k_2 \qquad \textbf{equation 2.8}$$

where $$4k_2 = 4\pi^2 mc^2 (\nu_2)^2 \qquad \textbf{equation 2.9}$$

Consequently, k_{Td} may be calculated using equation 2.7 and k_2 may be calculated using equation 2.9. These values are then substituted into equation 2.8 in order to calculate k_1. Using the equations 2.7,2.8 & 2.9 above, the force constants for the Si^{4+}-O^{2-} and Cr^{4+}-O^{2-} bonds can be estimated. They are summarised in table 2.10 below.

Table 2.10 Force constants calculated for the $[SiO]_4$ and $[CrO]_4$ tetrahedra in malayaite and forsterite.

Mineral	MO_4^{4-}	ν_1, cm^{-1}	ν_2, cm^{-1}	k_{Td}, mdyn/Å	k_1, mdyn/Å	k_2, mdyn/Å
Malayaite	SiO_4^{4-}	851	441	6.83	4.99	0.46
	CrO_4^{4-}	735	489[1]	5.09	2.84	0.56
Forsterite[2]	SiO_4^{4-}	835	440	6.57	4.75	0.46
	CrO_4^{4-}	764	489	5.50	3.25	0.56

[1] Assumed value - see later discussion.

[2] [18;32]

From table 2.10 above it can be seen that there is a significant decrease in the force constant when chromium substitutes for the silicon in malayaite and forsterite. The relative percentage decrease (Δ) in the Cr^{4+}-O force constant, if compared to the Si^{4+}-O force constant [$\Delta=\{(k_{1\ Cr\text{-}O} - k_{1\ Si\text{-}O})/k_{1\ Si\text{-}O}\}$ x100(%)], is

43% for malayaite. This may be compared with a value of 32% for forsterite. The greater decrease in malayaite is most likely due to the fact that the CrO_4^{4-} groups bridge the Sn-ions which are also covalently bonded to the respective oxygen atoms. In forsterite, on the other hand, the [SiO_4] tetrahedron behaves like an independent molecular complex inside the crystal since the Si-O force constant is at least four times larger than any other force constant in forsterite [20].

From the resonance Raman spectrum of malayaite, figure I-2.2 (appendix I), it is evident that in addition to the totally symmetric stretching frequency of the Cr-O bond, ν_1, occurring at 735 cm^{-1}, and the 489 cm^{-1} band which has been assigned to ν_2, there is a relatively intense band at 934 cm^{-1} with a prominent shoulder at 974 cm^{-1}, and weaker shoulders at 893 and 856 cm^{-1}. The weaker shoulders most likely belong to Si-O stretching modes of the malayaite host lattice. Similar bands can be found in the Raman spectrum of the undoped malayaite (compare figures I-2.1 and I-2.2 - appendix I), and as will become apparent, also in the Raman and resonance Raman spectra of undoped and chromium doped titanite (chapter 3). The shoulder at 974 cm^{-1} can possibly be assigned to the overtone $2\nu_2$, but it is also possible that the bands at 974, 934, and 820 cm^{-1} are components of ν_3, thus giving rise to an average value of 909 cm^{-1} for ν_3. Either way, in this respect our results differ significantly from those obtained for ν_3 in chromium doped forsterite where the mean value for ν_3 for CrO_4^{4-} ions in forsterite is 715 cm^{-1} [18]. In the Raman spectrum of malayaite, the band at 445 cm^{-1} has been assigned to ν_4. The above assignments are justified in the following ways.

Firstly, in the valence force field of a tetrahedral molecule, XY_4, the respective force constants are related to the respective vibrational modes in a manner described by equations 2.10 and 2.11 below [31]:

$$k_{Td} = 4\pi^2 m_y c^2 (\nu_1)^2 \qquad \textbf{equation 2.10}$$

$$k_\delta / \ell^2 = \frac{4\pi^2 m_y \nu_2^2 c^2}{3} \qquad \textbf{equation 2.11}$$

where m_y is the mass of the oxygen atom, k_{Td} is the stretching force constant, k_δ is the bending force constant, ℓ is the length of the edge of the tetrahedron in the equilibrium position, and ν_n is the frequency of the nth mode.

From the above equations, k_{Td} = 5.09 mdyne/Å and k_δ / ℓ^2 = 0.75 mdyne/Å for malayaite. Consequently $\nu_3^2 + \nu_4^2$ can be calculated from the equation 2.12 below.

$$4\pi^2 c^2 \left[(\nu_3)^2 + (\nu_4)^2 \right] = k_{Td}/m_y \left(1 + \frac{4m_y}{3m_x} \right) + 2k_\delta / m_y \ell^2 \left(1 + \frac{8m_y}{3m_x} \right) \qquad \textbf{equation 2.12}$$

where m_x is the mass of the chromium atom. From equation 2.12 above $\nu_3^2 + \nu_4^2$ = 10.5882x10^5 cm^{-1} for CrO_4^{4-} in malayaite. Consequently, substituting an average value for $\nu_{3\ obs}$ of 909 cm^{-1} gives $\nu_{4\ calc}$ = 482 cm^{-1} which is in reasonable agreement with $\nu_{4\ obs}$ at 445 cm^{-1} , and, substituting a value for $\nu_{4\ obs}$ of 445 cm^{-1} gives $\nu_{3\ calc}$= 928 cm^{-1} which is in good agreement with $\nu_{3\ obs}$ = 934, 974 and 820 cm^{-1}. The observed values and calculated values are in good agreement with each other and consequently support the band assignments.

Secondly, for CrO_4^{4-}, the following relationship (equation 2.13) exists between the fundamental modes [31]:

$$\frac{\nu_3 \nu_4}{\nu_1 \nu_2} = \sqrt{\frac{2}{3}\left(1 + \frac{4m_y}{m_x} \right)} \qquad \textbf{equation 2.13}$$

If the mass of chromium and oxygen are substituted into the right hand side (RHS) of equation 2.13 above, then RHS = 1.22.

If the observed values for the fundamental modes are substituted into the left hand side (LHS) of equation 2.13 above, then LHS = 909x445/735x489 = 1.13.

The RHS and the LHS of the above equation correlate closely with each other in support of the above assignment.

It is evident from figure I-2.3 (appendix I), which shows the resonance Raman spectrum of bulk Cr^{4+}:$CaSnOSiO_4$ recorded with the 514.5 nm line of an Ar^+ laser, that two resonance enhanced Raman modes occur at 489 and 445 cm^{-1}, respectively. These lines are not due to Si-O modes since they are more intense than the most intense band of the Raman spectrum of undoped malayaite, namely the 570 cm^{-1} band. From the above results, it is not possible to show unequivocally which of these resonance enhanced bands is ν_2 and which is ν_4. In fact, the bands might represent two components of the same mode, either ν_2 or ν_4 since under the C_2 site symmetry, in which chromium finds itself in malayaite, ν_2 and ν_4 should split into two and three components, respectively. In chromium doped forsterite, a band at 498 and another at 480 cm^{-1} have been assigned as components of ν_2 respectively, and a band at 290 and another at 253 cm^{-1} have been assigned as components of ν_4 respectively. Consequently, if the 489 cm^{-1} band in chromium doped malayaite is assigned to ν_2 then it is in excellent agreement with the corresponding mode in chromium doped forsterite. However, no bands were observed in chromium doped malayaite below 300 cm^{-1} which could be assigned to ν_4. Instead the band at 445 cm^{-1} has been assigned to ν_4. Calculations involving equations 2.10-2.13 above support this assignment.

Further support for the assignments of the fundamental modes may be found in the analysis of the combination and overtone bands. These are summarised in table 2.5 above and can be seen in figure I-2.5 (appendix I). They include combinations of $\nu_1+\nu_2$ and $\nu_1+\nu_3$. These combinations, and others, confirm the assignment of the resonance enhanced bands at 735, 934 and 445 cm^{-1} as fundamental modes. Furthermore, a distinct band at 1222 cm^{-1} in the resonance enhanced spectrum of chromium doped malayaite can only arise from a

combination of the bands at 735 and 489 cm^{-1} confirming the assignment of the band at 489 cm^{-1} to a fundamental mode.

In addition to the combination bands there are also overtones of ν_1, ν_2 and ν_3. From the overtones of ν_1, $n\nu_1(n=2,3)$, it is evident that the anharmonicity constant χ_{11} must have a positive value. If the values of $\nu_{(n)}/n$ are plotted against n, a value of $\chi_{11} = 1.2 \pm 0.4$ cm^{-1} is obtained and the harmonic value of ν_1 is $\omega_1 =$ 736cm^{-1}. This can be explained in terms of the bonding of the Sn-ions to the oxygen ions. In $AgMnO_4$ a positive χ_{11} value has been ascribed to the polarising effect of the Ag^+-ions [33].

2.5 CONCLUSION

2.5.1 SYNTHESIS

Undoped malayaite was synthesised at 1550°C. At this temperature, the reaction product was found to be in the initial stages of sintering. The reaction was repeated at 1500°C. The resulting product was broken down into a coarse white powder. Chromium doped malayaite was synthesised at 1450 and 1300°C. The products of these reactions were coarse powders with a strong maroon coloration. In addition, chromium doped malayaite was also synthesised at lower temperatures using a mineraliser mixture of boric acid and potassium nitrate. With the mineraliser mixture it was possible to synthesis a pigment of good quality at ~1200°C. Below ~1200°C it was not possible to synthesis pigments of suitably high quality. The coloration was weak and not very clean. In addition, XRD data showed that a large amount of by-products and unreacted starting materials remained after calcining.

The chromium doped malayaite was subjected to water and acid leaching treatments. The acid leaching treatments resulted in slight discoloration of the pigment. This was successfully countered by adding a slight excess of silica to the reaction mixture before calcining. This is of coarse not desirable for the

spectroscopic investigation of the pigment since the excess silica produces its own bands in the respective spectra. The pigments were also applied to tiles as part of the glaze mixture. The results were found to be satisfactory. They are not discussed here in any detail since the optimisation of the glaze and firing conditions is not a trivial task and was beyond the scope of the current investigation.

2.5.2 SPECTROSCOPY

The vibrational spectra of the undoped malayaite were recorded. The Raman and infrared spectra were found to be in good agreement with those recorded elsewhere. A tentative assignment of the bands in the Raman spectrum of undoped malayaite was undertaken.

The electronic spectrum of chromium doped malayaite was recorded. It showed a broad band in the 500-600 nm range indicating the possibility of recording the resonance Raman spectrum of chromium doped malayaite. The vibrational spectra of chromium doped malayaite were recorded. No significant changes were found in the infrared spectrum of doped malayaite when compared with the infrared spectrum of undoped malayaite. In contrast, new bands were found to be present in the Raman spectra of the chromium doped malayaite. Both micro and macro Raman spectra were recorded of the reaction products. These new features were shown to be sensitive to the amount of chromium in the host lattice. Consequently, they were shown to be resonance Raman bands due to Cr^{4+} in malayaite. Furthermore, progressions of ν_1(Cr-O) and subsidiary progressions of the Cr^{4+} bands were found in the Raman spectrum of Cr^{4+}:$CaSnOSiO_4$. These new features were investigated and tentatively assigned.

Chromium was found to exists in malayaite in its fourth oxidation state and to substitute for Si-ions which are in tetrahedral coordination with a site symmetry of C_2. Furthermore, the Cr-O bond lengths of the Cr^{4+}-ions in malayaite were calculated to be 1.752 Å. This is an average length since the maximum symmetry that the CrO_4^{4-}-ions can attain in malayaite substituting for silicon

atoms is C_2 which means that two different bond lengths are expected. The ionic radii sum of Cr and O is larger than that of Si and O. Consequently, the Cr-O bond was shown to have strong covalent character in chromium doped malayaite resulting in bond lengths which are shorter than those predicted by the ionic radii calculations. The bond length calculated for Cr^{4+}:$CaSnOSiO_4$ agree well with those of other tetra coordinated Cr^{4+} species.

An average bond order of 1.05 was calculated for the Cr^{4+}-O bond in chromium doped malayaite. This is an average value, once again due to the maximum site symmetry that the Cr-ion can attain in the malayaite structure. This value is well within the limits of the value expected for tetra coordinated Cr^{4+}. Furthermore, this value compares favourably with that of Cr^{4+} in forsterite.

The force constants for the Cr-O bond in chromium doped malayaite were also calculated. The stretching force constant was calculated to be 2.87 mdyne/Å. Calculations involving the force constants of the Cr-O bond were found to support the tentative assignments the Cr-O bands in the Raman spectrum of Cr^{4+}:$CaSnOSiO_4$.

Resonance Raman spectroscopy was used to effectively show the presence of Cr^{4+}-ions in the lattice of $CaSnOSiO_4$. A comparison of our results on Cr^{4+}:$CaSnOSiO_4$ with those obtained in the investigation of Cr^{4+}:Mg_2SiO_4 and Cr^{4+}:YAG leaves little doubt that CrO_4^{4-}-ions do in fact exist in chromium doped malayaite.

Chapter 3

The Titanite Compounds

3.1 INTRODUCTION

Titanite (calcium titanium silicate) is a naturally occurring mineral with the general chemical formula $CaTiOSiO_4$ or simply $CaTiSiO_5$. It was first described by Pictet in 1787 and designated the name titanite by Klaproth in 1795 in accordance with its chemical composition [34]. It is also commonly called sphene, a name which originated from a Greek word meaning wedge, in accordance with its common wedge shaped habit. Titanite is a sparse yet widely distributed accessory mineral commonly found in metamorphic and igneous rocks and their associated pegamites. Because of its extreme dispersive power, birefringence and colour, titanite has been cut into spectacular gemstones. They are however not highly prized due to their being soft and consequently, not very durable [34].

The crystal structure of naturally occurring titanite was first investigated by Zachariasen who, in 1930, described it as consisting of independent silicate ions bonded together with $[TiO_6]$ octahedra to form a network with 7-fold coordinated Ca-ions accommodated in the resulting cavities [34]. The crystals which came from Norway were assumed to have a composition sufficiently close to the ideal formula $CaTiSiO_5$. Initially, titanite was thought to belong to the monoclinic space group C2/c (or A2/a). Consequently, when malayaite was discovered in 1960, and its structure determined, it was thought that titanite and malayaite were isostructural. Then, in 1968, it was discovered that synthetic titanite belonged in fact to the monoclinic space group $P2_1/a$ (No. 14) [35]. Subsequently, it was shown that long-exposure single-crystal photographs of several natural titanite specimens also showed diffuse reflections in violation of the diffraction rules of A2/a [34].

It has been shown that the structure of titanite and malayaite are very similar. In fact, the only naturally occurring silicate isostructural with titanite is malayaite [34]. Both have chains of octahedra ($[SnO_6]$ or $[TiO_6]$ as the case may be) and they differ only in that the titanium atoms in titanite are slightly offset within the $[TiO_6]$ octahedra resulting in the slight lowering of symmetry. Titanite therefore belongs to a group of ferroelectric and antiferroelectric titanates where the

electric polarisation results from the displacement of the titanium atom from the centre of the $[TiO_6]$ octahedron.

Notwithstanding, there does appear to be a difference between synthetic and natural titanite which can be seen in the X-ray patterns. It is thought that this might be related to the domain texture of titanite [34]. It has been suggested that natural titanites might consist of numerous domains of $P2_1/a$ titanite related by a half turn parallel to *b*. This would bring all atoms into coincidence except the titanium atoms due to their off-centring within the $[TiO_6]$ octahedra. This non-coincidence would yield the necessary linear disorder required by the space-averaging effect of the scattered X-rays. Thus, the addition of a half-turn to the $P2_1/a$ space group would give the apparent A2/a space group of natural titanites [34].

Another difference between natural and synthetic titanites is that natural titanites contain various amounts of impurities like Fe^{3+}, Al^{3+}, OH^-, Cl^- and F^- [36;34]. It has been shown that coupled substitution of Fe^{3+} or Al^{3+} for Ti^{4+}, and OH^-, Cl^- or F^- for the oxygen atom shared by two Ti atoms, $O_{(1)}$, appears to favour domain formation. Synthetic titanite is essentially a single domain which results in it belonging to the space group $P2_1/a$, which results in the weak but sharp *k+l* odd reflections. Natural titanites on the other hand show only diffuse *k+l* odd reflections, or none at all. In a study of numerous samples of naturally occurring titanites, it was found that increased Al and Fe substitution increases the frequency of domains resulting in the *k+l* reflections becoming diffuse, and eventually disappearing as the average structure attains a space group of A2/a [36]. Convention reasonably suggests that if one titanium atom in a $[TiO_6]$ chain is off-set in one direction, that all the other titanium atoms in that chain will be off-set in the same direction as a result of the polarisation of the common oxygen atom. As Fe and Al substitute for Ti, with a coupled substitution of OH, Cl or F for $O_{(1)}$, the electronic configuration changes. This could disrupt the direction in which the titanium atoms are off-set along a $[TiO_6]$ chain, thus resulting in the diffuse *k+l* odd reflections [34]. This matter will be discussed in section 3.5 below.

That titanite and malayaite have such similar structures should come as no surprise since they are found naturally in a solid solution. The malayaite found in Perak in 1960 contained little titanium, but it has been reported that in some cases naturally occurring malayaite contains between 10 and 20 percent of titanium. It was this fact that initially inspired the assumption that a solid solution exists between the two, and that they are isostructural [8]. The region of a high temperature solid solution between malayaite and titanite has been determined. An x-ray powder diffraction investigation of the solid solution showed a successive change from malayaite to sphene as the composition was changed at 700°C and 1 kbar [8]. Below ~615°C and 1 kbar, the peak of the asymmetric solvus has experimentally been determined to be $Ca(Sn_{0.25}Ti_{0.75})OSiO_4$. It has been argued that the reason that tin-rich titanite, and titanium-rich malayaite are uncommon in nature is that the formation temperatures of tin ore deposits are probably lower than 500°C [8].

In 1976 it was reported that titanite undergoes a thermal phase transition [37]. This reversible, displacive phase transition occurs at ~493 K (220°C) and results in a change of the space group symmetry of titanite from $P2_1/a$ to A2/a. Consequently, at temperatures greater than ~220°C, malayaite and titanite are truly isostructural.

Subsequently, numerous studies have been undertaken of the paraelectric-antiferroelectric phase transition in titanite because of its non-classical behaviour [38]. They include a high temperature X-ray diffraction study of the order parameter and the transition mechanism [37;39], electron diffraction and electron microscopic studies of the transition dynamics [40], a combined linear birefringence and X-ray diffraction study [41], an investigation of the temperature dependence of the Ti-site electric-field gradient in titanite using perturbed-angular-correlation (PAC) spectroscopy [42], a Raman spectroscopic investigation of the phase transition [43], an infrared spectroscopic, dielectric response and heat capacity study [44], which, in addition to investigating the known phase transition at ~500 K, reported the possibility of a second anomaly at around 900 K which is related to the first. Further proof of a two step phase

transition in titanite has been reported after a synchrotron radiation study [38]. This study has shown that the antiferrodistortive phase transition in titanite is a stepwise process.

In addition to the temperature phase transition(s), a high pressure phase transition has been reported in titanite [45]. This study, using X-ray powder diffraction techniques, reports a $P2_1/a$ to A/2a phase transition which is related to the temperature phase transition. The pressure phase transition is discussed in detail in section 3.5 below.

Owing to the similarities between the structures of malayaite and titanite and malayaites reseptiveness to chromium as a guest chromophore, in the present study, undoped and chromium doped titanite were synthesised and their structural properties examined and compared with those of malayaite. The resonance Raman spectra of the doped titanite are also used as a probe to investigate both the temperature and pressure paraelectric-antiferroelectric phase transitions in titanite.

3.2 SYNTHESIS

3.2.1 SYNTHESIS

3.2.1.1 Synthesis of Titanite

Stoichiometric amounts of calcium, titanium and silicon in the form of calcium carbonate ($CaCO_3$), titanium dioxide (TiO_2), and silicon dioxide (SiO_2) were intimately wet mixed. The titanium dioxide and the silicon dioxide were milled prior to mixing to a particle size of 98% < 5μm, 75% < 2μm. After wet mixing, the reaction mixture was dried and dry mixed with a mortar and pestle, and then calcined. The reaction mixture was heated from room temperature to 1300°C. The temperature was held constant for two hours after which the oven was switched off. The resulting product was allowed to cool slowly to room temperature inside the oven. The reaction product was found to have shrunk slightly and was crystalline and hard. The reaction product was broken down into a powder with a mortar and pestle.

3.2.1.2 Synthesis of Chromium Doped Titanite

Chromium doped titanite was prepared in the same way as undoped titanite above except that one atom percent[1] of chromium, in the form of potassium dichromate ($K_2Cr_2O_7$), was added to the calcium carbonate, titanium dioxide and silicon dioxide before wet mixing. The reaction mixture was heated from room temperature to 1300°C. The temperature was held constant for two hours after which the oven was turned off. The reaction product was allowed to cool to room temperature inside the oven. It was then broken down into a powder with a mortar and pestle and leached in boiling water for one hour and dried. The product was then hot acid leached for 30 minutes.

3.2.1.3 Synthesis of Titanite Using Mineralisers

The titanite reactions, both doped and undoped were repeated at various temperatures between 1100 and 1300°C. It was found that titanite was not formed at temperatures below ~1100°C. In addition, it was found that while at temperatures between 1100 and 1200°C titanite was formed, a large amount of unreacted starting materials remained after calcining, and that $CaTiO_3$ was formed as a by-product. Consequently, the mineraliser mixture which proved effective in the synthesis of malayaite was tested on the titanite reaction mixtures and found to be effective as well. As was the case for malayaite, a mixture of five percent[2] of boric acid (H_3BO_3) and one percent of potassium nitrate (KNO_3) was used.

3.2.2 RESULTS AND DISCUSSION

3.2.2.1 Titanite Synthesised at 1300°C

This reaction product was synthesised to be use as an undoped reference sample for comparison with the doped reaction products of titanite using SEM analysis, XRD data and various forms of spectroscopy. The high temperatures at which these reactions were calcined also gives useful information about the thermal stability of the starting materials and of the reaction products. For

---

1 1% Cr as a percentage of the total number of calcium, tin and silicon atoms before calcining.

2 5 & 1% of H_3BO_3 and KNO_3, respectively, as a percentage of the total number of calcium, tin and silicon atoms before calcining.

example, at 1450°C malayaite forms from the respective raw materials but titanite sinters at this temperature. On the other hand neither sinter at ~1200°C which shows that from a thermal stability point of view, they are both suitable for use as ceramic pigments since most ceramic articles are calcined at temperatures of 1200°C and below. It must of course be remembered that though these materials do not sinter at ~1200°C, it is possible that they will undergo a solid state reaction with one of the many components of the ceramic body and glaze.

3.2.2.2 Titanite Doped with Chromium at 1300°C

The product of the doped reaction calcined at 1300°C was an intense, dirty maroon colour and also showed signs of considerable shrinkage. While the product was in the form of a solid mass, it could be broken down into a powder form with a mortar and pestle. A SEM analysis was done and XRD data collected on the product.

The SEM analysis results showed the presence of chromium in doped titanite though the technique was not found to be sensitive enough to yield accurate quantitative information about the chromium since it is present in such small quantities, as was the case in chromium doped malayaite. The XRD data of the product of the reaction at 1300°C and other reaction products calcined at lower temperatures are summarised in table 3.1 below. They show that at 1300°C the only compound formed in the firing process was $CaTiOSiO_4$ and that no starting materials remained unreacted. As was the case with the SEM analysis results, this technique was not sensitive enough to yield information about the dopants.

3.2.2.3 Titanite Synthesised with Mineralisers

Both doped and undoped titanite can be synthesised at 1300°C with no raw materials remaining unreacted, or by-products being formed. From a synthesis point of view, however, it is desirable to synthesis pigments at as low a temperature as possible. The results of the reactions carried out between 1100 and 1300°C with, and without the mineraliser mixture are summarised in table 3.1 below.

Table 3.1 XRD analysis results for titanite reaction mixtures, with and without mineraliser, doped with chromium, and calcined at temperatures ranging between 1100 and 1300°C.

Reaction Number	Temperature, °C	Mineraliser	TiO_2	SiO_2	$CaTiO_3$	$CaTiOSiO_4$
1	1300	✔	✗	✗	✗	✔
2	1300	✗	✗	✗	✗	✔
3	1200	✔	✗	✗	✗	✔
4	1200	✗	(✔)	✔	✔	✔
5	1150	✔	(✔)	(✔)	✔	✔
6	1150	✗	✔	✔	✔	✔
7	1100	✔	✔	✔	✔	✔
8	1100	✗	✔	✔	✗	✗

(✔) - Very little present.

3.2.2.4 Discussion

The most desirable result is that the only product formed is titanite and that no unreacted raw materials are left after calcining. Consequently, a few conclusions can be drawn from table 3.1 above. They are as follows:

- At 1300°C the only product of the reactions without mineraliser is titanite.
- At temperatures below 1300°C, the best results are achieved in the titanite reactions with the mineraliser mixture. Reaction mixtures without mineraliser do produce titanite at temperatures of as low as 1150°C, but also other by-products. In addition, the lower the temperature the more starting materials are left unreacted after calcining. Temperatures above 1300°C are not suitable for the synthesis of titanite since titanite melts congruently at ~1382°C [35].
- At 1200°C the only product of the reactions with mineraliser is titanite. At temperatures below 1200°C the reaction mixtures with mineraliser still produce titanite, but to a lesser extent as the calcining temperature gets lower. Correspondingly, the amount of raw materials left unreacted increase.
- At temperatures between 1100 and 1200°C, the colour of the chromium doped products synthesised with mineraliser is a function of the amount of titanite formed. For example, the colour of the product fired at 1200°C is more intense than that of the reaction fired at 1150°C. This is because the unreacted raw materials in the reaction product of the 1150°C reaction tend to dilute the intensity of the colour of the pigment.
- Since the only reaction product formed at 1200°C and above is titanite, the colour of the pigment above 1200°C is a function of the crystallinity of the product, and to a lesser extent, doping efficiency. The reaction product becomes more crystalline as the temperature increases resulting in a more intense colour. This advantage must be weighed up against the disadvantages of increased expense of calcining at higher temperatures, and the fact that the particle size of the product increases as the particles become more crystalline.
- When all factors are taken into account, it appears that the most appropriate temperature for calcining these pigments is 1200°C.

3.3 STRUCTURE

3.3.1 CRYSTAL STRUCTURE OF TITANITE

The crystal structure of titanite has been published [34]. It belongs to the monoclinic space group $P2_1/a$ (No.14). The most recent lattice constants of the crystal at 297 K are as follows: a = 7.0697 Å, b = 8.7223 Å, c = 6.5654 Å; β = 113.853°; V=370.27 Å, with Z = 4 and two molecules per Bravais unit cell [38]. The main difference between the structures of titanite and malayaite is shown schematically in figure 3.1 below.

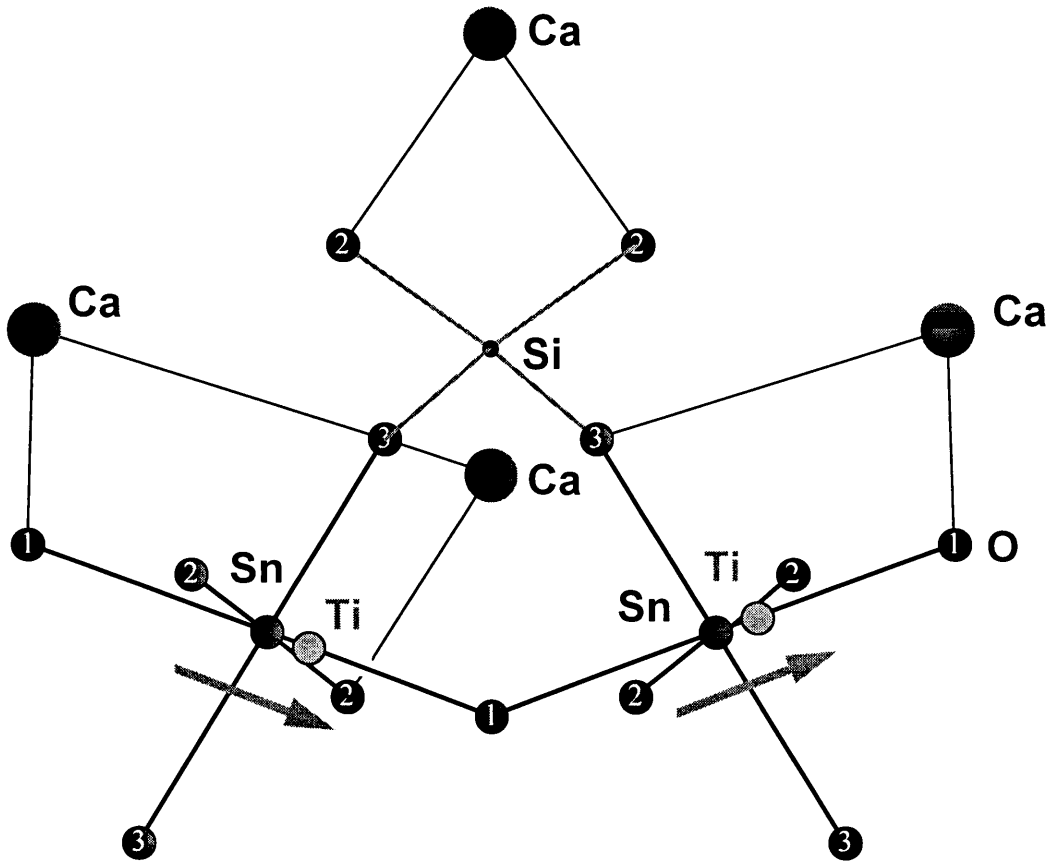

Figure 3.1 Schematic representation of the main difference between the titanite and malayaite structures, adapted from a figure published by Higgens and Ribbe [10].

The titanium atoms are displaced from the centre of the $[TiO_6]$ octahedron. It is this displacement of the Ti atom that results in the lowering of the symmetry of titanite as compared with that of malayaite in which the Sn atom is in the centre of the [Sn-O] octahedron.

The dominant structural units in titanite are chains of corner-sharing [TiO_6] octahedra running parallel to the *a* edge of the unit cell. The repeat unit in the chain is defined by two tilted octahedra which share a common oxygen atom (designated $O_{(1)}$ in figure 3.1 above). The oxygen atoms surrounding the [TiO_6] octahedron form a nearly regular octahedron. The titanium atoms are displaced within this octahedron. This results in alternating long (1.988 Å) and short (1.756 Å) Ti-$O_{(1)}$ bonds along the chain. The four remaining Ti-O bonds are longer than the axial Ti-$O_{(1)}$ bonds and range between 1.991 and 2.023 Å [38]. The $O_{(1)}$-Ti-O angles also reflect the off-centred displacement of the Ti atoms with the average of the four angles involving the shorter Ti-$O_{(1)}$ bond being wider than those involving the longer bond. Two chains per unit cell are related by a centre of symmetry, with one chain having the titanium ion displaced in the +*a* direction from the geometric centre of the octahedron, and the other in the -*a* direction. These chains are cross-linked by silicate tetrahedra sharing the remaining four oxygens, $O_{(2)}$, $O_{(3)}$, $O_{(4)}$, and $O_{(5)}$ respectively. The silicate tetrahedra share oxygen atoms with four separate chains. Oxygen atoms $O_{(3)}$ and $O_{(5)}$ belong to the same chain while $O_{(2)}$ and $O_{(4)}$ are shared by two chains. This produces a $[TiOSiO_4]^{2-}$ framework with large cavities enclosing calcium ions in irregular 7-coordination polyhedra [34].

The off-centred displacement of the titanium atom in the octahedron is characteristic of oxygen-octahedral ferroelectrics [34]. The antiparallel displacements of the titanium atoms in adjacent chains in titanite would compensate for the electric moments produced by the ionic displacements, thus resulting in a net zero electric polarisation for the unit cell. This state for a dielectric crystal is called antiferroelectric [34].

All atoms in titanite have C_1 site group symmetry. The bond lengths and bond angles found in titanite are summarised in table 3.2 below.

Table 3.2 Bond lengths and bond angles found in titanite [38].

Atom M	Bond length range, Å M-O	Bond angle range, ° O-M-O
Ti	1.756 - 2.023 *mean = 1.959*	84.8 - 95.2 *mean = 90*
Si	1.645 - 1.651 *mean = 1.647*	103.4 - 112.9 *mean = 109.4*
Ca	2.275 - 2.672 *mean = 2.432*	irregular

3.4 SPECTROSCOPY

3.4.1 THE SELECTION RULES OF TITANITE

As is the case with malayaite, a complete assignment of the Raman spectrum of titanite has not yet been undertaken, and once again it was not the aim of the current study to undertake such a task. Such a task, the details of which have been discussed in section 2.3.2 above, is not a trivial matter, and since titanite has lower symmetry than malayaite its Raman spectrum is expected to be even more complex than that of malayaite. The number of optical modes expected for titanite, calculated from equation 2.2 above, is 93 compared with the 45 optical modes calculated for malayaite. Titanite undergoes a phase transition at ~500 K which is discussed in section 3.3 above. After the phase transition, titanite belongs to space group A2/a (no.15), the same as that of malayaite, and it could therefore reasonably be expected that the number of bands in the Raman spectrum would be fewer after the phase transition has taken place. However, this turns out not to be the case. The high temperature and pressure phase transitions will be discussed in detail in section 3.5 below.

The first order phonon spectra of titanite in the two phases $P2_1/a$ and $A2/a$ are described by the following optically active representations obtained from a factor

group analysis performed on titanite by applying the correlation method (the Halford-Hornig or HH method).

$$\Gamma_{optic}^{P2_1/a} = 24A_g + 24B_g + 23A_u + 22B_u$$
$$\Gamma_{acoustic}^{P2_1/a} = 1A_u + 2B_u$$
$$\Gamma_{optic}^{A2/a} = 9A_g + 12B_g + 11A_u + 13B_u$$
$$\Gamma_{acoustic}^{A2/a} = 1A_u + 2B_u$$

Consequently, there are 93 optically active modes in the $P2_1/a$ phase as expected, 48 of which are Raman active and 45 of which are infrared active. The modes can further be divided into internal and external (or lattice) modes following the same procedure used for malayaite (section 2.4.1). The following results are obtained from this approximation.

$$\Gamma_{internal}^{P2_1/a} = 12A_g + 12B_g + 12A_u + 12B_u$$

Consequently the Raman spectrum of titanite is expected to contain 24 internal modes (12 totally symmetric and 12 antisymmetric modes) and the infrared spectrum is also expected to contain 24 internal modes (12 symmetric and 12 antisymmetric modes). The Raman spectrum of undoped titanite can be seen in figure I-3.1 (appendix I). The details of the spectrum are also summarised in table 3.4 in section 3.4.2.1. It is clear from the selection rules that many more bands are expected in the Raman and infrared spectra of titanite than in those of malayaite. As a result only the Si-O bands of titanite were tentatively assigned. This was done in conjunction with the assignments of the Si-O bands in malayaite. The assignments of these bands are in agreement with those reported elsewhere [46]. These assignments are also listed in table 3.4 below.

3.4.2 SPECTROSCOPY : TITANITE THE HOST AND CHROMIUM THE GUEST

3.4.2.1 Resonance Raman Effect of Chromium in Titanite

Chromium has to be incorporated into titanite, the host lattice. There are a number of ways in which this may be achieved. The most likely is a substitution reaction. This occurs when the chromium atom substitutes for a host lattice

atom. The same possibilities exist for titanite as for malayaite. Firstly, the chromium atom can substitute for a silicon atom which is tetrahedrally coordinated, secondly the chromium atom can substitute for a titanium atom which is octahedrally coordinated, and thirdly, substitution of the seven coordinated calcium ion is possible. As stated above, all of these atoms have C_1 site symmetry.

The arguments for the respective possibilities are similar to those for malayaite (section 2.4.2.1) and are not repeated here. The results are the same. Chromium is incorporated into the lattice of titanite by the substitution of a silicon atom by a chromium (IV) ion. This substitution is substantiated by the chromium-oxygen bond length, bond order, and force constant calculations which are discussed below.

The undistorted SiO^{4-}-ion has T_d-symmetry, with nine internal modes as described by the following representation.

$$\Gamma_{Td} = A_1 + E + 2T_2$$

All of these modes are Raman active. Should chromium substitute for silicon, then the undistorted CrO_4^{4-}-ion will have the same symmetry, and consequently, the same number of modes. The correlation between the modes of the free tetrahedron and those under the respective site and factor group symmetries are shown in table 3.3 below.

Table 3.3 Modes of the 'free' CrO_4^{4-}-ions of T_d symmetry correlated with those under C_1-site- and C_{2h}-factor group symmetries.

T_d	C_1	C_{2h}
ν_1 - A_1	A	A_g
		A_u
		B_g
		B_u
ν_2 - E	A	A_g
		A_u
		B_g
		B_u
	A	A_g
		A_u
		B_g
		B_u
ν_3, ν_4 - F_2	A	A_g
		A_u
		B_g
		B_u
	A	A_g
		A_u
		B_g
		B_u
	A	A_g
		A_u
		B_g
		B_u

The above correlation shows that six symmetric A_g and six non-symmetric B_g resonance enhanced Raman modes could be expected if chromium ions in their fourth oxidation state substitute for silicon ions under C_{2h} factor group symmetry. The totally symmetric modes are the ones expected to be the most enhanced. Although there are six symmetric modes predicted for chromium under C_{2h} factor group symmetry, only one of these is symmetric under the original T_d symmetry of the free ion.

Figure I-3.5 (appendix I) shows the electronic spectrum of chromium doped titanite. It very much resembles that of the corresponding malayaite analogue (Figure I-2.6 - appendix I). It is characterised by a abroad absorption peak at ~510 nm which represents the transition between the $^3A_2$ ground state of the d^2-Cr^{4+}-ion, and the $^3T_1$ state, assuming tetrahedral symmetry for CrO_4^{4-} (see section 2.4.2.1). The transition between the $^3A_2$ ground state and the $^3T_1$ state is known to occur in the 500-700 nm region for chromium doped YAG [22], chromium doped forsterite [18] and chromium doped malayaite (chapter 2). This transition is both electric- and spin- allowed and known to give rise to resonance enhanced stretching Raman bands in these compounds. The site symmetry of the SiO_4^{4-} -ions in the low symmetry antiferroelectric phase ($P2_1/a$) of titanite is C_1 and consequently a splitting of the electronic energy levels will occur. In Cr^{4+}:YAG, components of the $^3T_1$ state are also found in the near infrared region (~1000 nm) [22]. However, in the diffuse reflectance electronic spectrum of titanite, only a broad absorption peak at ~510 nm can be seen. A cryogenic diffuse electronic spectrum may help in the resolution of the broad absorption peak. Irrespective of whether the feature at ~510 nm consists of one or more components of the $^3A_2 \rightarrow {}^3T_1$ transition, it indicates that resonance enhancement of the Cr-O Raman bands should be achieved using the 514.5 nm excitation line of an Ar^+ laser.

The Raman spectra of undoped and chromium doped titanite can be seen in figures I-3.1 and I-3.2 (appendix I). The bands found in these spectra are summarised in table 3.4 below.

Table 3.4 Raman bands in undoped and chromium doped titanite

$CaTiOSiO_4$, ν/cm^{-1}, 514.5 nm			Cr^{4+}:$CaTiOSiO_4$ ν/cm^{-1}, 514.5 nm		Assignments
Salje[1]	Griffith[2]	This Study	293 K	513 K	
251 s		255	255	255 sh	
279 s		286	286 sh		
294 s		302	301		
305.6 vs		313	315	315 sh	
321 s		328	329	322	
340.5 vs		349	350	350	
374 w		384			
412 s	425	424	423	413	$\nu_4(Si\text{-}O)^2$
447 vw					
452.5 s	467	465	465	458	$\nu_4(Si\text{-}O)^2$
508 s			521 sh		
522 s	548	535	536	530	$\nu_4(Si\text{-}O)^2$
543 w		553			
594 vs	608	605	599	590	
690 vw					
			764 sh		$\nu_1(Cr\text{-}O)$
			800	780	$\nu_1(Cr\text{-}O)$
802 w		815			
836 s	856	855	852	848	$\nu_1(Si\text{-}O)^2$
851 w		871	869	866	
863 w	874	883	879		$\nu_3(Si\text{-}O)^2$
895 w	920	910	908	900	$\nu_3(Si\text{-}O)^2$
			952	944	$\nu_3(Cr\text{-}O)$
			989	979	$\nu_3(Cr\text{-}O)$
972 vw		991			
			~1063		
			~1170	~1163	
			1529		$2\nu_1(Cr\text{-}O)$
			1588		$2\nu_1(Cr\text{-}O)$
			1754	~1743	$\nu_1+\nu_3$ (Cr-O)
			2286		$3\nu_1(Cr\text{-}O)$
			2370	~2314	$3\nu_1(Cr\text{-}O)$

vw - very weak; w - weak; s - strong; vs - very strong; sh - shoulder

1 The Raman spectrum of titanite at 110K in diagonal polarisation using a Ar^+ 488 nm laser as light source [43].

2 The Raman spectrum of titanite at 293K , with assignments for Si-O bands [46].

The Raman bands in the above table of titanite are in reasonably good agreement. That they differ is most likely due to the fact that the spectrum recorded by Salje et al were recorded at 100 K using a different excitation source and that the spectrum recorded by Griffith were recorded prior to 1969. Table 3.4 above shows the presence of resonance enhanced Raman bands in the Raman spectrum of chromium doped titanite recorded with the 514.5 nm excitation laser line. The most noticeable change is the appearance of a new band at 800 cm^{-1} with a shoulder at 764 cm^{-1}. The insert in figure I-3.2 (appendix I) shows that the totally symmetric breathing mode could have more features than the ones at 800 and 764 cm^{-1} but since they could not be clearly resolved they are not listed here (with a cryogenic cell it might be possible to resolve these bands). Consequently, this band and shoulder have been assigned as components of the totally symmetric breathing mode ν_1. They occur in the region in which ν_1(Cr-O) is found in the Raman spectra of Cr^{4+}:$CaSnOSiO_4$ and Cr^{4+}:Mg_2SiO_4. In addition, weaker bands are also observed at 954 and 989 cm^{-1}. These bands have tentatively been assigned as components of ν_3. Details of combinations and overtones of the resonance enhanced bands, and the tentative assignment of some of the SiO_4^{4-} bands [46] can also be found in table 3.4.

3.4.2.2 Chromium-Oxygen Bond Length in Titanite

Using the empirical relationship between the Raman stretching frequency and the Cr-O bond length (equation 2.3) described in section 2.4.2.2 above, the bond lengths for the Cr-O bonds in chromium doped titanite may be calculated. Substituting 800 and 764 cm^{-1} into equation 2.3 yields Cr-O bond lengths of 1.700 and 1.729 Å respectively. The Cr-O bond lengths calculated in chapter 2 are 1.752 Å for chromium in malayaite, and 1.729 Å for chromium in forsterite, respectively. The values calculated here for titanite compare well with the values calculated for malayaite and forsterite.

There are four different Si-O bond lengths in titanite, 1.645, 1.646, 1.647 and 1.651 Å, yielding an average Si-O bond length of 1.647 Å [38]. This may be compared with an average Si-O bond length of 1.641 Å in malayaite [10] and 1.6354 Å in forsterite [28;29]. Clearly in all three cases, the Cr-O bond lengths

are longer than the Si-O bond lengths. This is supported by the ionic radii data in section 2.4.2.2 which gives values of 1.62 and 1.64 Å for $R(Si^{4+}\text{-}O^{2-})$, and 1.77 and 1.79 Å for $R(Cr^{4+}\text{-}O^{2-})$. Consequently, the chromium-oxygen bonds in titanite also have strong covalent character.

3.4.2.3 Chromium-Oxygen Bond Order in Titanite

The bond lengths calculated above for the Cr-O bonds in chromium doped titanite may be substituted into equation 2.4 which is a general relationship described in section 2.4.2.3, relating bond order or bond valence to the interatomic distance (Cr-O). Substitution of the respective values yields the results in table 3.5 below.

Table 3.5 Bond order and valence sum of chromium in titanite compared with chromium in other materials.

Material	$R(Cr^{4+}\text{-}O^{2-})$ Å	Coord^{n} No.	Bond Order	Valence Sum
Cr^{4+}:$CaTiSiO_5$	1.700	4	1.23	(4.92)
	1.729	4	1.13	(4.52)
				mean (4.72)
Cr^{4+}:$CaSnSiO_5$	1.752	4	1.05	(4.22)
Cr^{4+}:Mg_2SiO_4	1.729	4	1.13	(4.52)

The values in the valence sum column are bracketed since strictly speaking, the valence sum rule can only be applied to chromium oxides having four identical Cr-O bond lengths. Titanite has four different Cr-O bond lengths, while malayaite and forsterite have two or more different bond lengths. This results in their valence sum calculations not correlating that closely with their formal oxidation states. Nonetheless, they do correlate closely enough to support the assignment of the fourth oxidation state to chromium in titanite. Consequently, as was the

case in chromium doped malayaite, the bond order calculations support the substitution of Si^{4+} by Cr^{4+} in titanite.

3.4.2.4 Chromium-Oxygen Force Constants in Titanite

Table 3.4 above shows the tentative assignments of some of the bands found in the Raman spectra of undoped and chromium doped titanite. The tentative assignment of the bands in the Raman spectra of titanite was not as complete as that of malayaite since the spectra are more complex, as expected from the selection rules. In the Raman spectrum of undoped titanite only the Si-O bands were tentatively assigned. The Si-O bands in the 815-991 cm^{-1} region are a finger print of the bands found in the Raman spectra of malayaite. They have similar intensities though they are shifted to slightly higher wavenumbers. They are assigned to ν_1, and components of ν_3, in both cases. The Raman bands assigned to ν_4(Si-O) in malayaite and titanite also occur in more or less the same regions (~500 cm^{-1}).

Unfortunately, ν_2 could not be located for the SiO_4^{4-} -ions in chromium doped titanite. This band is expected to occur in the region of 400-500 cm^{-1}. As has been observed for both titanite and malayaite, the Raman bands due to the SiO_4^{4-} -ions are rather weak. This is in accordance with the type of Raman bands expected for orthosilicates [46]. This is because of the small degree of π-bonding in Si-O bonds. In addition, it has been shown in studies involving other orthosilicate materials that the ν_2 mode is particularly difficult to identify.

The Raman mode ν_2 for the Cr-O bond was also not observed in the resonance Raman spectrum of chromium doped titanite. Consequently, k_1 could not be calculated for the Si-O or Cr-O bonds in titanite. Another factor which makes the identification of ν_2 for the Si-O and Cr-O bonds in titanite difficult is the relative intensity of the bands in the Raman spectrum due to the Ti-O bonds. This is in line with numerous Ti-O containing materials. The most intense band in the Raman spectrum of titanite which can most probably be assigned to the Ti-O bond at 605 cm^{-1} is generally an order of magnitude greater than the Sn-O stretching frequency at 570 cm^{-1} in malayaite. In addition, all the bands in the

400-600 cm^{-1} region are intense. Consequently, the respective ν_2 modes are very likely to be hidden beneath these bands.

Since it was only possible to tentatively assign ν_1, ν_3 and ν_4 for titanite, only k_{Td} could be calculated using equation 2.7. While this value on its own is not fully descriptive, a useful comparison can be made between it and the values of k_{Td} for the Si-O and Cr-O bonds in malayaite and forsterite. These values are listed in table 3.6 below.

Table 3.6 Force constants calculated for titanite, malayaite and forsterite.

Mineral	MO_4^{4-}	ν_1, cm^{-1}	k_{Td}, mdyn/Å
Titanite	SiO_4^{4-}	856	6.90
	CrO_4^{4-}	782	5.76
Malayaite	SiO_4^{4-}	851	6.83
	CrO_4^{4-}	735	5.09
Forsterite	SiO_4^{4-}	835	6.57
	CrO_4^{4-}	764	5.50

From table 3.6 above it can be seen that the values calculated for k_{Td} for titanite are in good agreement with those calculated for malayaite and forsterite and thus support the substitution of Si^{4+} in titanite by Cr^{4+}.

3.5 THE PHASE TRANSITIONS

3.5.1 THE HIGH TEMPERATURE PHASE TRANSITION OF TITANITE

3.5.1.1 The Paraelectric-Antiferroelectric Phase Transition of Titanite : the Order Parameter and Transition Mechanism

The structure of titanite has been discussed in section 3.3 above. Diffraction data of the type *hkl: k+l* odd which violate the initially reported A/2a space group are ascribed to an off-centred displacement of the titanium atom from the geometric centre of the $[TiO_6]$ octahedron resulting in long and short Ti-O bonds alternating along the $[TiO_6]_n$ chains [34]. Two $[TiO_6]_n$ chains per unit cell are related by a centre of symmetry. In one of the chains, the displacement is such that the Ti^{4+}-ions are shifted in the *+a* direction, and in the other, the displacement is such that the Ti^{4+}-ions are shifted in the *-a* direction [34]. This arrangement results in $P2_1/a$ titanite being antiferroelectric [34].

In 1976 it was discovered by Taylor and Brown that titanite undergoes a reversible, displacive phase transition at 493 ± 20 K from space group $P2_1/a$ to A2/a [37]. In studies involving high temperature X-ray techniques, it was found that the transition is signalled by the disappearance of reflections of the type *hkl: k+l* odd. The principle structural change resulting from the phase transition was ascribed to a movement of the titanium atom from a position displaced towards one corner of the $[TiO_6]$ octahedron to a position at the geometric centre of the octahedron. The titanium atom was found to shift by 0.1 Å. Consequently, the axial Ti-O bond lengths were found to change from 1.766 and 1.973 Å at room temperature to ~1.87 Å at 543 K [34]. It was also shown that the Ca-ions shift near the transition temperature along *x* and *z* by 0.043 Å and -0.048 Å, respectively [37]. Above the transition temperature, further movement of the titanium atom was shown to be slight and consistent with simple cell expansion related to the increased temperature of the sample. It was suggested that the transition mechanism is similar to that of other displacive transitions in silicates and perovskite structure ferroelectrics and may lead to domain formation [37].

The rapid, non-quenchable behaviour of the phase transition and the structural data above and below the transition temperature indicated that the phase transition is displacive in nature and can be classified as a distortional transformation following the nomenclature of Buerger [47;48]. The behaviour of the crystal as the temperature is changed suggested a second order phase transition [37]. Taylor and Brown could however not distinguish between two possible models for the high temperature phase, namely, a single configuration with Ti strictly in the centre of the octahedron, or an average of two configurations with small Ti-displacements parallel and antiparallel to *a*. X-ray techniques look at long range order and consequently, if there are numerous small domains, it is possible that only their average might be seen.

A more recent X-ray diffraction study, in 1991, showed that the unit cell dimensions show a pronounced hysteresis effect in the 400-500 K range on heating and cooling [39]. This hysteresis effect was observed only during the first heating and cooling cycle and it was shown to result in a reduction of the transition temperature from ~500 K on heating to ~445 K on cooling. The hysteresis effect was shown to disappear on further heating. The displacement of the Ti-atoms was taken as the primary order parameter for the phase transition. The Ti-displacement plotted as a function of temperature [39], showed a typical second order behaviour. Furthermore, the Ti-displacements were shown to be coupled linearly to the Ca-displacements. Both displacements were shown to correlate exactly with displacements predicted from induced representation theory. It was shown that the Ca-displacements are essentially also parallel and antiparallel to *a*, and the nearest Ca and Ti atoms are displaced in the same direction [39]. As is the case for the Ti-displacements, the Ca-displacements are related by the A-centring and are equal and opposite to one another. The Ca-displacements (0.0559 Å) were however shown to be much smaller in magnitude than the Ti-displacements (0.0976 Å).

Ghose et al [39] have suggested that the phase transition is initially driven by a soft mode. Displacive phase transitions are believed to be associated with the instability of a lattice vibration [49]. A vibrational mode in the low temperature

phase effectively collapses at the critical temperature, T_c. Such a mode is called a soft mode. More specifically, a soft mode is a particular mode of vibration whose frequency tends towards zero as the critical temperature is approached [50]. This softening results in instability of the crystal against the low frequency phonon. Subsequently, the soft mode is followed by critical fluctuations which set in near T_c and an order-disorder mechanism finally drives the phase transition to completion, whereby parallel and antiparallel Ti-displacements related by [0;1/2;1/2] in adjacent domains are dynamically interchanged. Immediately above T_c, the high temperature A2/a phase is a statistical average of small dynamic antiphase domains of the low temperature $P2_1/a$ phase. The reflections of the type *hkl: k+l* odd do in fact not disappear completely, but become diffuse. Furthermore, Ghose et al have shown that it might reasonably be expected that vacancies and defects pinning the domain boundaries may drastically alter the transition behaviour and affect domain mobility. This is because the defects and vacancies rearrange themselves upon heating and cooling. Ghose et al proposed that it is this defect and vacancy rearrangement that is responsible for the hysteresis effect seen only during the first cycle of heating and cooling.

In addition, it has been suggested that impurities may also affect the phase transition. An example of this may be found in the effect of substituting Ti^{4+} with Al^{3+} or Fe^{3+}, or substituting OH^- for the $O_{(1)}$-ion [36] (see figure 3.1 above). Substitution of an Al^{3+} or Fe^{3+}-ion for a Ti^{4+}-ion will reduce the positive charge in the vicinity of $O_{(1)}$, thus favouring a domain boundary where both Ti atoms are displaced towards the substitution site [37]. On the other hand, substituting an OH^- for an $O_{(1)}$ will result in the withdrawal of electron density from the Ti-O bonds which will favour the displacement of both Ti atoms away from the site of substitution [37].

Ghose et al calculated a value of 0.32 for the effective critical exponent β. This value is close to a value of 1/3 which is the theoretical value for a 3D Ising model. Consequently, this value for the critical exponent indicates that the phase transition corresponds to three dimensional Ising behaviour.

An electron diffraction and electron microscopic study of the transition dynamics [40] confirmed the dynamic model proposed by Ghose et al. The electronic diffraction images showed that the average domain size depends on the thickness of the sample, demonstrating that the domain walls are generated after preparation of the sample, perhaps in a crushing process. On heating the sample with the electron beam, the interface density increases. In accordance, the average domain size decreases. The interfaces then become mobile until finally, their images disappear at T somewhat above T_c. These observations are in agreement with those obtained by Ghose et al in their X-ray studies. After repeated heating and cooling through T_c, the domain shape was found to change, with the domains becoming more elongated. If the sample is allowed to cool to well below T_c, the average domain size is seen to grow. In accordance, the interface density decreases [40]. These results show that the antiferroelectric-paraelectric phase transition is accompanied by the formation of an increasing density of mobile antiphase boundaries as T_c is approached [40].

A linear birefringence and X-ray diffraction study of the structural phase transition in titanite, undertaken by Bismayer et al [41] yielded a value of $\beta = 0.14 \pm 0.02$ for the critical exponent of the macroscopic order parameter from the linear birefringence data. This value is in sharp contrast to that of $\beta = 0.32$ suggested by Ghose et al [39]. Furthermore, a value of $\beta = 0.15 \pm 0.025$ was obtained using X-ray scattering. These values therefore suggest a 2D-Ising model as opposed to the 3D Ising model proposed by Ghose et al. The theoretical value of β for a 2D Ising model is 1/8. In addition, Bismayer et al did not find any evidence of a hysteresis effect as suggested by Ghose et al. It is possible that the hysteresis effects observed by Ghose et al are due to the influence of impurities or vacancies in the samples investigated by them. These impurities or vacancies might also be responsible for the high value that they obtain for the critical exponent β.

In a subsequent Raman spectroscopic investigation undertaken of the phase transition in titanite [43], a value of $\beta \approx 0.12$ for the effective critical exponent of the macroscopic order parameter was obtained which also supports a 2D Ising

behaviour. The structural phase transition in titanite was found to correlate with a strong temperature dependence of the Raman scattering cross sections and, to a lesser extent, with shifts of the phonon frequencies. Consequently, their quantitative temperature evolution in the low-symmetry phase ($P2_1/a$) was found to be compatible with a nearly 2D Ising model. Furthermore, it was found that at temperatures above 860 K, the phonon signals agree with A2/a symmetry but not between 497 and 860 K. In this temperature range, new structural states are proposed to give rise to additional phonon signals. It is thought that mobile antiphase boundaries, as proposed by van Heurk et al [40], are responsible for these signals between 497 and 860 K.

Subsequently, an infrared spectroscopic, dielectric response and heat capacity study of single crystals and powder samples of titanite was undertaken [44]. This investigation observed the structural phase transition at ~500 K, as expected, but in addition, a second anomaly was observed at ~900 K. Once again it was shown that the phase above ~500 K is not due to a uniform state with A2/a symmetry. Evidence suggests that either some short range order of the $P2_1/a$ phase exists up to temperature of ~850 K, or that an intermediate phase exists which undergoes a continuous phase transition at high temperatures. Either way, this temperature region cannot be described by a 2D Ising model nor by an antiferroelectric phase transition with a uniform paraelectric state [44]. This study also brings to light the presence of small Ti-displacement parallel to the *b* axis which appears to be too small to be observable as a critical mode with *b* axis polarisation.

A recent synchrotron radiation study [38] has shown that the antiferrodistortive phase transition in titanite is a stepwise process. An intermediate phase with Ca-disorder in split positions is suggested. The transition from the high temperature to the low temperature phase is reported to involve the displacement of the Ti atoms from the centres of the $[TiO_6]$ octahedra parallel to the *a*, *b* and *c* axes and additional shifts of Ca atoms from their high temperature positions, along *a* and *c*. In this study it is shown that the large excess quantities, the spectroscopic data and the diffuse X-ray scattering are compatible with the appearance of a

true thermodynamic state between 496 and 825 K. A stepwise transformation process involving two critical mechanisms is suggested for the region between 496 and 825 K. It is suggested that group theoretical considerations allow a symmetry breaking from A2/a to $P2_1/a$ via an intermediate disordered phase. The diffuse reflections in this study were found to disappear at ~825 K thus giving evidence of a second thermal anomaly at ~825 K. The intermediate modification is characterised by disordered Ca atoms in split positions. At temperatures above ~825 K, the Ca atoms are distributed freely among the two positions they occupy. Consequently, the occupational probability is 0.5 for each position. Below ~825 K, the Ca atoms do not move freely between these positions. Consequently, the occupational probability is no longer 0.5 for each position, and even a slight deviation from 0.5 leads to disorder, and consequently, to weak diffuse intensities of the reflections *hkl: k+l = 2n+1* (odd). At temperatures below 296 K variations of the atom positions in titanite are small (Ti-coordinates *x* and *y* show typical changes of the order of 0.001 Å).

In the second symmetry breaking step, at ~497 K, it is suggested that two critical mechanisms are involved. The first involves the ordering of the Ca atoms in the low symmetry $P2_1/a$ phase at one preferential 4e-position. The second involves a displacive mechanism characterised by further displacements of the Ca atoms. Simultaneously, major displacements of the Ti atoms occur. In the $P2_1/a$ phase, the Ti and Ca displacements are linearly related. Consequently, the two phenomena involved here are firstly an order-disorder one, and secondly, a displacive one [38].

From the above discussion, it is clear that the phase transition in titanite is still the object of debate. What is also clear is that X-ray diffraction techniques average over a length scale too large to reflect the symmetry of a material on an interatomic scale [38]. It has been attempted, in a previous study [42], to investigate the phase transition of titanite by substituting another atom for one of the titanite atoms. In this investigation, ^{181}Hf was substituted for Ti in order to be used as a probe. Perturbed-angular-correlation (PAC) spectroscopy uses the nuclear-electric-quadrupole moments of radioactive probe atoms to measure the

extranuclear electric-field gradient (EFG) at specific lattice sites where the probes are substituted. Unfortunately, the $^{181}Hf \rightarrow ^{181}Ta$ probe did not show any evidence of the phase transition in titanite. It is thought that this results from the fact that the displacement of the Ti atom occurs nearly along the *z* axis of the EFG and that it is the symmetry of this displacement which causes the EFG to remain relatively constant over the temperature range near T_c which results in the phase transition going unnoticed.

In the current study, the substitution of a Si atom of the host lattice by a Cr atom was undertaken. As shown above, the chromium in titanite gives rise to resonance Raman bands. Since the $[SiO_4]$ tetrahedra bridge the $[TiO_6]$ octahedra, and share edges with the $[CaO_7]$ polyhedra, the Cr atom, substituted into the Si position in titanite should be sensitive to the phase transition. Consequently, by observing the chromium in titanite, using resonance Raman spectroscopy, it should be possible to gain some information about the phase transition.

3.5.1.2 Chromium Doped Titanite and the High Temperature Phase Transition

It has been shown that Cr^{4+} substitutes for Si^{4+} in titanite (section 3.4). This substitution results in new features in the Raman spectrum of Cr^{4+}:$CaTiOSiO_4$. These resonance Raman bands have been attributed to the Cr-O bond in Cr^{4+}:$CaTiOSiO_4$. In the present study, the phase transition that titanite undergoes is investigated using the Cr^{4+} in titanite as a probe. As described above, the phase transition in titanite is characterised by the displacement of the Ti-ions, and to a lesser extent, the displacement of the Ca-ions. Since the $[SiO_4]$ tetrahedra bridge the $[TiO_6]$ octahedra, and share edges with the $[CaO_7]$ polyhedra, it might reasonably be expected that the effects of these displacements might be seen by observing the tetrahedron to which they are attached. It has been shown that the phase transition has very little effect on the structure of the $[SiO_4]$ tetrahedron [44]. Only very small bond length changes of the Si-O bonds may be associated with the phase transition. This is due to the increase in symmetry of titanite. This results in the four Si-O bond lengths of

1.645, 1.646, 1.647 and 1.651 Å, (mean = 1.6473 Å) under C_i symmetry changing to two Si-O bond lengths each of 1.644 and 1.649 Å, respectively. Thus the mean Si-O bond length after the phase transition (~500 K) is 1.6465 Å, an effective lengthening of the mean bond length of only 0.0008 Å. Consequently, any change in the Raman modes of the [SiO_4] tetrahedra at T_c should be as a result of changes in the [TiO_6] and [CaO_7] polyhedra.

The average bond lengths for the Cr-O bond in Cr^{4+}:$CaTiOSiO_4$ have been calculated above. As can be seen in section 3.4.2.2 above, the Cr-O bonds have bond lengths of 1.70 and 1.73 Å, respectively. These bond lengths are longer than those of the Si-O bonds and, consequently, the substitution of a Cr into a Si site will result in a tight fit which is consistent with the fact that the Cr-O bonds have been shown to have strong covalent character.

Consequently, any changes in the features of the Raman spectra resulting from the CrO_4^{4-} tetrahedra in Cr^{4+}:$CaTiOSiO_4$ are expected to be as a result of the displacements due to the antiferroelectric-paraelectric phase transition in titanite.

This method of analysis is based on the theory of hard mode spectroscopy. Vibrational spectroscopy is one of the most important tools for determining relationships between the macroscopic properties of crystals and their crystal structure. Traditionally, the investigation of phase transitions using Raman spectroscopy depended on the observation of soft modes [51]. This method is restricted to displacive systems. Optical hard mode spectroscopy (either as Hard Mode Raman Spectroscopy or Hard Mode Infrared Spectroscopy) has been shown to be amongst the most successful experimental methods used for the quantitative determination of order parameters in phase transitions [52]. Hard modes are optically active phonons which show systematic changes of their Raman and/or infrared spectra when the structural properties of a the material are changed as a result of the application of pressure, the change in temperature or some other parameter [53]. The underlying principal of hard mode spectroscopy is that high frequency phonons with low dispersion can be treated approximately as Einstein oscillators with their frequencies and optical cross

sections depending essentially on local bond properties. If such bond properties are changed during a phase transition, the phonon properties will change accordingly. It is irrelevant whether the phase transition is displacive, order-disorder, or of the Mott, Anderson or Peierls type. Since the characteristic length of high-frequency phonons is very short, the structural variations that might occur in a system are measured on an atomistic scale. This feature is of great advantage for the analysis of heterogeneous materials for example [53]. This gives hard mode spectroscopy wider application than soft mode spectroscopy.

As discussed above, the $[SiO_4]$ tetrahedron in Cr^{4+}:$CaSnOSiO_4$ is very rigid and remains largely unaffected by the phase transition. Consequently, any change in the Si-O bond properties should be as a result in changes in the polyhedra to which they are attached. The same can reasonably be expected for the Cr-O bonds. The frequencies of phonons with energies well above those of corresponding soft modes depend on the evolution of the structural order parameter as a function of temperature, pressure or chemical composition. The relative changes to the phonon frequencies is usually of the order of ~2% of their total energies. This enables the coupling between the phonon frequency, ω, and the order parameter, Q, as described by equation 3.1 below.

$$\Delta(\omega^2) \propto AQ + BQ^2 \qquad \textbf{equation 3.1}$$

The correlation length of hard modes is generally comparable with that of bond distances so that the order parameter is measured on an atomistic length scale.

The order parameter, is related to the critical exponent, β, as shown in equation 3.2 below [39],

$$Q = Q_o(T_c - T)^{\beta} \qquad \textbf{equation 3.2}$$

Consequently, it should be possible to determine a value for the critical exponent, β, from the Cr-O modes in Cr^{4+}:$CaTiOSiO_4$, using their frequencies, band widths and/or intensities as order parameters.

The temperature dependence of the Raman bands of undoped titanite has been described above (section 3.5.1). The Raman cross sections were found to be very temperature sensitive and the phonon frequencies also showed a temperature dependence. Some of the Raman mode intensities also changed with the change in temperature [43]. However, phonons which were predicted to disappear when the phase transition from the $P2_1/a$ to the A2/a structure had occurred were still observed at temperatures of as high as 860 K. This is further evidence of the fact that the A2/a phase at temperatures between ~500 and ~860 K is in fact a statistical average of small slabs of $P2_1/a$ material separated by anti-phase boundaries. Raman spectroscopy is very sensitive to these micro states in contrast to X-ray techniques which reflect symmetry on a larger that interatomic scale.

The Raman spectrum of chromium doped titanite can be seen in figure I-3.2 (appendix I). An enlargement of the totally symmetric Cr-O stretching mode is included as an insert. Clearly there are at least two features in this band. One occurs as a band, at 800 cm^{-1}, and the other as a distinct shoulder, at 764 cm^{-1}. There may be more features to this band. The Si^{4+} atom for which the Cr^{4+} is substituting finds itself in C_1 site symmetry with four different Si-O bond lengths. Consequently, the same might be expected for Cr^{4+}-ion in this position.

It can be seen in figure I-3.3 (appendix I) which shows the Raman spectra of Cr^{4+}:$CaTiOSiO_4$ at 290 and 510 K, that the Cr-O modes are indeed sensitive to the increase of temperature. The temperature dependence of the totally symmetric Cr^{4+}-O stretching mode at 800 cm^{-1} can be seen in figure 3.2 below.

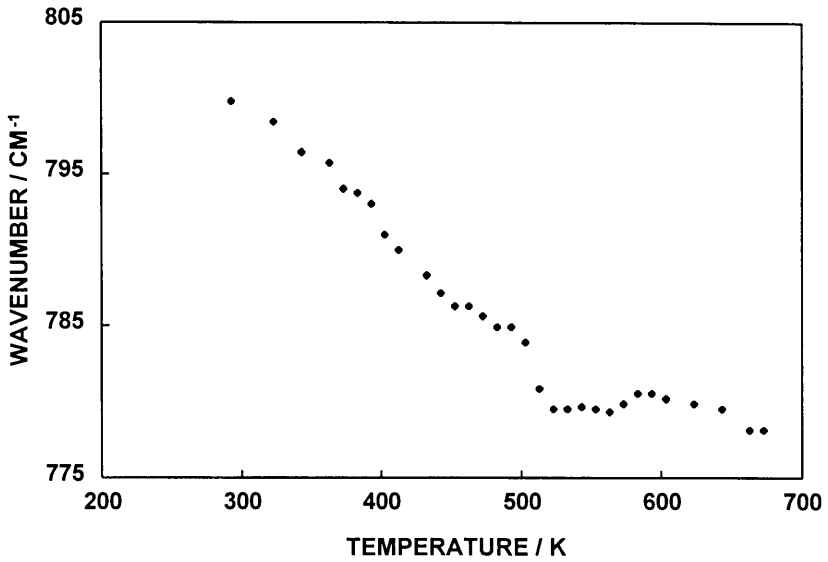

Figure 3.2 Temperature dependence of the peak position of the totally symmetric Cr^{4+}-O stretching mode in Cr^{4+}:$CaTiOSiO_4$.

The occurrence of the phase transition at ~500 K is clearly evident in this figure indicating that the Cr-O bonds are affected by the phase transition in titanite. The decrease in wavenumbers as the temperature is increased is also reflected in the temperature dependence of other Raman active modes such as the totally symmetric Ti-O stretching mode at 599 cm^{-1} and the bending Si-O mode at 536 cm^{-1}. This behaviour has previously been observed in the Raman spectrum of undoped titanite [43]. The behaviour of the Si-O and Ti-O modes in chromium doped titanite were found to correlate closely with those in undoped titanite. Therefore, the chromium in chromium doped titanite does not appear to affect the phase transition in a measurable way.

The second Cr^{4+}-O stretching mode (or asymmetry) at 764 cm^{-1} could not be observed over a broad temperature range. It was found to shift to higher wavenumbers as the temperature was increased, and to merge with the 800 cm^{-1} band at higher temperatures. This anomalous behaviour could be considered as an order parameter. However, since the exact position of the 764 cm^{-1} is difficult to determine as the temperature is increased, the change in distance between the 800 cm^{-1} and 764 cm^{-1} band as a function of temperature did not

yield reproducible results for β, the critical exponent of the macroscopic order parameter.

The temperature dependence of the intensity of the Cr-O stretching frequency at ~800 cm^{-1} can be seen in figure 3.3 below. It closely resembles the temperature dependence of the intensity of the Ti-O stretching mode at 599 cm^{-1} of A_g-symmetry.

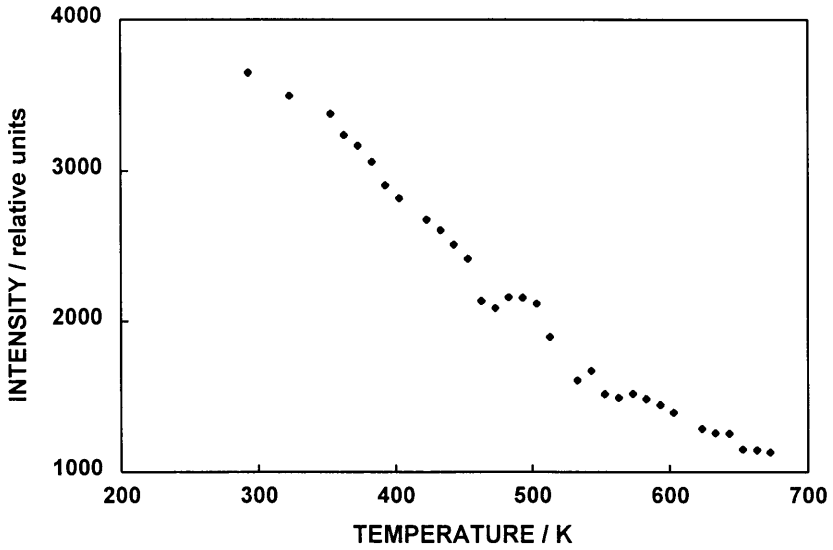

Figure 3.3 The temperature dependence of the intensity of the Cr^{4+}-O stretching mode at 800 cm^{-1} in Cr^{4+}:$CaTiOSiO_4$.

Once again, evidence of the phase transition is found in the change in intensity of this Cr-O band as a function of temperature. If the natural logarithm of the intensity of this band is plotted against $\ln(T_c-T)$, where T_c is the transition temperature at 497 K, a straight line is obtained with a correlation coefficient of r = 0.995. This plot may be seen in figure 3.4 below.

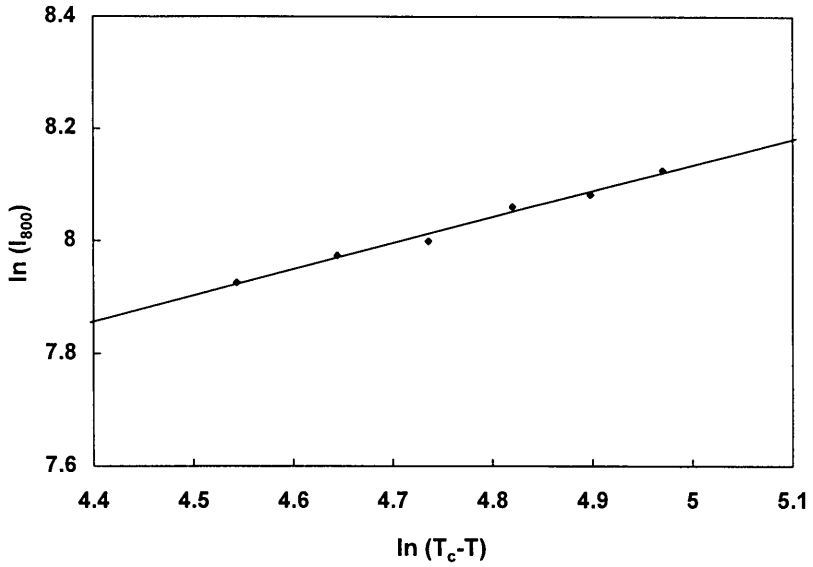

Figure 3.4 The natural logarithm of the relative intensity of the 800 cm^{-1} Raman band in Cr^{4+}:$CaTiOSiO_4$ (I_{800}) plotted against ln(T_c-T), where T_c represents the phase transition temperature at 497 K.

From the slope of this graph, a value for the critical exponent of the macroscopic order parameter of $\beta = 0.115 \pm 0.005$ is obtained which corresponds well with the theoretical value of $\beta = 1/8$, as predicted by the 2D Ising model.

This is significant since it is in reasonable agreement with the values obtained for β in studies of undoped synthetic titanite, using X-ray and Raman spectroscopic techniques. It is also significant since it is in contrast to a value of ~1/3 obtained in another previous study. The reason for this high value was thought to be impurities within the titanite. However, chromium in titanite does not appear to affect the behaviour of the phase transition.

If the ratios of the Cr-O mode at 800 cm^{-1} and the Ti-O mode at 599 cm^{-1} are plotted against temperature, the occurrence of the phase transition at ~497 K is once again clearly seen. This graph may be seen in figure 3.5 below.

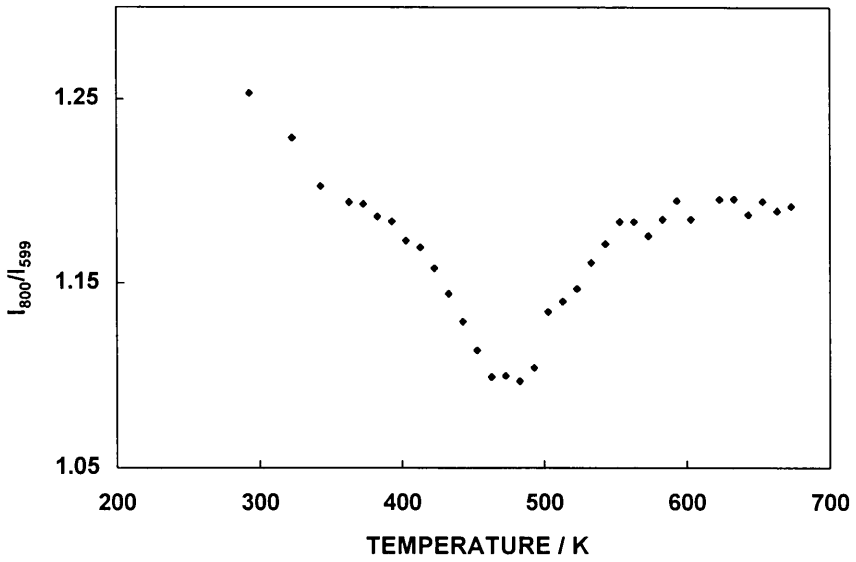

Figure 3.5 The ratio of the intensities of the 800 cm^{-1}(Cr^{4+}-O) and 599 cm^{-1} (Ti^{4+}-O) (I_{800}/I_{599}) plotted against temperature.

This is significant since both bands reflect the phase transition, though not to the same extent. The Ti-$O_{(1)}$ bond distance in titanite changes significantly with increasing temperatures, particularly near the phase transition temperature.

However, the change in the bond length of the Ti-$O_{(1)}$ bond is not reflected to a great extent in the temperature dependence of ν(Ti-O). This is most probably because this totally symmetric stretching mode reflects the average Ti-O bond length in the [TiO_6] octahedron which hardly changes in the antiferroelectric phase [39]. It changes from 1.959 Å at 295 K to 1.962 Å at 530 K [38], a change of only ~0.0027 Å.

Since Cr^{4+} substitutes for Si^{4+} in titanite, it is not surprising that the temperature dependence of ν(Cr-O) at 800cm^{-1} and the Si-O stretching mode at 536 cm^{-1} show close correspondence as can be seen in figure 3.6 below. In this graph, the percentage shifts of the respective Cr-O, Ti-O and Si-O bands are plotted against temperature. It is clearly seen that the Cr-O and Si-O bands show a close correspondence in their temperature dependence, with the Cr-O bands being the most sensitive to the change in temperature. This is significant since it

has been shown that the [SiO_4] tetrahedrons bond lengths are hardly effected at all by the shifting of the Ti and Ca atoms in the phase transition. Consequently, the evidence of the phase transition in the Raman bands of the [SiO_4] tetrahedron is as a direct result of the phase transition resulting from the movement of the Ti and Ca atoms. That the Cr-O band behaves similarly is evidence that it is also sensitive to the movement of the Ti and Ca atoms to which it is attached, and consequently, to the phase transition. In fact, it is even more sensitive to the phase transition than the [SiO_4] tetrahedron. The peak position of the Ti-O stretching mode has a more gradual, almost linear dependence on the change in temperature. It does nonetheless also reflect the phase transition.

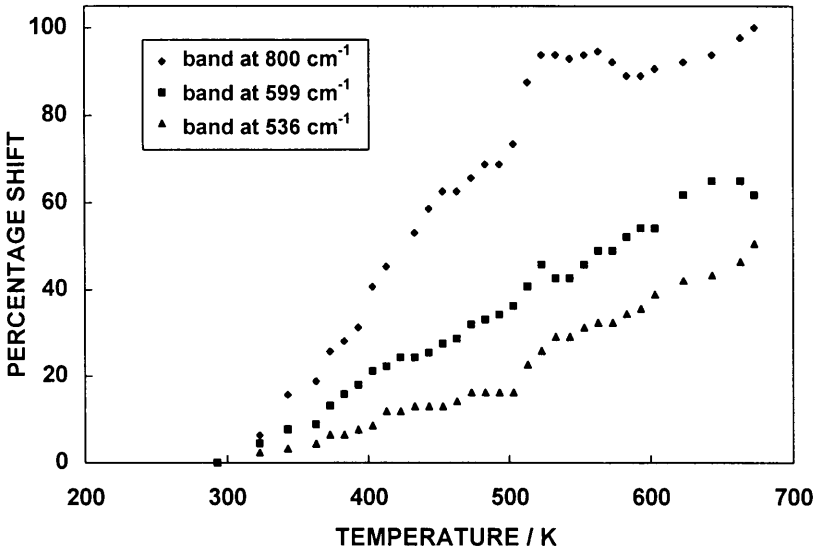

Figure 3.6 The percentage shifts of the 536, 599, 800 cm^{-1} modes in Cr^{4+}:$CaTiOSiO_4$ upon heating the sample.

The band widths of the respective bands can also be used to study the phase transition. The spectral line widths of the bands in the Raman spectrum of undoped titanite, the full-width-at-half-maximum (FWHM), showed weak increases as the temperature was raised. An example of this is the band at 423 cm^{-1}. In Cr^{4+}:$CaTiOSiO_4$ an anomaly is seen in the case of the totally symmetric stretching mode of Cr-O at 800 cm^{-1} as the temperature is increased from 297 K.

Most band widths increase as the temperature is increased. This band however is seen to decrease in width. Above ~500 K, only one band is seen at 780cm^{-1}. At this temperature, two bands at 944 and 979 cm^{-1} represent ν_3, and $2\nu_1$ is such a broad and weakly defined feature that its peak maximum could not be determined with absolute certainty. It occurs in the region of ~1550 cm^{-1}. The temperature dependence of the FWHM of the 800 cm^{-1} band can be seen in figure 3.7 below.

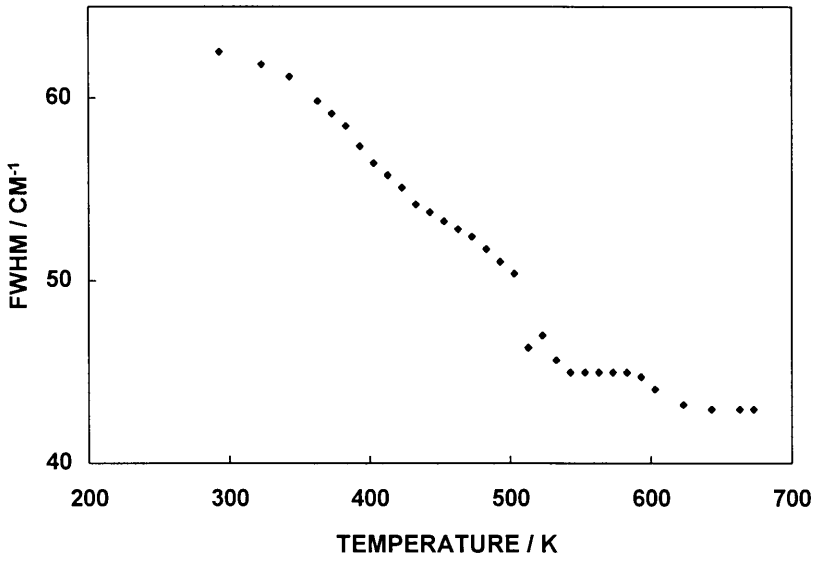

Figure 3.7 The temperature dependence of the line width (FWHM) of the Cr^{4+}-O symmetric stretching mode at 800 cm^{-1} in Cr^{4+}:$CaTiOSiO_4$.

From figure 3.7 above, it is seen that the line width of the 800 cm^{-1} band decreases until the phase transition temperature is reached. After this the line width remains almost constant. This behaviour is due to the unresolved components of this band and as soon as only one component is observed above the transition temperature, the line width remains almost constant. The Raman spectrum of titanite above the phase transition temperature may be compared with the Raman spectrum of Cr^{4+}:$CaSnOSiO_4$ where only one band represents the totally symmetric Cr-O stretching frequency. In the high temperature phase of titanite, it is isostructural with malayaite. It has been shown using various techniques that titanites A2/a structure is only a statistical average of $P2_1/a$

domains. This is seen Raman spectroscopically by the fact that Raman bands that are expected to disappear in the high symmetry phase do not in fact disappear. However, it appears from figure 3.7 above that Cr^{4+} in both malayaite and the high temperature phase of titanite have C_2 site symmetry since in the case of the high temperature titanite, only one band represents the totally symmetric Cr-O stretching mode.

In order to compensate for the normal temperature effects on the line widths of Raman bands, the ratio of the line widths of the 800 and 599 cm^{-1} bands are plotted against temperature in figure 3.8 below.

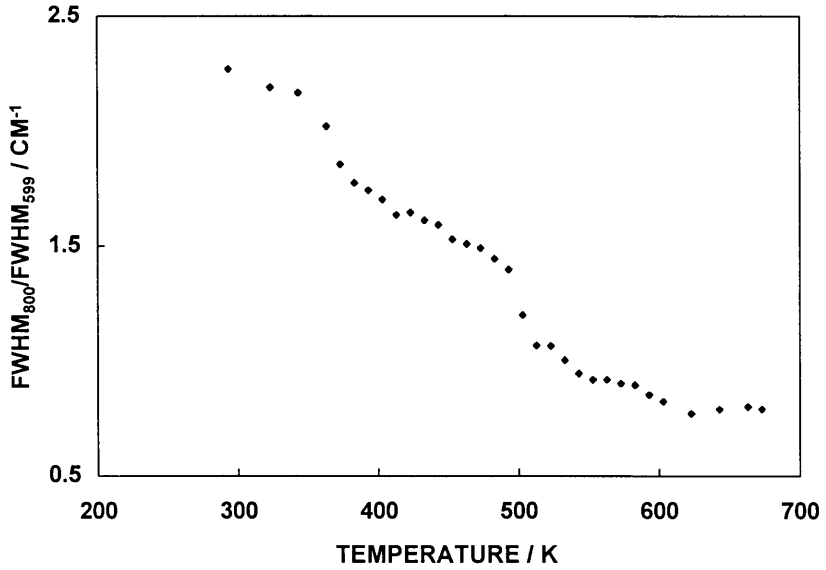

Figure 3.8 The temperature dependence of the ratio of the line widths of the 800 and 599 cm^{-1} Raman bands ($FMHM_{800}/FWHM_{599}$) in Cr^{4+}:$CaTiOSiO_4$

A decrease in this ratio can be seen in the antiferroelectric phase. This is followed by a discontinuity at the phase transition temperature. After ~500 K there is a further slight decrease in the 500 - 580 K temperature range. At higher temperatures, the values remain almost constant. This suggests that at higher temperatures the behaviour of the Cr-O bands are consistent with normal cell behaviour due to the rising temperature.

This anomalous behaviour of the line width of the 800 cm^{-1} band can be used as an order parameter. If the natural logarithm of the full width at half maximum of the 800 cm^{-1} band is plotted against $\ln(T_c-T)$ where T_c is the phase transition temperature at 497 K, a straight line is obtained. This can be seen in figure 3.9 below.

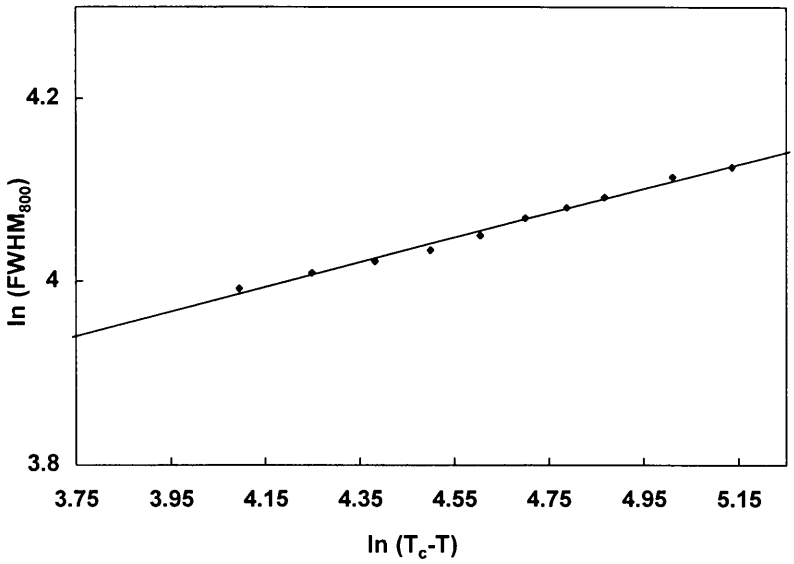

Figure 3.9 The natural logarithm of line widths (FWHM) of the totally symmetric stretching mode in Cr^{4+}:$CaTiOSiO_4$ graphically represented against $\ln(T_c-T)$ where T_c is the transition temperature at 497 K.

The correlation coefficient of the above graph was found to be r = 0.996, and the slope of the line gives a value of $\beta = 0.134 \pm 0.010$. This latter value for the critical exponent β agrees very well with the value of $\beta = 0.14$ as determined by Bismayer et al [41], and $\beta = 0.12$ as obtained by Salje et al for undoped titanite [43]. This once again indicates that the chromium doped into titanite does not adversely effect the behaviour of the phase transition.

3.5.2 THE HIGH PRESSURE PHASE TRANSITION OF TITANITE

3.5.2.1 The Paraelectric-Antiferroelectric Phase Transition of Titanite : Transition Mechanism

A pressure induced phase transition has been observed in a sample of synthetic titanite [45], using synchrotron radiation on material in a diamond anvil cell. The

high pressure phase was refined in space group A2/a at 69.5 kbar. At this pressure, the cell dimensions were found to be a = 6.8912, b = 8.6234 and c = 6.4065 Å, and β = 113.057°.

The observed reversible symmetry change from $P2_1/a \rightarrow A2/a$ is identical to that of the high temperature paraelectric-antiferroelectric phase transition at 497 K discussed above. However, the mechanism for the phase transition is proposed to be different. While in the temperature phase transition the phase between ~500 and ~825 K may be described as a statistical average of small domains of $P2_1/a$ material, it is reported that the high pressure phase transition is a response to increasing over-bonding of the Ti atoms. This has the effect of forcing individual Ti atoms into the geometric centres of their coordination octahedra. The result is that in the high pressure phase, titanite has both long and short range A2/a symmetry. In contrast, the high temperature phase between ~500 and ~825 K has only long range A2/a symmetry. Above ~825 K, the high temperature phase also has short range A2/a symmetry.

The synchrotron radiation investigation studied titanite at ambient pressure, 12.8, 21.0 and 69.5 kbar [45]. The phase transition is reported to occur between 21.0 and 69.5 kbar. Consequently, the exact or approximate pressure at which the phase transition occurs could not be determined. In the present investigation, the resonance Raman bands of Cr^{4+}:$CaTiOSiO_4$ are used to investigate the high pressure phase transition of titanite.

3.5.2.2 Chromium Doped Titanite and the High Pressure Phase Transition

In the current study, a preliminary high pressure Raman spectroscopic investigation was undertaken of chromium doped titanite using the 514.5 nm laser excitation line of an Ar^+ laser and a diamond anvil cell. Chromium doped titanite was placed under pressures between ~3 and ~46 kbar. Three of the spectra recorded at pressures of 3.12, 35.2 and 45.8 kbar can be seen in figure I-3.4 (appendix I). From this figure it is clearly seen that the respective spectra

vary considerably from one another. One of the most marked differences is the change in positions of the various bands in these Raman spectra.

The pressure dependence of the position of the totally symmetric Cr^{4+}-O stretching mode at ~800 cm^{-1} can be seen in figure 3.10 below.

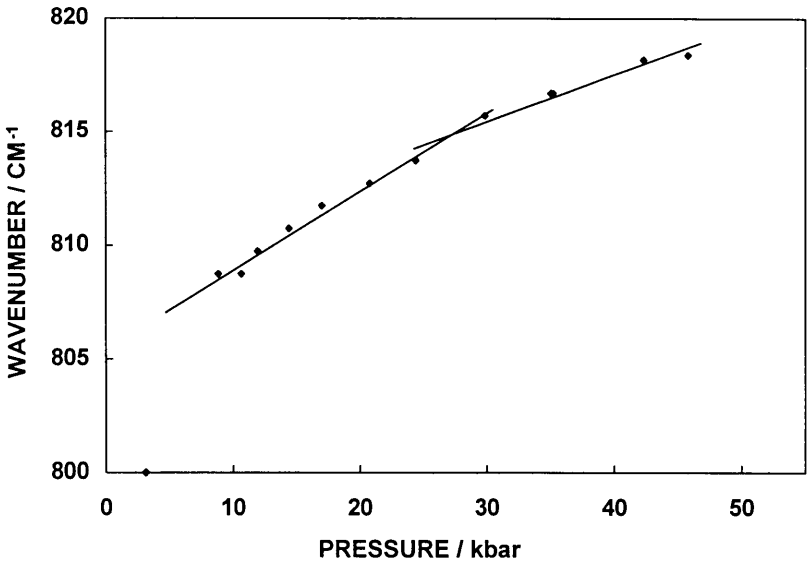

Figure 3.10 The pressure dependence of the peak position of the totally symmetric Cr^{4+}-O stretching mode in Cr^{4+}:$CaTiOSiO_4$.

This band moves to higher wave numbers as the pressure is increased. The pressure dependence of the Cr-O band assigned as ν_3 can be seen in figure 3.11 below.

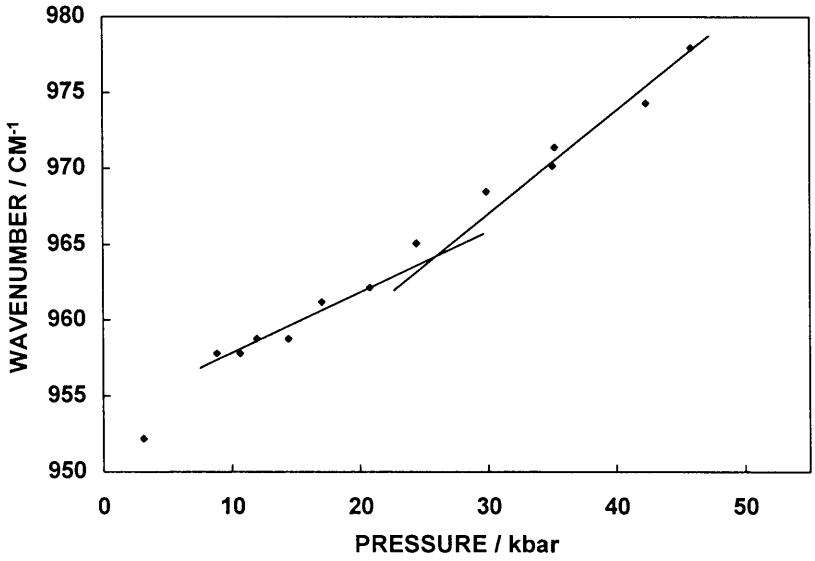

Figure 3.11 The pressure dependence of the peak position of ν_3(Cr^{4+}-O) in Cr^{4+}:$CaTiOSiO_4$.

From figure 3.11 above, it is clearly seen that this Cr-O band is also sensitive to the increase of pressure and it also moves to higher wave numbers as the pressure is increased. There appears to be a discontinuity in the rate of shift of both Cr-O bands as the pressure is increased. This occurs at ~27.5 kbar. The shift of the two Cr-O bands above ~27.5 kbar is however different. Whereas the 800 cm^{-1} band tends to shift at a faster rate above ~25 kbar, the 960 cm^{-1} band tends to shift at a slower rate above this pressure.

The effect of increasing pressure on the position of ν_4(Si-O) at 460 cm^{-1} can be seen in figure 3.12.

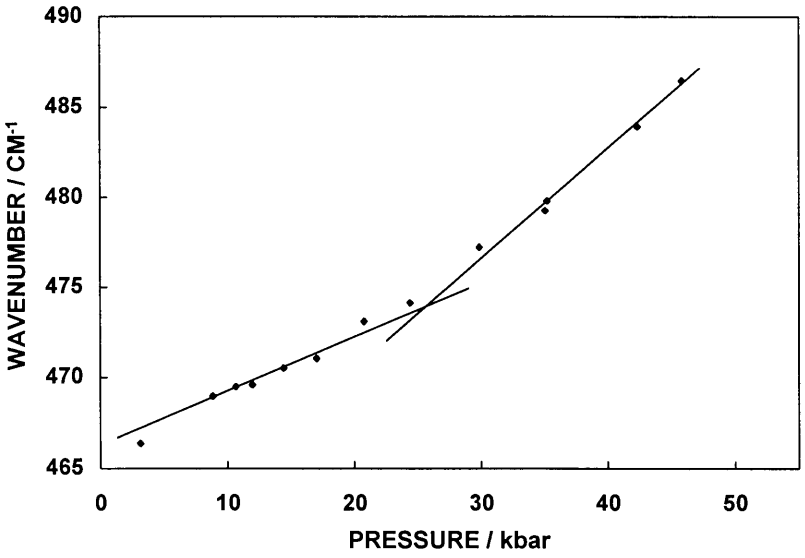

Figure 3.12 The pressure dependence of the peak position of $\nu_4(Si^{4+}\text{-}O)$ in Cr^{4+}:$CaTiOSiO_4$.

This band behaves in a similar way to the Cr-O bands in that it also moves to higher wave numbers as the pressure is increased. This is as expected since Cr substitutes for Si in Cr^{4+}:$CaTiOSiO_4$. That the bands move to higher wavenumbers is due to the dimensions of the unit cell which get smaller as the pressure is increased. Furthermore, the Si-O band also shows a discontinuity in the rate of shift at ~27.5 kbar. Above the transition pressure, it behaves like ν_3(Cr-O) in that the rate of shift of the band increases above ~27.5 kbar.

The effect of increasing pressure on the position of ν_1(Ti-O) can be seen in figure 3.13 below.

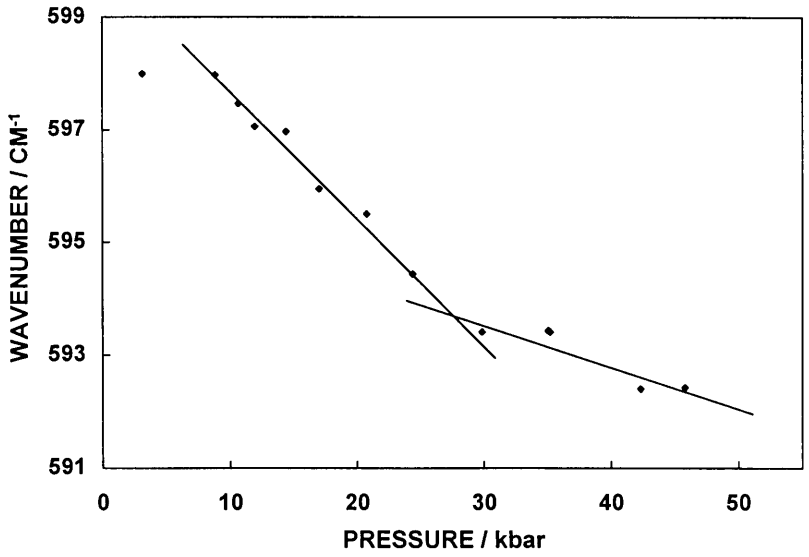

Figure 3.13 The pressure dependence of the peak position of ν_1(Ti-O) in Cr^{4+}:$CaTiOSiO_4$.

This band is also sensitive to the increase in pressure but it shows anomalous behaviour as compared with that of the Si-O and Cr-O bands in Cr^{4+}:$CaTiOSiO_4$. Whereas the Cr-O and Si-O bands were seen to move to higher wavenumbers as the pressure was increased, the Ti-O band is seen to move to lower wavenumbers. The shift is not as large as that of the other bands. The Ti-O band also show a change in the rate of shift of the Raman band at ~27.5 kbar, as is the case for the Cr-O and Si-O band shifts.

That the Ti-O band is moving to shorter wave numbers might be justified by the shift of the Ti atom within the [TiO_6] octahedron and that the average bond lengths of the Ti-O bonds are getting longer. That all of the other bands observed are moving to higher wave numbers is not surprising since the unit cell gets smaller as the pressure is increased. There appears to be an anomaly at ~27.5 kbar which could be as a result of the $P2_1/a \rightarrow A2/a$ phase transition. The Raman

bands followed through the increase in pressure were chosen because they were relatively well resolved in spectra with relatively weak intensity. The other bands were broad, diffuse and of low intensity. Consequently, it is difficult to follow them accurately. The Raman spectra were recorded by focusing the laser on the sample in the diamond anvil cell in the macro phase. Spectra with higher resolution might be obtained under the microscope. This would allow for the suggestion that the pressure phase transition results in the centring of the Ti atom within the [TiO_6] octahedron [45] to be verified more accurately. Should this be the case, then some of the bands in the Raman spectrum of the low pressure phase would be expected to disappear in the high pressure phase. From the spectra recorded, it does however not appear that bands disappear. There is however strong preliminary evidence that the $P2_1/a \rightarrow A2/a$ pressure phase transition takes place at ~27.5 kbar.

3.5.3 DISCUSSION

Some general remarks may be made with regards to the temperature and pressure phase transitions of titanite discussed above.

The Raman cross sections, frequencies and intensities of the Cr-O bands in Cr^{4+}:$CaTiOSiO_4$ were found to be very temperature and pressure sensitive. Furthermore, the Si-O and Ti-O bands were also found to be temperature and pressure sensitive.

The Cr-O and Si-O bands in both the temperature and pressure investigations were found to behave in similar ways as expected since Cr substitutes for Si in Cr^{4+}:$CaTiOSiO_4$.

Increasing the temperature of titanite is expected to result in the shift of the Raman modes to lower wavenumbers and to result in band broadening. Conversely, increasing the pressure of titanite is expected to result in a shift of the Raman modes to higher wavenumbers. At least two anomalies may be found in the Raman spectra of titanite at different temperatures and pressures.

The first anomaly occurs with respect of the position and width of the totally symmetric Cr-stretching vibration with increasing temperature. This mode is seen to move to lower wavenumbers and get narrower as the temperature is increased. This can be ascribed to the increase in symmetry of the $[CrO_4]$ tetrahedron at the higher temperature. This results in the various components of the Cr-O band merging. Consequently, the band narrows, and shifts to a lower frequency as a result of the phase transition in titanite.

The totally symmetric Cr-O stretching vibration in Cr^{4+}:$CaTiOSiO_4$ was also found to narrow in the pressure investigation. Unfortunately, the resolution of the spectra was not sufficient to quantify this apparent band narrowing.

The second anomaly appears in the pressure investigation of titanite. The Ti-O band which is expected to move to higher wavenumbers as the pressure is increased, moves in fact to lower wavenumbers. Once again, this anomalous behaviour may be ascribed to the phase transition in titanite.

3.6 CONCLUSION

3.6.1 SYNTHESIS

Undoped titanite was synthesised at 1300°C. At this temperature the reaction product was found to be on the verge of sintering. The reaction product was broken down to a powder form with a mortar and pestle. The resulting powder was a white powder with a slight yellow coloration. Undoped titanite was also synthesised at 1200°C using a mineraliser mixture of boric acid and potassium nitrate. Chromium doped titanite was synthesise at 1300°C. The product was an intensely coloured brown-maroon powder. Doped titanite was also synthesised at 1200°C using the mineraliser mixture used for the undoped titanite. As was the case with malayaite, while it was possible to synthesis titanite at temperatures below ~1200°C, these reaction products were a mixture of starting materials, by-products and titanite. In addition, the colour of the reaction product indicated that the doping was not very efficient.

3.6.2 SPECTROSCOPY

Vibrational spectra of undoped titanite were recorded. They were found to be in good agreement with those recorded elsewhere. The Si-O bands in the Raman spectrum of titanite were tentatively assigned.

The electronic spectrum of chromium doped titanite was recorded and found to be in good agreement with the electronic spectrum of chromium doped malayaite. It shows a broad absorption peak at ~510 nm indicating the possibility of recording the resonance Raman spectrum of chromium doped titanite. The vibrational spectra of chromium doped titanite were recorded. As was the case with chromium doped malayaite, no significant changes were found in the infrared spectrum of doped titanite as compared with that of undoped titanite. The Raman spectra did however show a difference. Resonance Raman bands were found which could be attributed to the chromium in titanite. Various overtones and combinations of these resonance Raman bands were also identified. These new features were found to be sensitive to the amount of chromium with which titanite was doped. They were investigated and tentatively assigned.

As was the case with chromium doped malayaite, chromium in titanite was found to substitute for Si-ions in tetrahedral coordination. In the case of titanite, the Si-ions have C_i site symmetry. At least two features were found in the totally symmetric stretching mode of Cr-O. This is in line with the low C_i site symmetry of the Si-ion which it is substituting. This band could not be satisfactorily resolved. However, at least two features were discernible.

From these features, the average bond lengths of the Cr-O bonds in chromium doped titanite were calculated. They were calculated to be 1.700 and 1.729 Å respectively. This may be compared with a value of 1.752 Å obtained for the Cr-O bond length in chromium doped malayaite. As was the case in Cr^{4+}:$CaSnOSiO_4$, the ionic radii sum of Cr and O is larger than that of Si and O. Consequently, the Cr-O bond has strong covalent character in chromium doped

titanite resulting in bond lengths which are shorter than those predicted by the ionic radii calculations.

An average bond order of 1.18 was calculated for the Cr-O bond in Cr^{4+}:$CaTiOSiO_4$. This value is consistent with tetrahedral coordination and similar to the bond orders of chromium in malayaite and forsterite.

The ν_2 Raman modes for Cr-O and Si-O in Cr^{4+}:$CaTiOSiO_4$ could not be found. Consequently, only values for k_{Td} of the Cr-O and the Si-O bonds could be calculated in Cr^{4+}:$CaTiOSiO_4$. They are 6.90 and 5.76 mdyn/Å, respectively. These values compare favourably with the k_{Td} values calculated for Cr^{4+}:$CaSnOSiO_4$ and Cr^{4+}:Mg_2SiO_4.

Resonance Raman spectroscopy was used effectively to elucidate the coordination state of chromium in titanite.

3.6.3 THE PHASE TRANSITIONS

The antiferroelectric-paraelectric phase transition has been extensively investigated. Numerous models have been suggested for the phase transition. As yet the exact details of the phase transition have not yet been conclusively determined. In this study chromium was successfully doped into the structure of titanite. In other studies, the impurities substituting for the Ti-ions or the O -ions shared by the Ti-ions were found to affect the phase transition mechanism. Furthermore, an investigation of the phase transition by substituting Ti-ions by Hf-ions using perturbed angular correlation spectroscopy did not yield any information about the phase transition. In this study the chromium ions were substituted into the position of the Si-ions.

This substitution was found to be very sensitive to the structural phase transitions underway in titanite. Furthermore, it did not appear to affect the phase transition mechanism in any way. Consequently, it was shown to be a very sensitive probe to the phase transition in titanite. The Raman modes due to Si-O bonds were found to react in a similar way to the modes due to the Cr-O bonds. This is as expected since the Cr-ions have been shown to substitute for Si-ions

in titanite. While the Ti-O bands were also found to be sensitive to the phase transition, the Cr-O bands were found to be the most sensitive of the Cr-O, Si-O and Ti-O bands.

The intensity of the totally symmetric Cr-O mode was used to determine a value for the critical exponent of the macroscopic order parameter, $\beta = 0.1150 \pm 0.005$. In addition a value of $\beta = 0.134 \pm 0.010$ was obtained using the line width at half maximum of the totally symmetric Cr-O mode. Both these values are in good agreement with those obtained elsewhere. They are close to the theoretical value predicted for a 2D Ising model.

The current study shows strong support for a transition mechanism whereby the low temperature phase may be described by a 2D Ising model, while the high temperature phase between ~500 K and ~825 K is a statistical average of small domains of $P2_1/a$ titanite as opposed to the Ti-ions shifting to the geometric centres of the $[TiO_6]$ octahedra. This is evident from the fact that bands which should disappear if the Ti-ions shift to the geometric centres of the $[TiO_6]$ octahedra do in fact not disappear.

The high pressure phase transition of titanite has not been extensively investigated. It has been reported that titanite has a low pressure $P2_1/a$ phase below ~21 kbar, and a high pressure A2/a phase above ~69 kbar. The mechanism for the transition is proposed to be different to that of the temperature phase transition in that the A2/a phase is as a result of the actual centring of the Ti atoms in the $[TiO_6]$ octahedron rather than the statistical average of small domains of differently orientated $P2_1/a$ domains.

The Cr-O bands in Cr^{4+}:$CaTiOSiO_4$ were found to be sensitive to the increase in pressure. The positions of some Cr-O, Si-O and Ti-O bands were investigated as a function of pressure. The Raman modes due to Si-O bonds were found to react in a similar way to the modes due to the Cr-O bonds. This is as expected since the Cr-ions substitute for Si-ions in titanite. While the Ti-O bands were also found to be sensitive to the phase transition, their shift was much smaller than that of

the Cr-O and Si-O bands. Furthermore, the Ti-O band investigated showed anomalous behaviour by shifting to lower wavenumbers as the pressure was increased.

All bands showed discontinuity in the rate of shift at ~27.5 kbar. Consequently, this preliminary investigations shows that the phase transition occurs at around 27.5 kbar. From the spectra recorded, it does not appear that various bands disappear in the spectra of the high pressure phase. While spectra with greater resolution are required to qualify this more accurately, it does not appear that the high pressure phase is as a result of the centring of the Ti atom in the $[TiO_6]$ octahedron between ~27.5 and ~45 kbar, but rather as a result of the statistical average of differently orientated $P2_1/a$ titanite as is the case for titanite at temperatures between ~497 K and ~825 K at ambient pressure.

Chapter 4

The Pyrochlore Compounds

4.1 INTRODUCTION

Pyrochlore is a naturally occurring mineral with the general chemical formula $(Na,Ca)_2(Nb,Ti)_2(O,F)_7$ [54]. The pyrochlore structure was first determined by Gaertener in 1930 [55]. Subsequently, numerous oxide compounds were discovered that have the pyrochlore structure. These compounds have been the subject of investigation for many years. Bystrom, using X-ray powder diffraction diagrams, first showed in 1944 that the paraelectric form of cadmium niobate has the pyrochlore structure [56]. Interest in this compound was stimulated in 1952 when Cook and Jaffe discovered that it is ferroelectric below room temperature [56]. Consequently, interest in isostructural compounds was also stimulated. In 1955, Jona et al refined the structure reported by Bystrom with data collected on single crystals. The pyrochlore compounds were shown to belong to the cubic space group Fd3m, with 8 formula units per unit cell.

Minerals with the pyrochlore structure have the general chemical formula $A_2B_2O_7$ or $A_2O'B_2O_6$. Their structure may be viewed as a three dimensional network of corner sharing $[BO_6]$ octahedra with the A-ions and the O'-ions occupying large open spaces in the network. The network of linked octahedra results in a B:O ratio of 2:6.

Various investigations of systems yielding $A_2B_2O_7$ compounds with the pyrochlore structure have been undertaken [56;57]. There are numerous different families of pyrochlore minerals with A^{III} and B^{IV} cations. These include

- the zirconates and hafnates which have the general chemical formula $A_2^{III}B_2^{IV}O_7$ (A=La,Nd; B=Zr,Hf) [58].
- the rare-earth titanites with the general chemical formula $Ln_2^{III}Ti_2^{IV}O_7$ (Ln=Sm,Gd,Yb;Y) [59].
- the rare-earth stannates with the general chemical formula $Ln_2^{III}Sn_2^{IV}O_7$ (Ln=La,Sm,Gd,Tb,Dy,Ho,Tm,Yb,Lu;Y) [59;60].

Pyrochlores with the A and B ions in oxidation states other than (III) and (IV), respectively, also exist. Examples include

- pyrochlore compounds with the general chemical formula $Cd_2^{II}B_2^{V}O_7$ (B=Ta, Nb, Sb) [61].
- pyrochlore compounds with the general chemical formula $Ca_2^{II}B_2^{V}O_7$ (B=Sb,Ta) [54].

This study focuses on two compounds with the pyrochlore structure, and the effect that doping with vanadium and calcium has on their properties. The chemical states of the dopants are also investigated. The two compounds investigated here are as follows:

I $Y_2Sn_2O_7$
II $Y_2Ti_2O_7$

Previous studies on $Y_2Sn_2O_7$ include X-ray diffraction data for $Y_2Sn_2O_7$ and various other rare earth stannates [56], the study of $Y_2Sn_2O_7$ and various other rare earth stannates using ^{119}Sn MAS NMR, more specifically with the use of paramagnetic shift probes, in the solid state [62], and a structure refinement and calculated X-ray powder data study of $Y_2Sn_2O_7$ derived from powder neutron data [63].

Complete vibrational studies of the two compounds have also been undertaken. The vibrational spectra have been investigated in relation to order-disorder phenomena [64]. They have also yielded the force fields of $Y_2Sn_2O_7$ and $Y_2Ti_2O_7$ along with numerous other compounds and families of compounds with the pyrochlore structure [57;59].

The chemical state of vanadium in $Y_2Sn_2O_7$ has been reported [65]. Vanadium tin composites are reported to have various applications including the colouring of ceramic glazes [66], and the selective oxidation of hydrocarbons [65]. There are a number of ceramic pigments used for colouring ceramics, and all have draw backs. As a yellow pigment, the V-SnO_2 yellow is said to be superior in cost, and strength

of colour but inferior in cleanness and brightness when compared with the praseodymium yellow [66]. Furthermore, lead and cadmium containing yellow pigments such as $Pb_2Sb_2O_7$, $PbCrO_4$, and CdS can no longer be used in many countries because of the regulatory trend against toxic products [67]. While the toxic properties of vanadium are well known, there are two factors which render $V:Y_2Sn_2O_7$ and $V:Y_2Ti_2O_7$ pigments safer than the above mentioned pigments. The first is that whereas in the above pigments the toxic component makes up a large portion of the material (lead makes up 50% of the cations in $Pb_2Sb_2O_7$), in a doped pigment, the toxic component(s) are present in substantially smaller amounts (in the order of ~1%). The second is that the small amounts of toxic compound(s) that are present are incorporated into the structure of the host lattice in such a way that they cannot get out under ambient conditions of temperature and pressure. These doped host lattice structures are generally, by the nature of their being, very stable and unreactive. The stability of ceramic pigments is of coarse of paramount importance since in their application they are subject to extreme conditions of temperature and very corrosive environments which they must withstand. Consequently, there is room for improved yellow ceramic pigments and $V:Y_2Sn_2O_7$ and $V:Y_2Ti_2O_7$ are good candidates for such compounds.

4.2 SYNTHESIS

4.2.1 SYNTHESIS

4.2.1.1 Synthesis of $Y_2Sn_2O_7$ and $Y_2Ti_2O_7$

Stoichiometric amounts of yttrium and tin in the form of yttrium oxide (Y_2O_3) and stannic oxide (SnO_2) were intimately wet mixed. The stannic oxide was milled to a particle size of 98%<5 µm and 75%<2 µm prior to mixing. After wet mixing, the reaction mixture was dried and dry mixed with a mortar and pestle, and then calcined. The reaction mixture was heated from room temperature to 1450°C. The temperature was held constant for four hours after which the oven was switched off. The resulting product was allowed to cool to room temperature inside the oven.

The $Y_2Ti_2O_7$ compound was synthesised in the same way except that titanium in the form of titanium dioxide (TiO_2) was used in stead of the stannic oxide. In addition, the reaction mixture was fired at the lower temperature of 1300°C. The lower temperature is required since the titanium containing reaction mixture sinters at higher temperatures.

4.2.1.2 Synthesis of Calcium and Vanadium Co-Doped $Y_2Sn_2O_7$ and $Y_2Ti_2O_7$

Calcium and vanadium co-doped $Y_2Sn_2O_7$ and $Y_2Ti_2O_7$ were prepared in the same way as their undoped analogues except that between 0.5 and 2 atom percent[1], respectively, of calcium, in the form of calcium carbonate ($CaCO_3$), and vanadium, in the form of ammonium metavanadate (NH_3VO_3), were added to the yttrium-tin or yttrium-titanium reaction mixtures before wet mixing. After wet mixing and dry mixing, the yttrium-tin and the yttrium-titanium reaction mixtures were heated to 1450° and 1300°C, respectively. The temperature was held constant for four hours after which the oven was switched off. The reaction products were allowed to cool to room temperature inside the oven.

The resulting powders were then water leached for one hour and dried. This was followed by hot acid leaching treatment for 30 minutes.

4.2.2 RESULTS AND DISCUSSION

4.2.2.1 Undoped $Y_2Sn_2O_7$ and $Y_2Ti_2O_7$

The resulting products were fine white powders. The average particle size of the powders was found to be in the region of 50 μm. In addition to the Raman spectra of the reaction products being recorded, the IR spectra were recorded, XRD data was collected and a SEM analysis was carried out.

Undoped $Y_2Sn_2O_7$ and $Y_2Ti_2O_7$ were synthesised to be used as reference samples for comparison with the co-doped reaction products using the aforementioned techniques. The high temperatures at which these reactions were carried out also

[1] 0.5-2% Ca and V as a percentage of the total number of yttrium and tin (or titanium) atoms.

gives a good indication of the thermal stability of the reaction mixtures. As an example, the titanium pyrochlore reaction mixture was found to sinter at the higher temperatures at which the tin analogue was prepared. This is of little consequence here though since thermal stability of ~1300°C is more than sufficient for use as a ceramic pigment. Consequently, both the tin and titanium analogues have sufficient thermal stability for use as ceramic pigments.

The results of the spectroscopic investigation of the undoped and doped reaction products will be discussed separately in section 4.4 below. The SEM analysis results show that the yttrium and tin (or titanium as the case may be) added to the reaction mixture are present in equal portions after calcining, indicating that none of the starting materials were lost upon firing. The XRD data show that at 1450 and 1300°C respectively, the only compounds formed in the firing process were $Y_2Sn_2O_7$ or $Y_2Ti_2O_7$, as the case may be, and that no starting materials remained unreacted.

4.2.2.2 $Y_2Sn_2O_7$ and $Y_2Ti_2O_7$ Co-Doped with Calcium and Vanadium

The resulting products were fine, intensely coloured yellow powders. The average particle size of the powders without milling were found to be in the region of 50 μm, as was the case with their undoped counterparts. Once again, in addition to the Raman spectra of the reaction products being recorded, the IR spectra were recorded, XRD data was collected and a SEM analysis was carried out.

The SEM analysis results showed the presence of calcium and vanadium in the doped pyrochlores though the technique was not found to be sensitive enough to give accurate quantitative information about the dopants since they are present in such small quantities. The XRD data are summarised in table 4.1 below. They show that at 1450 and 1300°C respectively, the only compounds formed in the firing process were $Y_2Sn_2O_7$ or $Y_2Ti_2O_7$, as the case may be, and that no starting materials remained unreacted. As was the case with the SEM analysis results, this technique was not sensitive enough to yield information about the dopants.

Table 4.1 X-ray powder diffraction analysis results for the undoped and calcium and vanadium co-doped $Y_2Sn_2O_7$ and $Y_2Ti_2O_7$ reactions calcined at temperatures between 1200 and 1450°C.

Reaction Number	Pyrochlore Type	Temperature, °C	Y_2O_3	BO_2 (B=Sn,Ti)	Other Compound(s)	$Y_2B_2O_7$ (B=Sn,Ti)
1	Sn	1450	✗	✗	✗	✔
2	Sn	1300	✗	✗	✗	✔
3	Sn	1200	✔	✔	✗	✗
4	Ti	1450	product sintered	-	-	-
5	Ti	1300	✗	✗	✗	✔
6	Ti	1200	✔	✔	✗	✗

4.2.2.3 Discussion

The most desirable result is that the strongest possible pigment is produced at the lowest possible temperature with all of the starting materials having reacted to yield the desired product. In addition, the minimum amount of dopants should be used. This will result in the minimum amount of pigment being required to achieve the desired colouring effect of a ceramic article and the minimum amount of energy being used to synthesis the pigment. A number of conclusions may be drawn from the effect of various parameters on the synthesis of the pyrochlores, and the analysis of the pyrochlores synthesised. They are as follows:

- Neither of the calcium and vanadium co-doped pyrochlores could be synthesised successfully at temperatures below 1300°C. While a sol-gel technique did produce the desired host material at temperatures as low as 1150°C, it was not successful in producing the co-doped pyrochlores. In any event, the sol-gel technique is expensive to carry out on a bulk scale. In addition, no mineraliser mixture was found to be successful in lowering the temperatures required to produce either the pyrochlore host material or pigments with suitable colour properties.
- At 1300°C, in both the case of the tin and the titanium pyrochlores, the XRD data showed that only the respective pyrochlore was produced and that no unreacted raw materials remained after calcination. In addition the co-doped samples showed a very intense and clean yellow coloration.
- At 1450°C, the titanium pyrochlore sintered. The tin pyrochlore produced a pigment with a coloration more intense than the pigment produced at lower temperatures. Furthermore, the increased calcination temperature did not increase the crystallinity (or particle size) of the product.
- The intensity of the colour of the pigments in the case of both the tin and the titanium pyrochlores was found to improve as the amount of dopant was increased. In heavily doped $Y_2Sn_2O_7$, YVO_4 was detected in small amounts as a by-product.
- All of the doped products were subject to an acid leaching treatment. After 30 minutes of acid leaching, no discoloration was found to have occurred in any of the samples.

- When all factors are taken into account, it appears that the most appropriate temperature for calcining the pyrochlore pigments is 1300°C.

4.3 STRUCTURE

4.3.1 CRYSTAL STRUCTURE OF $Y_2Sn_2O_7$ and $Y_2Ti_2O_7$

The crystal structures of $Y_2Sn_2O_7$ and $Y_2Ti_2O_7$ have been published [54;63]. They belong to the cubic space group Fd3m (No.227). Their unit cells contain eight $A_2B_2O_7$ formula units with two units per Bravais unit cell. Minerals with this structure, have cell edges close to 10.3 Å. $Y_2Sn_2O_7$ has a cell edge of 10.3723 Å. As expected due to the smaller ionic radius of the titanium ion, $Y_2Ti_2O_7$ has a smaller cell edge of 10.095 Å. Their general chemical formula may be described as $A_2O'B_2O_6$ with their structures being made up of a network of $[BO_6]$ octahedra sharing all their corners around hexagonal vacancies with a lattice of $[A_4O']$ tetrahedra positioned inside the vacancies [57]. Figures 4.1 and 4.2 below illustrate portions of the octahedral and tetrahedral networks of the pyrochlore structure.

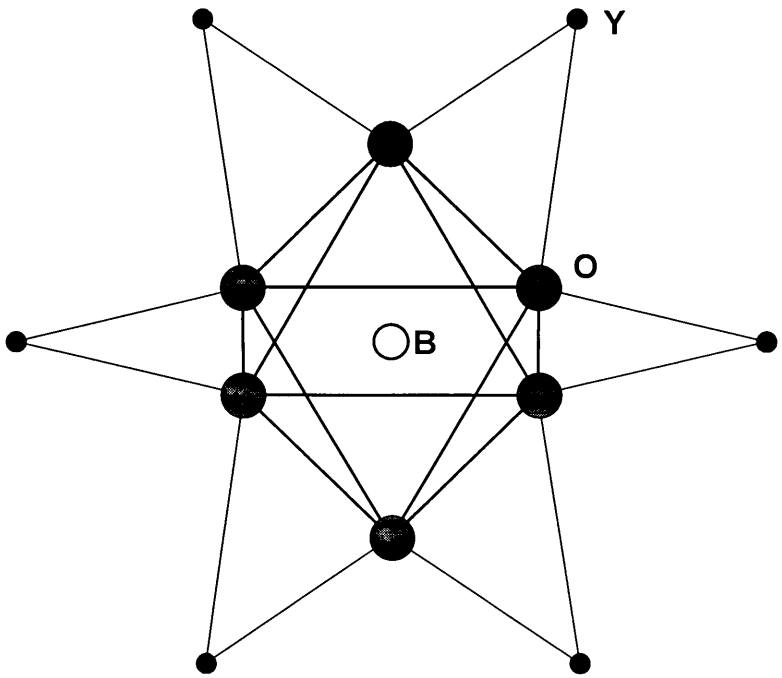

Figure 4.1 Schematic representation of the $[BO_6]$ octahedra in the pyrochlore structure and the way in which the Y(A)-ions are bonded to these octahedra [62].

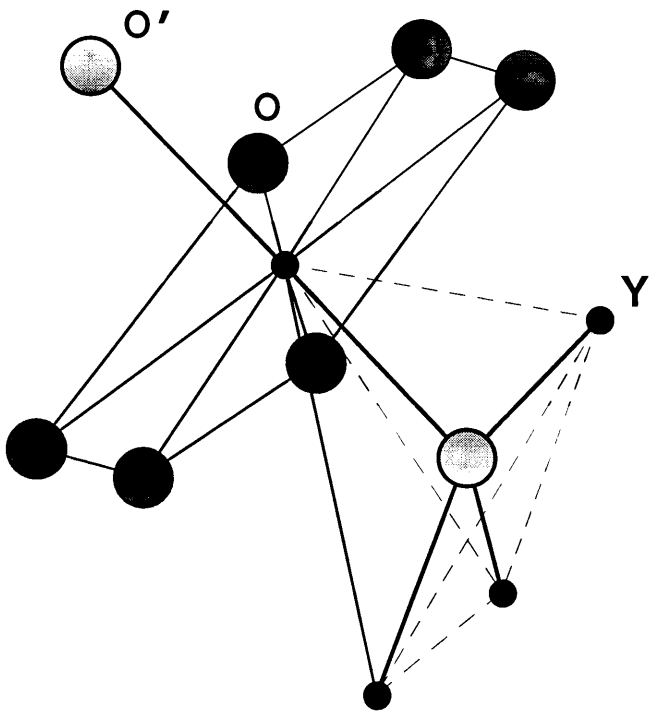

Figure 4.2 Schematic representation showing the tetrahedral environment of the Y(A)-ions in the pyrochlore structure [59].

The $[BO_6]$ octahedra are linked by their corners to form hexagonal 'crowns' whose centres are filled with Y^{3+}-ions. Four crowns are grouped together in such a way that four Y^{3+} cations form a tetrahedron in the centre of which an O' oxygen atom is located. Consequently, the pyrochlore structure may be viewed as two separate overlapping lattices, one composed of the $[BO_6]$ units, the other composed of a lattice of $[Y_4O']$ tetrahedra.

Each O atom is bonded to two B^{4+}-ions and two Y^{3+}-ions. The length of the B-O bonds is about 2.0 Å. The Y-O and Y-O' bonds have lengths of about 2.5 and 2.2 Å, respectively. Since the Y^{3+}-ions occupy the large vacancies left in between the $[BO_6]$ lattice, they do not contribute directly to the cohesion of the three dimensional lattice [59]. From a structure refinement of the $Y_2Sn_2O_7$ compound [63], the bond lengths of the tin pyrochlore are known more accurately. The bond lengths of $Y_2Ti_2O_7$ are also known [59], though not as accurately. These bond

lengths are summarised in table 4.2 below. As expected, the bonds of the titanium pyrochlore are shorter than those of its tin counterpart.

Table 4.2 Bond lengths in $Y_2Sn_2O_7$ and $Y_2Ti_2O_7$.

M-O	$Y_2Sn_2O_7$, Å	$Y_2Ti_2O_7$, Å
Y-O	2.494	2.48
Y-O'	2.246	2.18
B-O	2.043	1.95

The site group symmetries and Wyckoff letters of the atoms in $Y_2Sn_2O_7$ and $Y_2Ti_2O_7$ are listed in table 4.3 below.

Table 4.3 Site group symmetries and Wyckoff letters of the atoms in $Y_2Sn_2O_7$ and $Y_2Ti_2O_7$.

Ion	Site Group Symmetry	Wyckoff Notation
Y^{3+}	D_{3d}	16c
Sn^{4+} or Ti^{4+}	D_{3d}	16d
O^{2-}	C_{2v}	48f
O'^{2-}	T_d	8b

It has been shown that in the pyrochlore structure, the $[BO_6]$ octahedra are squashed along the *3* axis if the *u*(48*f*) parameter (origin on B; 3m) differs from 0.3125 [55]. It has also been shown that when the $[BO_6]$ polyhedra are more regular, the $[AO_8]$ polyhedra become more distorted, and vice versa. It has been suggested that the relative bond directions of the B-O bonds (and the A-O bonds) and the $[BO_6]$ bond lengths vary slightly as do the repulsion forces between the

oxygen atoms of the same basal plane ($O_{(1)}$ and $O_{(2)}$ in figure 4.3) and the oxygen atoms of the two opposite planes ($O_{(1)}$ and $O_{(3)}$ in figure 4.3).

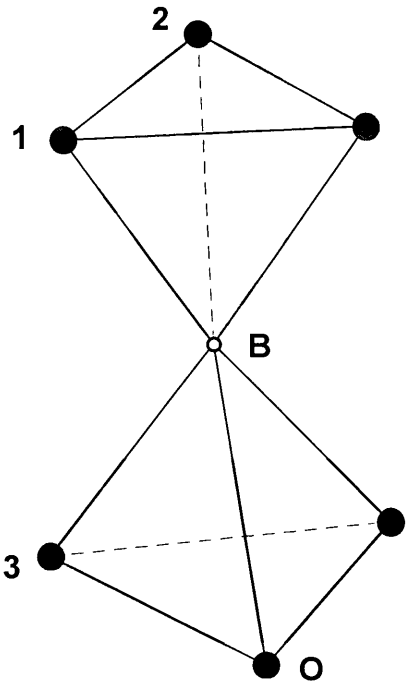

This would induce a variation in the polarisability of the B-O (and A-O) bonds, which might be expected to lead to more intense Raman lines when the polyhedron is more distorted. Consequently, in the Raman spectrum of $A_2B_2O_7$, the bands resulting from the $[BO_6]$ and the $[AO_8]$ polyhedra might be expected to be strongly influenced by even a very slight variation in their structure geometry. Such a variation in their structure geometry may result from the doping of the host lattice.

Figure 4.3 Deformation of the $[BO_6]$ octahedron [57].

4.4 SPECTROSCOPY

4.4.1 THE SELECTION RULES

The vibrational spectra of various rare earth stannates and titanates have been studied. The vibrational spectra of $Y_2Sn_2O_7$ and $Y_2Ti_2O_7$ have also been investigated [57;59]. The bands have been assigned and are summarised in table 4.4 below. Bhagavantam's method yields the following representation for the vibrations of the pyrochlore structure:

$$\Gamma_{optic} = \underset{(R)}{A_g} + \underset{(R)}{E_g} + \underset{(i)}{2F_{1g}} + \underset{(R)}{4F_{2g}} + \underset{(i)}{3A_{2u}} + \underset{(I)}{3E_u} + \underset{(IR)}{7F_{1u}} + \underset{(i)}{F_{2u}}$$

$$\Gamma_{acoustic} = F_{1u}$$

where (R) indicates the Raman active vibrations, (IR) the infrared active vibrations, and (i) the inactive modes. Consequently, six Raman modes and seven infrared bands are expected in the vibrational spectra of the respective pyrochlores.

4.4.2 SPECTROSCOPY : VANADIUM AND CALCIUM CO-DOPED $Y_2Sn_2O_7$ AND $Y_2Ti_2O_7$

4.4.2.1 Electronic Spectra of $Y_2Sn_2O_7$ and $Y_2Ti_2O_7$

The electronic spectra of the co-doped pyrochlores were recorded (see figures I-4.7 and I-4.8 - appendix I). The vanadium in the co-doped pyrochlores is most likely to be in its fifth and most stable oxidation state [65]. Vanadium in its fifth oxidation state does not have any electrons in its 3d orbitals. Consequently, no bands are expected to be found in the visible region of the electronic spectra. In accordance, neither of the pyrochlore spectra show an absorption maximum in the visible region of the electromagnetic spectrum. Both show a very broad feature between 300 and 450 nm. This feature must therefore represent a charge transfer band from the filled non-bonding ligand (oxide) orbitals $(t_{1g})^6$ and $(t_{1u})^6$ to the empty $t_{2g}(\pi^*)$ orbitals of the V^{5+}-ion, or in other words, a ligand to metal charge transfer (LMCT). These spectra are in good agreement with the literature [65]. Using the broad feature described above and using the 514.5 nm line of an Ar^+ laser it was possible to record the pre-resonance Raman spectra of the V^{5+} and Ca^{2+} co-doped pyrochlores.

4.4.2.2 Raman Effect of Calcium and Vanadium in $Y_2Sn_2O_7$ and $Y_2Ti_2O_7$

For the calcium and vanadium co-doped pyrochlores to be useful as ceramic pigments, the dopants need to be incorporated into the host lattice which must be stable in a corrosive environment at excess temperatures to prevent the colour of the pigment from being destroyed when the ceramic article is fired. As already stated, the vanadium in these doped pyrochlores is expected to be in its fifth oxidation state. In addition, it was found that the colour of the pigment develops only if calcium is added as a co-dopant in equal amounts. Since the calcium cations will enter the host lattice in their second oxidation state, if the vanadium cations are in their fifth oxidation state, the co-substitution will maintain the over all

electroneutrality of the compound since the combined charges of the yttrium and tin or yttrium and titanium cations that they will be substituting is +7. The effective substitution is thus $Ca^{2+} + V^{5+} \rightleftarrows Y^{3+} + Sn^{4+}$(or Ti^{4+}).

The question arises whether or not some other compound is being formed which is responsible for the intense yellow colour. Possibilities for this might include YVO_4 and $Ca_2V_2O_7$. While $Ca_2V_2O_7$ has the same general chemical formula as the pyrochlores under investigation, it does not have the pyrochlore structure. It belongs to the triclinic space group P_1 (No.1). The electronic spectra of YVO_4 and $Ca_2V_2O_7$ have been published [67]. As might be expected, they resemble those of the co-doped pyrochlores under investigation here since they also have a yellow coloration which results from vanadium in its fifth oxidation state.

The Raman spectra of undoped and calcium and vanadium co-doped $Y_2Sn_2O_7$ were recorded (see Figures I-4.1, I-4.2 & I-4.3 - appendix I). The Raman spectra of undoped and calcium and vanadium co-doped $Y_2Ti_2O_7$ were also recorded (see Figures I-4.4 & I-4.5 - appendix I). The bands of the respective spectra are summarised in table 4.4 below along with their assignments from the literature.

From table 4.4 it can be seen that the band positions in the undoped pyrochlores are in good agreement with those recorded elsewhere. The selection rules have been discussed above. Under O_h^7-symmetry the atoms are situated in the following positions: A(4c - D_{3d}); B(4d - D_{3d}); O'(2b - T_d) and O(12f - C_{2v}). The A and B cations do not contribute to the Raman active modes since they are located on inversion centres. Consequently, only vibrations of the oxygen atoms are allowed [57]. It is clear from table 4.4 below, and from the Raman spectra of the pyrochlore compounds in appendix I that features are observed in the spectra of the V^{5+} and Ca^{2+} co-doped species that can be assigned to V-O stretching modes. These features are absent in the Raman spectra of the undoped pyrochlores and they have been found to be dependant on the concentration of the dopants. This is seen if figure I-4.2 and I-4.3 in appendix I are compared. The bands due to the V-O bonds are more intense in the spectrum of the more highly doped pyrochlore. In addition, these features are also dependent on the excitation line used to record the Raman spectra and are thus pre-resonance Raman modes resulting from the dopants.

Table 4.4 Raman bands in undoped and in calcium and vanadium co-doped $Y_2Sn_2O_7$ and $Y_2Ti_2O_7$.

Undoped $Y_2Sn_2O_7$	Undoped $Y_2Sn_2O_7$		Ca & V doped $Y_2Sn_2O_7$	Undoped $Y_2Ti_2O_7$	Undoped $Y_2Ti_2O_7$	Ca & V doped $Y_2Ti_2O_7$	Assignment	*Bonds
This Study	[57;59]	[64]	This Study	This Study	[57;59]	This Study	[57;59]	[57;59]
-	-	-	803	-	-	824		
756	-	766	-	-	-	755		
			750					
	-			705	717	713		
-	610	-	-	585	586	597	F_{2g}	1
530 sh	530	-	-	519	527	520	F_{2g}	2 & 3†
508	505	514	505	519	527	520	A_{1g}	1, 2 & 3†
410	418	420	405	-	333	-	E_g	1, 2 & 3
349	355	355	~340 sh	305	318	305	E_g	1, 2‡, 3 & 4†
308	315	315	302	-	227	232	F_{2g}	2†, 3 & 4
				217	218	-		
-	-	-	145 sh	-	-	154		
				110	114	-		
-	-	-	90			113		

* M=Sn orTi; 1 = M-O; 2 = O-M-O; 3 = Y-O 4 = O-Y-O

† $Y_2Sn_2O_7$ only; ‡ $Y_2Ti_2O_7$ only

4.4.2.3 Vanadium-Oxygen Bond Lengths in $Y_2Sn_2O_7$ and $Y_2Ti_2O_7$

Using an empirical relation (eqn 4.1) developed by Hardcastle and Wachs [68], which relates the Raman stretching frequencies of vanadium-oxygen (V-O) bonds to their bond lengths, the V-O bond lengths of the vanadium in the pyrochlore compounds may be calculated.

$$\nu = 21349\exp(-1.9176R) \qquad \textbf{equation 4.1}$$

The V-O bands and their respective calculated bond lengths are listed in table 4.5 below.

Table 4.5 Bond lengths of the V^{5+}-O bonds in Ca^{2+} and V^{5+} co-doped $Y_2Sn_2O_7$ and $Y_2Ti_2O_7$.

	V-O Raman Band, cm^{-1}	V-O Bond Length, Å
V:$Y_2Sn_2O_7$	803	1.711
	750	1.746
	145	2.603
	90	2.852
V:$Y_2Ti_2O_7$	824	1.697
	755	1.743
	154	2.572
	113	2.733

As was the case with similar calculations in previous chapters involving the calculation of bond lengths, the diatomic approximation was used which assumes that vibrational interactions between neighbouring chemical bonds in complex transition metal oxides may be neglected [68]. This approximation assumes that a direct relationship exists between a metal-oxygen bond length and its Raman stretching frequency which allows the metal-oxygen bond lengths to be calculated

directly from the measurement of the Raman stretching frequency. It is valid if the error associated with the experimental observable of interest is comparable to, or less than, the interactions between the neighbouring metal-oxygen bonds. This assumption was shown by Hardcastle and Wachs to be valid in all cases involving V-O Raman modes investigated by them [68].

The co-doping is likely to result in Ca^{2+} -ions substituting for Y^{3+} -ions and V^{5+} -ions substituting for B^{4+} -ions in the respective pyrochlores. The ionic radii of Ca^{2+} (1.12 Å) and Y^{3+} (1.019 Å) are similar, with the ionic radii of the dopant being slightly larger than that of the ion it is substituting. The Ca^{2+} -ion is very flexible and has the ability to assume various coordination states. This is evident from numerous calcium compounds. In β-$Ca_2P_2O_7$, the Ca^{2+} -cations are found in four different calcium-oxygen coordination polyhedra [69]. Two of these polyhedra exhibit a coordination number of 7, one of 8 and one of 9. The average bond lengths of the respective polyhedra are 2.448, 2.434, 2.534, and 2.570 Å, respectively, with bond lengths ranging from 2.318 to 2.927 Å. In $Ca_2V_2O_7.H_2O$, the Ca^{2+} -ions find themselves in two distinct calcium-oxygen polyhedra [70]. The first Ca^{2+} -ion is 7-fold coordinated with an average Ca-O bond length of 2.42 Å, and bond lengths ranging from 2.34 to 2.60 Å. The second Ca^{2+} -ion is 8-fold coordinated with an average bond length of 2.49 Å, and bond lengths ranging from 2.37 to 2.70 Å. The bond lengths of the Y-O bonds in the tin and titania pyrochlores are 2.494 and 2.48 Å, respectively (table 4.2 above). This is in good agreement with the average Ca-O bond lengths in other compounds considered above. The Y-O' bonds are somewhat shorter at 2.246 and 2.18Å, respectively. However, numerous pyrochlore structures with Ca^{2+} -ions in the A position of the $A_2B_2O_7$ molecule are known [54]. Therefore, Ca^{2+} should comfortably be able to substitute for Y^{3+} in $Y_2Sn_2O_7$ and $Y_2Ti_2O_7$.

The B-O bond lengths for the tin and titania pyrochlores are 2.043 and 1.95 Å respectively. Of the V-O bond lengths calculated above (table 4.5), two are somewhat shorter, and two somewhat longer than the B-O bond lengths. The ionic radii of V^{5+} (0.54 Å), and Sn^{4+} (0.69 Å) and Ti^{4+} (0.605 Å) are similar, as is the case with Ca^{2+} and Y^{3+}. In this case, however, the ionic radii of the dopant is smaller

than that of the ion it is substituting. The sum of the ionic radii [21] of the dopants are listed below along with the ionic radii of the ions that they replace in the respective pyrochlores.

$r(Ca^{2+} \& V^{5+}) = 1.12 + 0.54 = 1.66$ Å
$r(Y^{3+} \& Sn^{4+}) = 1.019 + 0.690 = 1.709$ Å
$r(Y^{3+} \& Ti^{4+}) = 1.019 + 0.605 = 1.624$ Å

While the Ca^{2+} -ions are slightly larger than the Y^{3+} -ions, and the V^{5+} -ions are slightly smaller than the Sn^{4+} - and Ti^{4+} -ions, the combined ionic radii of Ca^{2+} and V^{5+} are very close to those of Y^{3+} and Sn^{4+}, and Y^{3+} and Ti^{4+}, respectively. Consequently, the combined ionic radii of the calcium and vanadium suggest that they should fit well into the structures of the respective pyrochlores. In addition to supporting a co-substitution of calcium and vanadium in the respective pyrochlores, the ionic radii calculations also suggest that the calcium and vanadium atoms will substitute in adjacent positions within the host lattice.

Crystals of composition $A_2B_2O_7$ may belong to one of a small number of groups of related structures. Crystals for which the ionic radius of the B- ion, generally the more electronegative one, is greater than 0.60 Å tend to crystallise into structures such as pyrochlore and weberite in which the B atom is octahedrally coordinated [71]. The ionic radius of V^{5+} is only 0.54 Å which suggests that the V^{5+} -ion might be in a coordination state other than octahedral. Indeed, if the bond lengths calculated above (table 4.5) from the Raman modes at around 800 cm^{-1} are compared with the bond lengths and the corresponding stretching frequencies of numerous V^{5+}-O compounds [68], they are found to be consistent in number and frequency with V^{5+}-O compounds with the vanadium tetrahedrally coordinated. A number of $A_2B_2O_7$ compounds with tetrahedrally coordinated vanadium are known. $Cd_2V_2O_7$, is an example [72]. In this compound there are three distinct V-O bond lengths of 1.764, 1.717, and 1.672 Å. Another example is $Mg_2V_2O_7$ [73]. In this compound, there are two distinct VO_4 tetrahedra. The first has bond lengths ranging from 1.629 to 1.817 Å, with an average bond length of 1.715 Å. The second has bond lengths ranging from 1.682 to 1.784 Å, with an average bond

length of 1.729 Å. These bond lengths are in good agreement with the ones calculated for the vanadium-oxygen bonds in the co-doped pyrochlores (table 4.5).

Yet another example may be found in the form of β-$Sr_2V_2O_7$ [74], which is isostructural with $Ca_2V_2O_7$ [75]. This compound has two distinct divanadate structures. Consequently, there are four different [VO_4] tetrahedra in β-$Sr_2V_2O_7$. There are two types of V-O bonds in these divanadate structures, namely bridging $V_{(1)}$-O-$V_{(2)}$ bonds and outer V-O bonds. The bridging V-O bonds in β-$Sr_2V_2O_7$ are 1.80 and 1.82 Å in length, and the outer V-O bonds have an average bond length of 1.70 Å and range between 1.63 and 1.77 Å. These bond lengths compare very well with those of the vanadium doped pyrochlores. Bond lengths calculated for the V-O bonds are 1.711 and 1.746 Å in $Y_2Sn_2O_7$ and 1.697 and 1.743 Å in $Y_2Ti_2O_7$ (table 4.5 above).

The longer bond lengths correspond more closely with those of the bridging V-O bond lengths in β-$Sr_2V_2O_7$, while the shorter bond lengths correspond well with those of the outer V-O bonds of β-$Sr_2V_2O_7$. This might suggest that in addition to a calcium ion and a vanadium ion substituting in adjacent positions within the host lattice, two vanadium atoms might also substituting into adjacent positions with respect to each other which results in a divanadate type substitution with bridging V-O bonds and outer V-O bonds in the vanadium and calcium co-doped pyrochlores. The very broad V-O bands in the Raman spectrum of the doped pyrochlores suggest a wide range of V-O bond lengths which would result from the divanadate structure. $Ca_2V_2O_7$, β-$Sr_2V_2O_7$, $Mg_2V_2O_7$ and $Ca_2V_2O_7.H_2O$ all exhibit true divanadate type structures with two differently coordinated V^{5+} -cations sharing an oxygen atom resulting in a wide range of V-O bond lengths.

If a straight forward substitution of V^{5+} for Sn^{4+} or Ti^{4+} is considered, then it might reasonably be expected that the vanadium will be octahedrally coordinated. This does not appear to be the case. The numerous examples of octahedrally coordinated V^{5+}-cations studied by Hardcastle and Wachs [68] show a large number of bands which range from ~1000cm^{-1} to ~110cm^{-1}. The vanadium in the pyrochlores exhibit only two distinct bands each at ~810 and ~750cm^{-1},

respectively, in addition to the small features between ~90 and 150cm^{-1}. While it is possible that other V-O bands are hidden beneath the Raman bands of the host structure between 850 and 200 cm^{-1}, there are no features between ~850 and ~1000cm^{-1} to support octahedral coordination (see figures I-4.2 and I-4.5 - appendix I).

The small features between ~90 and 150cm^{-1} in the Raman spectrum of each of the doped pyrochlores can most likely be associated with the V-O bonds since they, like the modes in the 800 cm^{-1} region, are also only present in the Raman spectra of the doped pyrochlores. They are unlikely to be associated with the Ca-O bonds since these vibrations are expected to be at ~400cm^{-1} and are also expected to be weak [76]. Should they result from the V-O bonds, then they would belong to bonds with bond lengths of ~2.58 and 2.80Å, respectively. These are long compared to the other bond lengths calculated for the V-O bonds above. It was shown in the crystal structure studies of $Mg_2V_2O_7$ [73] that while the vanadium ions exhibit apparent tetrahedral coordination, each of the distinct tetrahedra exhibit a long and weak fifth V-O bond. The first tetrahedron exhibits a fifth bond length of 2.869 Å, and the second, a fifth bond length of 2.440 Å, respectively. In addition, it has been documented that it is the ability of the V^{5+}-cation to change easily from four-fold to five- or six-fold coordination which makes the structure of compounds like $Mg_2V_2O_7$ stable when similar diphosphate and disilicate structures are not stable [73].

The features between ~90 and ~150cm^{-1} in the Raman spectra of the tin and titania pyrochlores respectively, support the possibility of long fifth and sixth V^{5+}-O bonds in the two co-doped pyrochlores. Since the calcium ions are larger than the yttrium ions that they are substituting for, a distortion of the coordination of the adjacent vanadium ion is very likely. A distortion of the $[BO_6]$ octahedron has been shown to be dependent on the A-cation. It has been shown elsewhere that highly polarizable ions such as Ti^{4+}, Zr^{4+}, Nb^{5+} and Ta^{5+} with nd^0 electronic configurations can induce a distortion of the position of the B-cation leading to dynamic disorder [57]. An example of this is $Y_2Ti_2O_7$. Its structure, as determined by X-ray methods, was shown to be only statistically cubic [57]. The V^{5+}-cation also has a nd^0

configuration and this is consistent with the broad V-O bands in the co-doped pyrochlores. It has also been shown that the Raman spectra of pyrochlores are strongly influenced by very slight variations in the structural geometries of the $[BO_6]$ or $[AO_8]$ polyhedra [57] (section 4.3.1 above). That the entire structure is under pressure is also evident from the fact that the Raman bands belonging to the host lattice of the respective pyrochlores are broader in the co-doped pyrochlores than in the undoped pyrochlores.

From table 4.5 above it is readily seen that the V-O bands in the Raman spectrum of the co-doped titanium pyrochlore are ~25 cm^{-1} higher than the same bands in the Raman spectra of the tin pyrochlore. This is expected since the unit cell of the titanium pyrochlore is smaller than that of the tin pyrochlore. Since there is less space in the lattice of $Y_2Ti_2O_7$ the V-O bond lengths are expected to be shorter, resulting in the respective bands appearing at higher wave numbers. The fact that the V-O bands in $Y_2Ti_2O_7$ are at higher wave numbers than in $Y_2Sn_2O_7$ discounts the possibility that the colour of the pigments and the origin of the Raman bands are from YVO_4, $Ca_2V_2O_7$ or any other compound. If this were the case, the V-O Raman bands should appear at the same positions in both pyrochlores. In addition, the bands in the Raman spectra of the co-doped pyrochlores belonging to the host lattice would also remain unaffected which is not the case.

It was found that in heavily doped $Y_2Sn_2O_7$ samples YVO_4 was formed as a by-product. The Raman spectrum of such a sample (figure I-4-6 - appendix I) shows clearly the bands due to the host lattice, the V-O bands seen due to the vanadium incorporated into the host lattice structure and unique, intense bands at 260, 370, 808, 816 and 884 cm^{-1}. These bands correlate with those in the Raman spectrum of YVO_4 synthesised in this study, and recorded elsewhere [46]. These bands were not found in any of the doped $Y_2Ti_2O_7$ samples.

4.4.2.4 Vanadium-Oxygen Bond Order in $Y_2Sn_2O_7$ and $Y_2Ti_2O_7$

An empirical expression (eqn 4.2) has been developed which relates the observed Raman stretching frequency of a vanadium-oxygen bond to its bond order.

$$s(V-O) = \left[0.2912 \ln(21349/\nu)\right]^{-5.1} \qquad \textbf{equation 4.2}$$

The bond orders calculated from the Raman stretching frequencies in the calcium and vanadium co-doped pyrochlores are listed in table 4.6 below.

Table 4.6 Bond orders of the V^{5+}-O bonds in Ca^{2+} and V^{5+} co-doped $Y_2Sn_2O_7$ and $Y_2Ti_2O_7$.

	Raman Band, cm^{-1}	Bond Order
$V:Y_2Sn_2O_7$	803	1.26
	750	1.14
	145	0.15
	90	0.09
$V:Y_2Ti_2O_7$	824	1.31
	755	1.15
	154	0.16
	113	0.12

Vanadium in the co-doped pyrochlores is in its fifth oxidation state and so, theoretically, the valence sum of the bonds should be equal to 5. This has been shown to be true for numerous V^{5+} compounds in tetrahedral, pentacoordinated and octahedral coordination [68]. The divanadate substitution discussed in section 4.4.2.3 would result in there being one bridging V-O bond (803 and 824cm^{-1} respectively), three slightly longer outer V-O bonds (750 and 755cm^{-1} respectively) and two long V-O bonds (~150 and ~100cm^{-1}, respectively). This would result in a valence sum of 4.92 for the tin pyrochlore and 5.04 for the titanium pyrochlore. The higher valence sum for vanadium in the titanium pyrochlore is due to the unit cell of this pyrochlore being smaller which results in shorter V-O bonds. Although these valence sum calculations support the divalent structure discussed above, it should be noted that they are rough estimates. The Raman bands are broad and it is

possible that there are other V-O bands hidden under the host lattice bands. In addition, strictly speaking, valence sum calculations can only be calculated accurately for coordination states were all M-O bonds are of equal length. While the valence sums calculated above are an average value for the bonds, they are very close to the expected value of 5.

4.5 CONCLUSION

4.5.1 SYNTHESIS

Undoped $Y_2Sn_2O_7$ and $Y_2Ti_2O_7$ were successfully synthesised at high temperatures. The resulting products were fine white powders. These pyrochlores were also synthesised at temperatures of as low as 1150°C using sol-gel methods. Calcium and vanadium co-doped $Y_2Sn_2O_7$ and $Y_2Ti_2O_7$ were also successfully synthesised at high temperatures. It was found that the intensity of the pigments increased if the pigment was synthesised at higher temperatures but that the increased temperatures did not effect the particle size of the product noticeably. For the tin pyrochlore, the best results were obtained at temperatures of ~1450°C. A pigment with sufficiently intense coloration was also synthesised at 1300°C. At 1450°C, the titanium pyrochlore was found to sinter. The best results for the co-doped titanium pyrochlore were obtained at ~1300°C. It was not possible to synthesis the co-doped pyrochlores at temperatures as low as 1150°C using the sol-gel method or various mineraliser mixtures.

The co-doped pigments were subjected to acid leaching treatments and were found to be stable with no visible alteration or discoloration occurring. It addition, the pigments were also applied to tiles as part of the glaze mixture. The results were found to be satisfactory. They are not discussed here in any detail since the optimisation of the glaze and firing conditions is not a trivial matter and was beyond the scope of this investigation.

4.5.2 SPECTROSCOPY

The vibrational spectra were recorded of the undoped pyrochlores. Both the infrared and the Raman spectra were found to be in good agreement with those recorded elsewhere. The electronic spectra were recorded of the calcium and vanadium co-doped pyrochlores. They indicated the possibility of recording the pre-resonance Raman spectra of the doped pyrochlores. The vibrational spectra of the doped pyrochlores were recorded and new bands were found in the Raman spectra which could be assigned to the V-O bonds in the doped pyrochlores.

Four Raman bands were found which indicate that the vanadium has been incorporated into the lattice of the hosts. In all cases, the bands were found to be at higher wavenumbers in the titanium pyrochlores than in the tin pyrochlores. This is to be expected since the unit cell of the titanium pyrochlore is smaller. Consequently, the possibility of the yellow coloration coming from another compound was discounted.

While the exact coordination of the calcium and vanadium cations could not be determined unequivocally, strong evidence was found which shows that the calcium cations substitute for the yttrium cations and that the vanadium cations substitute for the tin or titania cations. Evidence was also found which shows that the entire host lattice is under pressure from the dopants.

Bond lengths were calculated for the V-O bonds from the Raman bands. In both cases two bond lengths were found which suggest that the vanadium is tetrahedrally coordinated within the pyrochlores. In addition, two long bond lengths were calculated for each of the pyrochlores. Consequently, it is most likely that the vanadium ions are octahedrally coordinated with four rather short bonds and two weak long bonds. This is supported by the bond order calculations. This has been shown to be the case for various other vanadium compounds which crystallographically appear to have a distorted tetrahedral coordination but in addition have an extra long bond. The broad V-O bands in these compounds most probably reflect disordered polyhedra in which the V^{5+}-ions occupy a site symmetry lower than D_{3d}, the site symmetry of the B-ions in $A_2B_2O_7$ pyrochlores.

Chapter 5

Conclusion

5.1 SOLID STATE CHEMISTRY

Solid state chemistry is one of a number of different disciplines involved in the broad field of material science research. Others include solid state physics and metallurgy. Material science relies heavily on a broad spectrum of disciplines with the various disciplines all contributing to the big picture. No one discipline can provide all of the answers. Solid state chemistry is a particularly useful discipline for the investigation of materials. This is because it is able to combine the two important aspects of material science. The first is that of synthesis. The solid state chemist is able to synthesise new materials based on a detailed understanding of the elements and of existing materials. This understanding of existing materials leads to the second favourable aspect of solid state chemistry, that of characterisation. The solid state chemist is able to characterise the materials synthesised using numerous techniques at his or her disposal and consequently to synthesise new materials based on this characterisation.

This solid state chemical investigation proceeded along the lines of these two important aspects of material science, namely synthesis and characterisation.

5.2 CERAMIC PIGMENTS

The chemistry of ceramic pigments is more often than not complicated. To a large extent ceramic pigment synthesis takes place on an empirical basis. Even in the most modern production facilities, pigments are synthesised in batches which tend to have colour properties which vary. The different batches are then blended together to yield a pigment with the desired pigmentation properties. The methods are often not well understood and reproducibility is often poor.

The reasons for the lack of knowledge about these pigments are numerous. They include the fact that the different types of ceramic pigments often have properties that vary substantially, even within the same family of pigments; the pigments are synthesised at high temperatures which makes the investigation of the synthesis mechanism difficult and, the literature available on these types of materials is not abundant and often vague. Certainly, one of the most difficult

properties of ceramic pigments to investigate, and one of the most important, is the origin of the colour of the pigments which results from the interaction of the host lattice with the very small quantities of dopant(s). This is because the host lattice tends to obscure the details of the very small amounts of dopant(s) present.

As stated in chapter 1, the vast number of elements that can potentially make up the host lattice, and the vast number of elements that might be used as dopants, and the vast number of compounds that might be useful as mineralisers, and the diverse conditions of synthesis make it an enormous, if not impossible task to synthesise new pigments or optimise pigment synthesis on an empirical basis. Consequently, what is needed for more efficient ceramic pigment synthesis, and the development of new pigments, is a better understanding of these pigments.

A better understanding of the chemical state of the dopant(s) within the host lattice will result in an informed approach to the design of new pigments. The knowledge of how the dopants interact with the host lattice in existing pigments can be combined with existing ionic ion radii data and other data on uncoordinated and coordinated ions to adapt existing pigments, and ultimately, design and synthesis new ones.

In the current investigation, numerous pigments were synthesised and the illusive chemical states of the dopants within the host lattices were revealed. With the information gained from this investigation, it was possible to design and synthesis materials with potential for use as new pigments. For completeness sake, some of these compounds are listed and briefly discussed in section 5.5 below.

5.3 SYNTHESIS OF THE PIGMENTS

The pigments synthesised in this investigation had to comply with different criteria. They had to be of suitable quality for application to ceramic articles, and for their characterisation. These two criteria do not necessarily amount to the same thing. For example, for most characterisation techniques, the more

crystalline the reaction product the better. Higher crystallinity is however not necessarily desirable for a pigment that is to be applied to a ceramic article since it results in a larger particle size. Furthermore, the higher temperatures required to synthesis more crystalline pigments are expensive on an industrial scale, and therefore not desirable. Another example may be found in the chromium doped malayaite pigment which was found to have greater stability when applied to a ceramic article if an excess of silica was used in the synthesis of the pigment. For characterisation purposes however, the excess silica is a problem since it can obscure or distort the characterisation of the properties of the pigment under investigation.

For the synthesis of pigments for application to ceramic articles, several factors were taken into account. The pigment should have the most intense colour possible, and be synthesised as cheaply as possible. These two criteria also tend to work against each other. For example, a more intense pigment is generally obtained at higher temperatures, but the higher temperatures result in higher manufacturing costs. Furthermore, the higher temperatures tend to result in larger particle sizes which is also an undesirable effect. This is however not always the case. Examples are the pyrochlore pigments investigated here where higher temperatures did not seem to affect their particle size noticeably.

It is noteworthy that no two pigments behave the same way when being synthesised. Examples of this include the two pyrochlore compounds investigated here, and the doping of malayaite with chromium as opposed to doping with a different chromophore. In the first example, the tin analogue can be calcined at much higher temperatures to produce a more intense pigment. However, at these higher temperatures, the titanium analogue sinters. In the second example, malayaite was also successfully doped with cobalt (see section 5.5 below). A large difference is found in the crystallinity of the chromium doped malayaite and cobalt doped malayaite. Small amounts of cobalt were found to enhance the crystallinity of the reaction product substantially. Consequently, malayaite containing cobalt was found to sinter at temperatures where malayaite containing chromium did not.

In all cases, pigments were synthesised that were of high purity and crystallinity, to be suitable for characterisation. The synthesis was also adapted to be more cost effective and produce a pigment of quality suitable for colouring ceramic articles.

5.4 CHARACTERISATION OF THE PIGMENTS

All pigments synthesised were characterised on a macroscopic scale, and on a microscopic scale. The macroscopic investigation involved the characterisation of the host material and the microscopic investigation involved the characterisation of the guest chromophores or dopants within the host lattice.

The host lattice was characterised using X-ray techniques and scatting electron microscopy (SEM). The X-ray powder diffraction results showed that all host materials can be found as naturally occurring minerals. X-ray powder diffraction was used to determine whether the desired reaction products had been formed, whether by-products had been formed, and whether raw materials had been left unreacted. It was also useful for estimating the amount of reaction products and raw materials left after calcining. SEM analysis was useful in quantifying the ratio of the elements of the host materials present after calcining. This is a useful technique for determining whether any raw materials are lost during the calcining process.

The guest chromophores were characterised inside their host lattices using SEM analysis, electronic spectroscopy and vibrational spectroscopy. SEM analysis was useful in showing that the dopants were indeed present in the host lattice after calcining. Unfortunately, it could not be used to quantify these amounts since the technique could not produce reproducible results at the low concentration levels at which the dopants are present. X-ray techniques could not provide any information about the chromophores since they are present in such small quantities. X-ray techniques look at bulk properties. They can yield information about the host lattice surrounding the chromophore, but no information about the chromophore itself. It is noteworthy that even when a pure

sample of host lattice material is being investigated, X-ray techniques can only yield information about long range properties of the material being investigated. A good example of this is the high temperature phase of titanite (T>500 K) where X-ray techniques show the space group to be C2/c. Raman studies conducted in this investigation and elsewhere show however that titanite above ~500 K exists rather as a mixture of $P2_1/a$ domains, the statistical average of which is perceived as C2/c by X-ray techniques. In fact, Raman spectroscopy is one of the few techniques able to focus on short range properties, even on an atomistic scale as demonstrated in the current investigation where the properties of a single atom isolated in a bulk host material were investigated.

Electronic and vibrational spectroscopy were used to elucidate the chemical state of the dopants within the host lattices. In all cases, resonance Raman spectroscopy was successfully applied to investigate the interaction of the host lattice with the guest chromophore. It is this interaction which results in the colour of the ceramic pigment. The strength of resonance Raman spectroscopy lies in its ability to selectively enhance the vibrational modes of the chromophores in the host lattice by a factor of 10^3 to 10^5. The resonance Raman effect is achieved by irradiating the pigment with a laser excitation line whose energy corresponds to that of the electronic transition of the chromophoric group in the host lattice.

The chemical state of chromium in malayaite was revealed. The chromium was found to substitute for tetrahedrally coordinated Si of C_2 site symmetry in malayaite, $CaSnOSiO_4$, and to be present in the relatively uncommon +4 oxidation state rather than the more common and generally more stable +3 or +6 oxidation states. An average Cr-O bond length for the chromium in malayaite of 1.752 Å was calculated which is in good agreement with Cr(IV)-O bonds in similar complexes. The ionic radii sum of Cr(IV) and O is larger than that of Si(IV) and O, and larger than the Cr(IV)-O bond calculated for chromium in malayaite. Consequently, the Cr-O bond was shown to have strong covalent character.

Furthermore, an average bond order of 1.05 was calculated for the Cr(IV)-O bond in Cr^{4+}:$CaSnOSiO_4$ which is well within the range expected for tetra coordinated Cr(IV). The force constants were calculated for Cr(IV)-O in malayaite. All of these parameters combine to yield a detailed analysis of the coordination chemistry of chromium in malayaite.

The chemical state of chromium in titanite was also determined. It was found to be in an oxidation state of +4 and to substitute for tetrahedrally coordinated Si, as was the case for Cr^{4+}:$CaSnOSiO_4$. Consequently, the Cr(IV) is in tetrahedral coordination. Bond lengths of 1.700 and 1.729 Å, and an average bond order of 1.18 were calculated for the Cr(IV)-O bond in Cr^{4+}:$CaTiOSiO_4$. These are in good agreement with those of chromium doped malayaite, the differences being attributed to the slightly smaller unit cell of titanite. The force constants calculated for chromium in titanite were also found to be in reasonable agreement with those of chromium in malayaite.

The resonance enhanced Raman modes in Cr^{4+}:$CaTiOSiO_4$ were subsequently used to investigate the high temperature reversible antiferroelectric-paraelectric phase transition which titanite undergoes at ~500 K, and which has been the object of extensive research since 1976. The Cr(IV) substituted into the host lattice was found to be very sensitive to the structural phase transition, without appearing to affect the phase transition mechanism. The current study shows strong support for a transition mechanism whereby the phase transition below T_c may be described by a 2D Ising model, while the high temperature phase between ~500 K and ~825 K is a statistical average of small domains of $P2_1/a$ titanite as opposed to the Ti-ions shifting to the geometric centres of the $[TiO_6]$ octahedra. This is evident from the fact that bands which should disappear if the Ti-ions shift to the geometric centres of the $[TiO_6]$ octahedra do in fact not disappear.

The resonance enhanced Raman modes in Cr^{4+}:$CaTiOSiO_4$ were also used to investigate the high pressure reversible antiferroelectric-paraelectric phase transition which titanite undergoes. The high pressure phase transition of titanite

has not been extensively investigated. It has been reported that titanite has a low pressure $P2_1/a$ phase below ~21 kbar, and a high pressure A2/a phase above ~69 kbar. The mechanism for the transition is proposed to be different to that of the temperature phase transition in that the A2/a phase is as a result of the actual centring of the Ti atoms in the $[TiO_6]$ octahedron rather than the statistical average of small domains of differently orientated $P2_1/a$ domains.

The current investigation suggests that this is however not the case. If this were the case, some of the Raman bands of Cr^{4+}:$CaTiOSiO_4$ would be expected to disappear as the symmetry of the host lattice increases. This does not appear to be the case however. Consequently, the high pressure phase is most likely a statistical average of small domains of differently orientated $P2_1/a$ domains as was the case in the temperature phase transition. Evidence was found for the existence of a soft mode (a Ti-O mode) which could possibly be responsible for driving the phase transition. Furthermore, the pressure at which the phase transition occurs was determined to be ~27.5 kbar.

The chemical state of vanadium in the pyrochlore compounds was also determined, though the exact coordination could not be elucidated unequivocally. The colour of the pyrochlore base pigments was found to be due to the co-substitution of Ca(II) and V(V) for Y(III) and Ti(IV) or Sn(IV) as the case may be. The resulting substitution of a 3+ and a 4+ -ion by a 2+ and a 5+ -ion preserves the electroneutrality of the host lattice. It was shown unequivocally that the colour of the pigments is as a result of the co-doping of the host lattice and not as a result of the formation of products other than the pyrochlores. The vanadium was found to be coordinated in a rather unusual fashion, exhibiting both tetrahedral and octahedral vanadium bonding characteristics. Strong evidence exists that the co-substitution results in local disordering of the host lattice.

5.5 THE SOLID STATE CHEMISTRY OF SOME TITANIA- AND TIN ..... *AND OTHER PIGMENTS*

The ideal situation for ceramic pigment synthesis and pigment synthesis in general is to have a knowledge of the pigments that allows for new pigments to

be designed and synthesised. In the current investigation, the properties of some ceramic pigments were revealed. This information was subsequently used successfully to synthesis various other related materials which show good potential for use as ceramic pigments or related materials. Some of these materials are listed below.

- Malayaite was doped with cobalt. The result was a blue pigment. Titanite was also doped with cobalt. The result of this reaction was a brown pigment. The chemical state of cobalt has still to be clarified. It appears to be in its +2 oxidation state in malayaite. It is highly unlikely that it substitutes for Ca^{2+} however since cobalt does not generally form such long bonds. Substitution of Sn^{4+} or Si^{4+} creates problems with the electroneutrality of the compound. Further work is required in the elucidation of the chemical state of cobalt in malayaite and titanite.

- Malayaite and titanite were co-doped with various transition metal ions and various lanthanide elements and yttrium. Rare earth elements have been shown to substitute for calcium in titanite [77;78]. They have 7 coordination ionic radii which are close to that of 7 coordinated calcium. Yttrium, lanthanum, cerium, praseodymium and neodymium were separately co-doped with the some of the first row transition metal atoms. Since the most favourable oxidation state of all of these rare earth elements is +3, and the only oxidation state of yttrium is +3, substitution of a Ca^{2+} by a M^{3+} will result in an extra positive charge. This should then allow for the substitution of a Si^{4+} or Sn^{4+} by a M^{3+}. Various interesting results were obtained. An example is the co-substitution of these rare earth elements and cobalt. Whereas the substitution of cobalt on its own produced a blue pigment, the co-substitution of cobalt with the above mentioned elements yields a pigment with an intense green colour. The properties of these co-doped malayaite and titanite materials require further investigation.

- Another co-doping reaction carried out was that of the co-doping of zircon with cerium and praseodymium to produce an orange pigment. Zircon yellow is zircon doped with praseodymium alone.

- Numerous other reactions were carried out based on the findings of the investigation of the other pigments.

From this solid state chemical investigation of some titania- and tin pigments it is clear that no two pigments behave in the same manner. They all require specialised synthesis techniques, and they all have unique properties. The scope for work in this field is immense. This includes work not only on pigments, but also related material like catalysts for example. The technique, used in this study to investigate the behaviour of materials (the phase transitions of titanite) must surely also find application in the investigation of other materials. Indeed, it will be through a greater understanding of the complex nature of ceramic pigments and related materials, that new pigments, better pigments, and other useful materials will be synthesised.

Appendix I

Vibrational and Electronic Spectra

I-1 LIST OF SPECTRA

I-2 VIBRATIONAL AND ELECTRONIC SPECTRA OF CHAPTER 2

I-2.1 Raman Spectra of Malayaite and Chromium Doped Malayaite

Figure I-2.1 Raman spectrum of undoped $CaSnOSiO_4$ in the wave number ranges of (a) 2800 - 200cm^{-1}, and (b) 400 - 50cm^{-1} (micro).

Figure I-2.2 Raman spectrum of chromium doped $CaSnOSiO_4$ (micro - 1%Cr).

Figure I-2.3 Raman spectrum of a bulk polycrystalline sample of chromium doped $CaSnOSiO_4$ (Macro - 1%Cr).

Figure I-2.4 Raman spectrum of a bulk polycrystalline sample of chromium doped $CaSnOSiO_4$ (Macro - 2%Cr).

Figure I-2.5 Raman spectrum of a bulk polycrystalline sample of chromium doped $CaSnOSiO_4$ showing progressions (ν_n (n = 2,3)) and subsidiary progressions ($\nu_n + v.\nu_1$ (v = 1,2)(n = 2,3)) of the Raman modes (Macro - 1%Cr).

I-2.2 Electronic Spectra of Chromium Doped Malayaite

Figure I-2.6 The diffuse reflectance electronic spectrum of chromium doped $CaSnOSiO_4$.

I-3 VIBRATIONAL AND ELECTRONIC SPECTRA OF CHAPTER 3

I-3.1 Raman Spectra of Titanite and Chromium Doped Titanite

Figure I-3.1 Raman spectrum of undoped $CaTiOSiO_4$ (micro).

Figure I-3.2 Raman spectrum of chromium doped $CaTiOSiO_4$ (Macro-0.5%Cr).

Figure I-3.3 Raman spectrum of chromium doped $CaTiOSiO_4$ at 290 and 510 K (Macro -0.5%Cr).

Figure I-3.4 Raman spectrum of chromium doped $CaTiOSiO_4$ at 3.1, 35.2 and 45.8 kbar (Macro - 0.5%Cr).

I-3.2 Electronic Spectra of Chromium Doped Titanite

Figure I-3.5 Diffuse reflectance electronic spectrum of chromium doped $CaTiOSiO_4$.

I-4 VIBRATIONAL AND ELECTRONIC SPECTRA OF CHAPTER 4

I-4.1 Raman Spectra of Undoped and Calcium and Vanadium Co-Doped $Y_2Sn_2O_7$ and $Y_2Ti_2O_7$

Figure I-4.1 Raman spectrum of undoped $Y_2Sn_2O_7$ (micro).

Figure I-4.2 Raman spectrum of calcium and vanadium co-doped $Y_2Sn_2O_7$ (micro - 2 atom% Ca & V).

Figure I-4.3 Raman spectrum of calcium and vanadium co-doped $Y_2Sn_2O_7$ (Macro - 4 atom % Ca&V).

Figure I-4.4 Raman spectrum of undoped $Y_2Ti_2O_7$ (micro).

Figure I-4.5 Raman spectrum of calcium and vanadium co-doped $Y_2Ti_2O_7$ (micro - 2 atom% Ca & V).

Figure I-4.6 Raman spectrum of $Y_2Sn_2O_7$ and YVO_4 (Macro).

I-4.2 Electronic Spectra of Calcium and Vanadium Co-Doped $Y_2Sn_2O_7$ and $Y_2Ti_2O_7$

Figure I-4.7 Diffuse reflectance electronic spectrum of calcium and vanadium co-doped $Y_2Sn_2O_7$.

Figure I-4.8 Diffuse reflectance electronic spectrum of calcium and vanadium co-doped $Y_2Ti_2O_7$.

I-2 VIBRATIONAL AND ELECTRONIC SPECTRA OF CHAPTER 2

I-2.1 Raman Spectra of Malayaite and Chromium Doped Malayaite

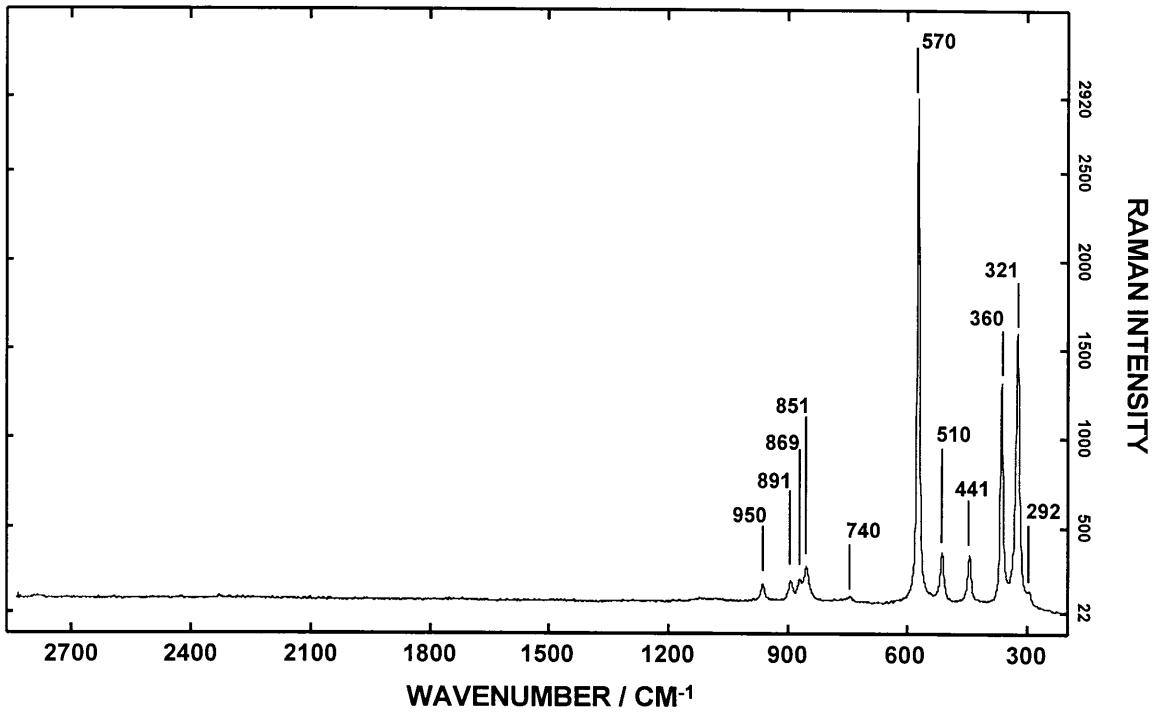

(a)

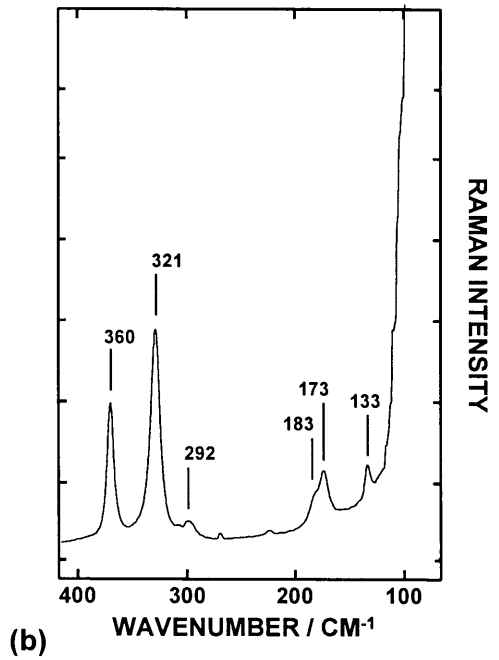

(b)

Figure I-2.1 Raman spectrum of undoped $CaSnOSiO_4$ in the wave number ranges of (a) 2800 - 200cm^{-1}, and (b) 400 - 50cm^{-1} (micro).

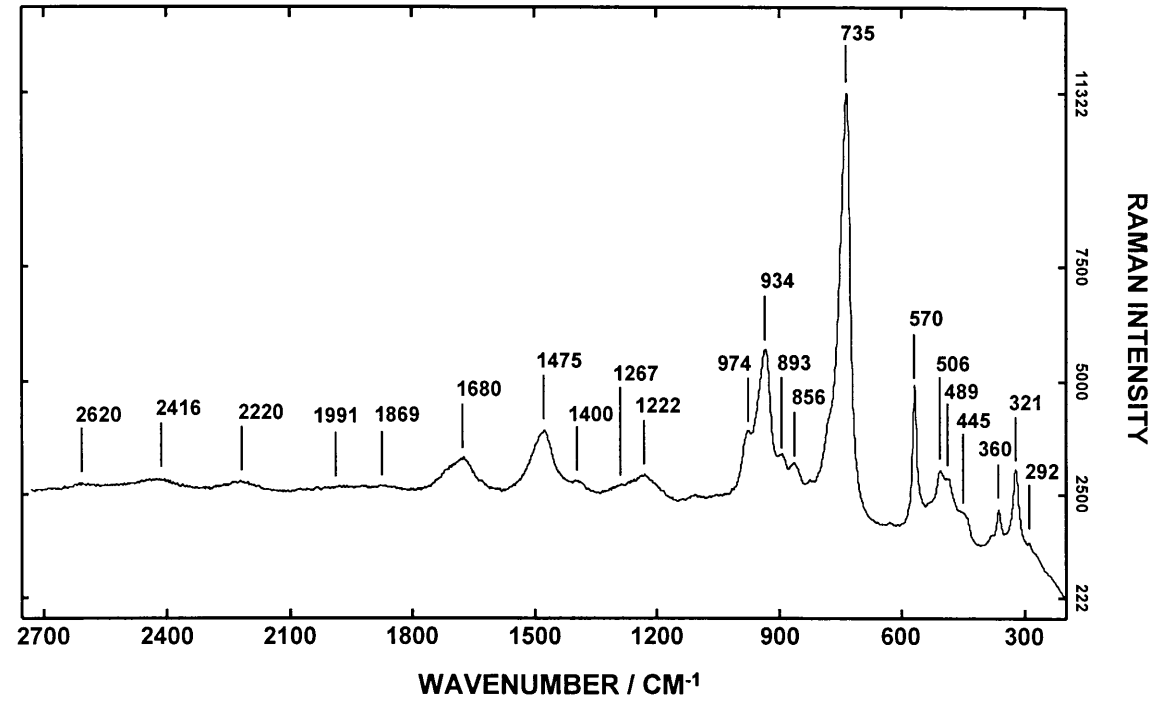

Figure I-2.2 Raman spectrum of chromium doped $CaSnOSiO_4$ (micro - 1%Cr).

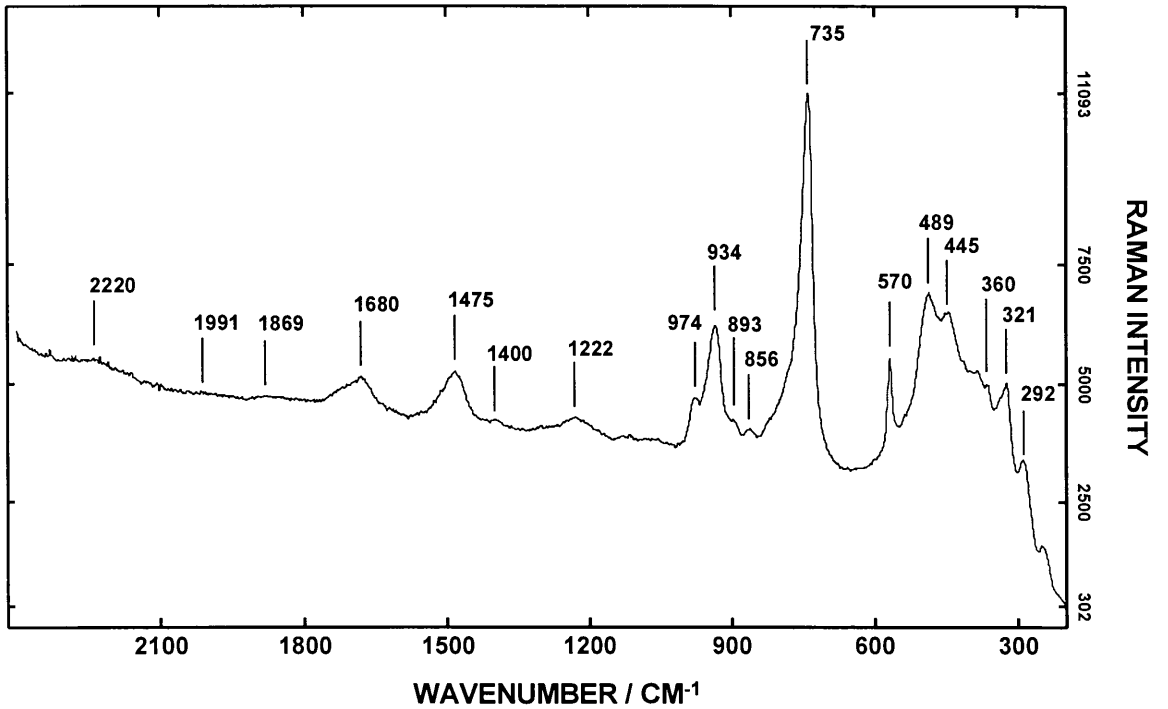

Figure I-2.3 Raman spectrum of a bulk polycrystalline sample of chromium doped $CaSnOSiO_4$ (Macro - 1%Cr).

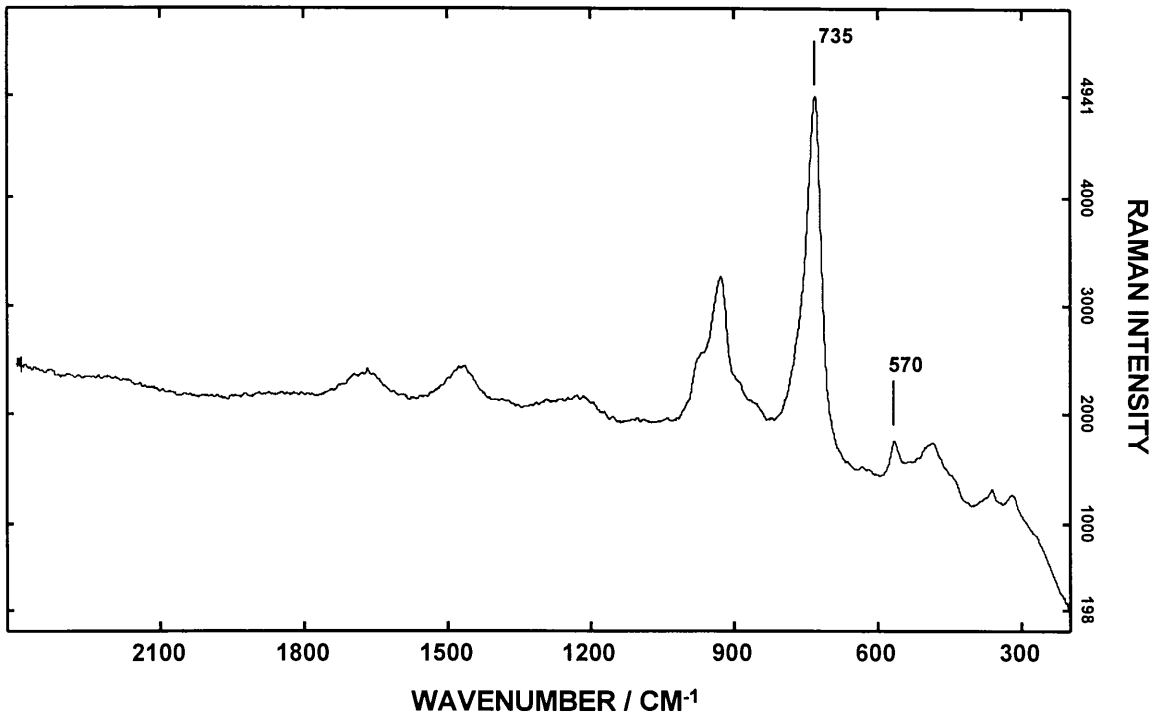

Figure I-2.4 Raman spectrum of a bulk polycrystalline sample of chromium doped $CaSnOSiO_4$ (Macro - 2%Cr).

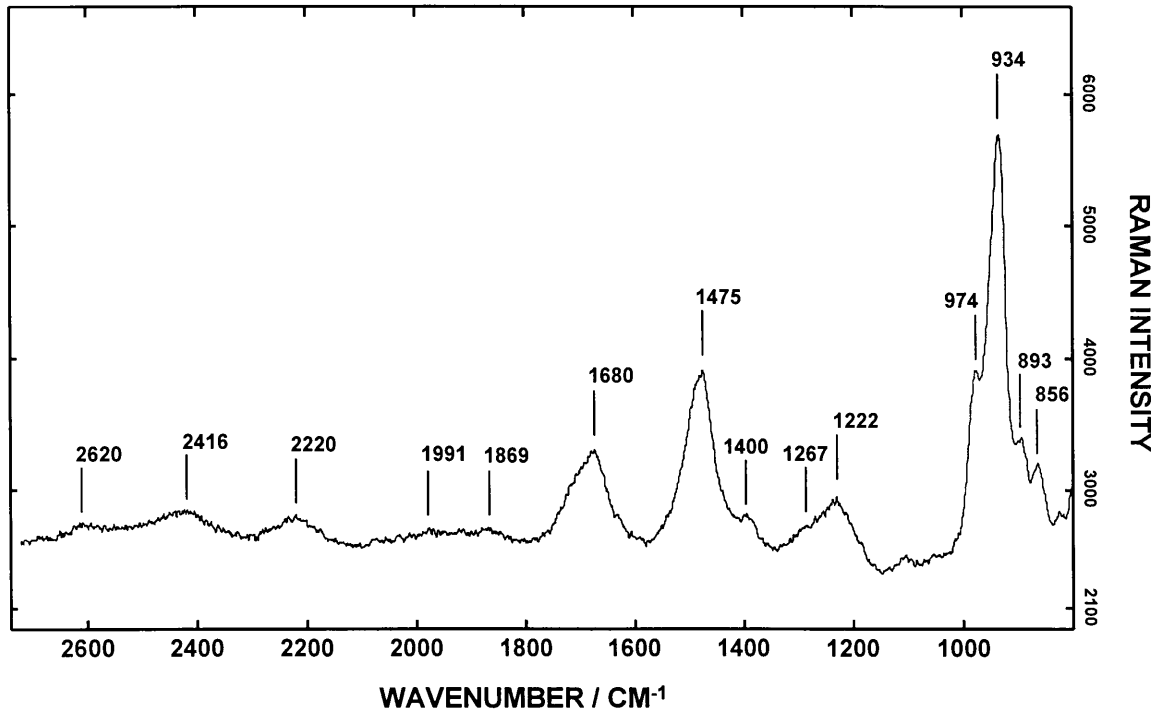

Figure I-2.5 Raman spectrum of a bulk polycrystalline sample of chromium doped $CaSnOSiO_4$ showing progressions (ν_n (n = 2,3)) and subsidiary progressions ($\nu_n + v.\nu_1$ (v = 1,2)(n = 2,3)) of the Raman modes (Macro - 1%Cr).

I-2.2 Electronic Spectra of Chromium Doped Malayaite

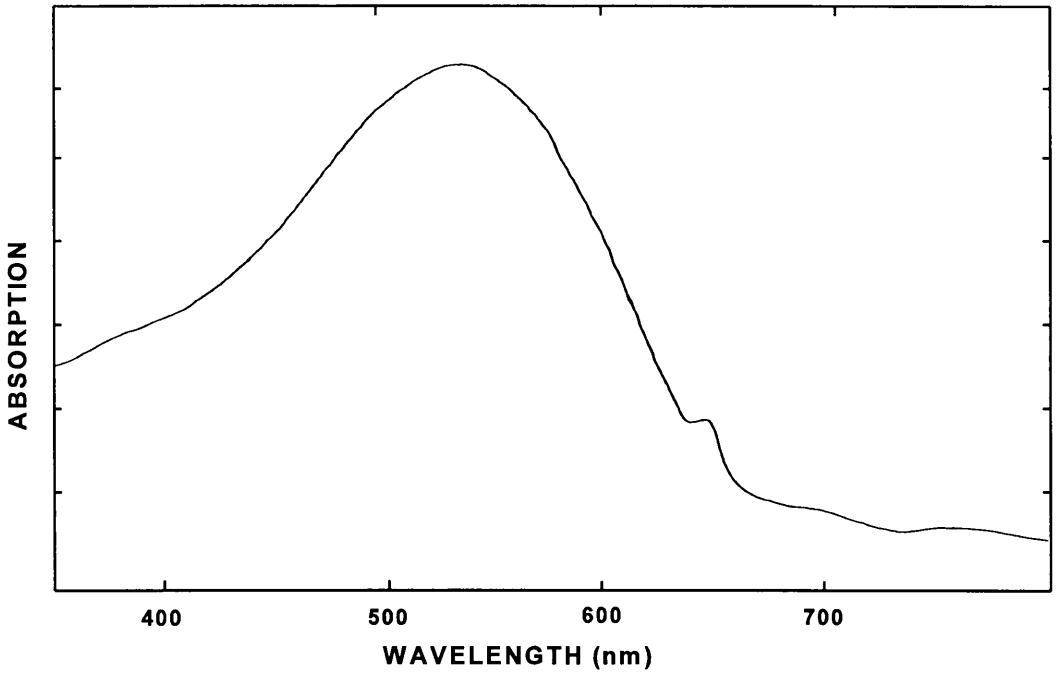

Figure I-2.6 Diffuse reflectance electronic spectrum of chromium doped $CaSnOSiO_4$.

I-3 VIBRATIONAL AND ELECTRONIC SPECTRA OF CHAPTER 3

I-3.1 Raman Spectra of Titanite and Chromium Doped Titanite

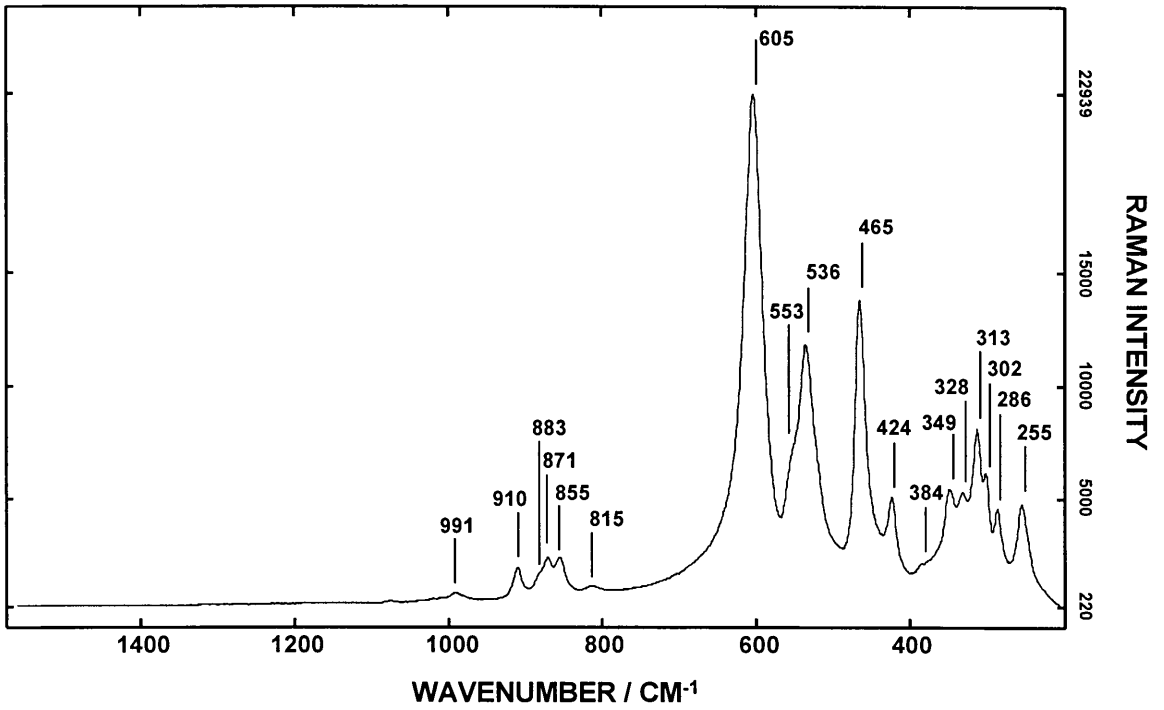

Figure I-3.1 Raman spectrum of undoped $CaTiOSiO_4$ (micro).

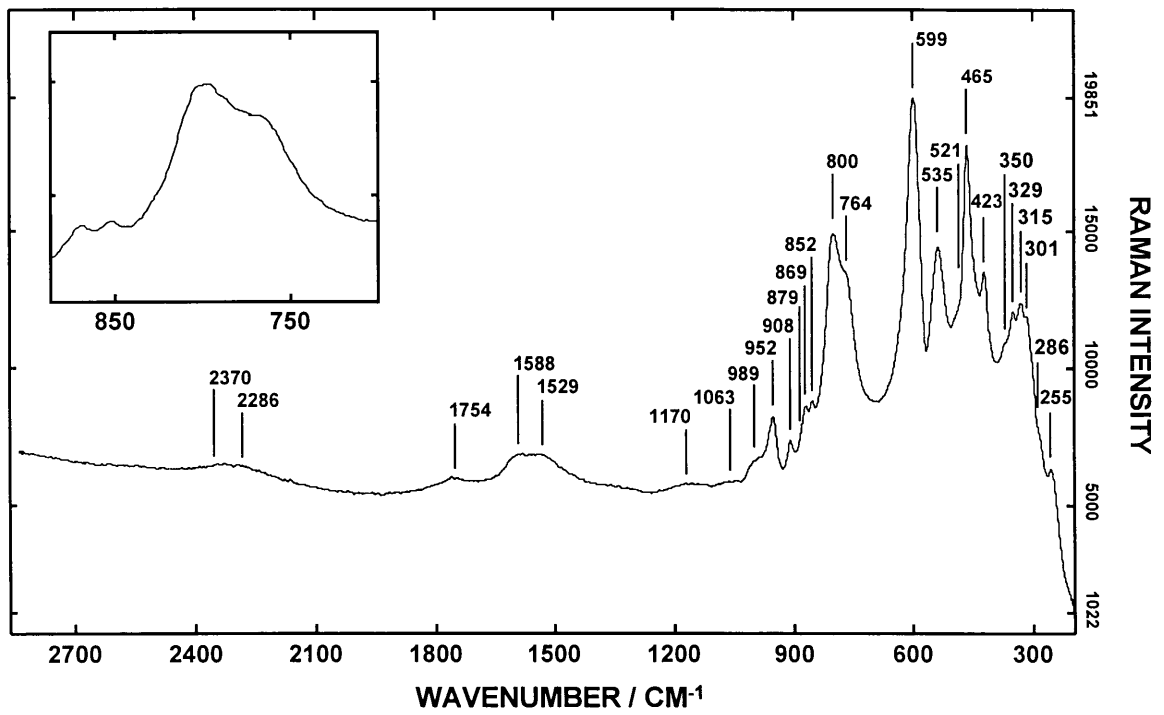

Figure I-3.2 Raman spectrum of chromium doped $CaTiOSiO_4$ (Macro-0.5%Cr).

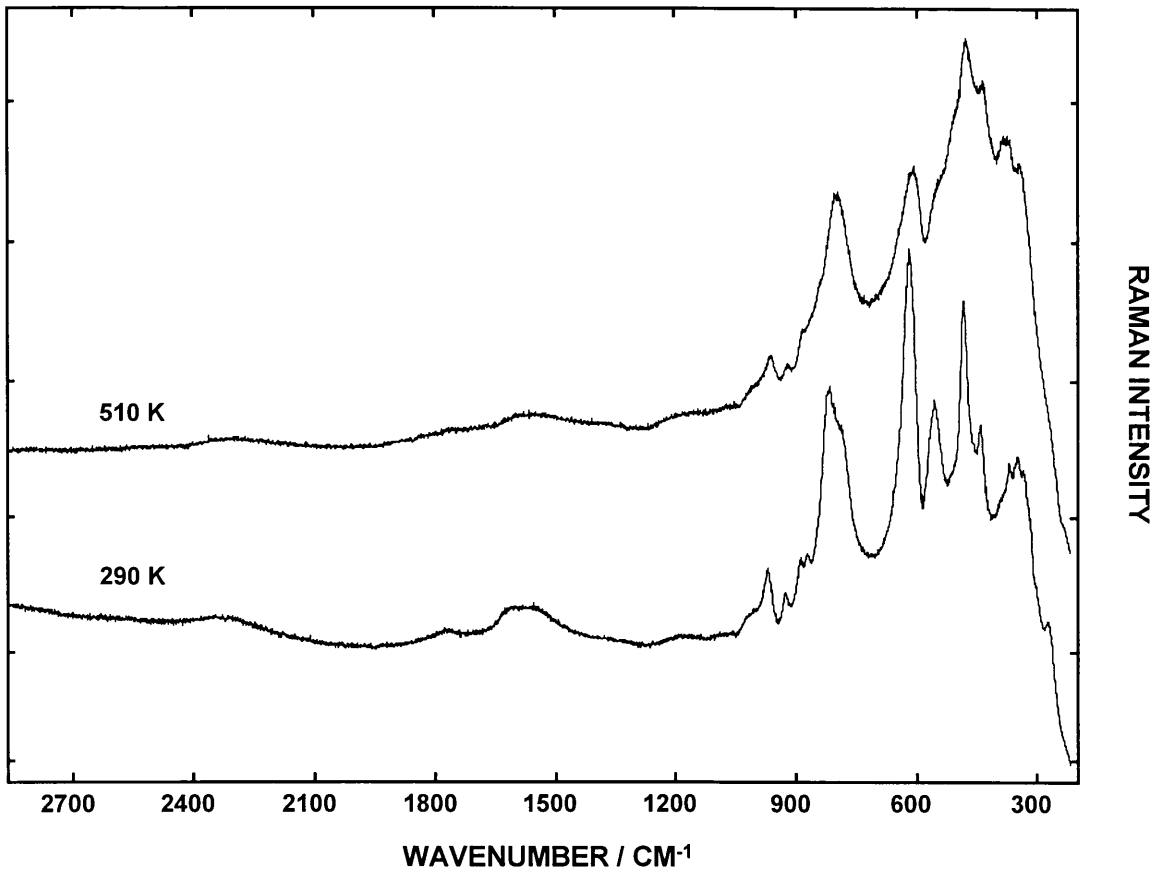

Figure I-3.3 Raman spectrum of chromium doped $CaTiOSiO_4$ at 290 and 510 K (Macro -0.5%Cr).

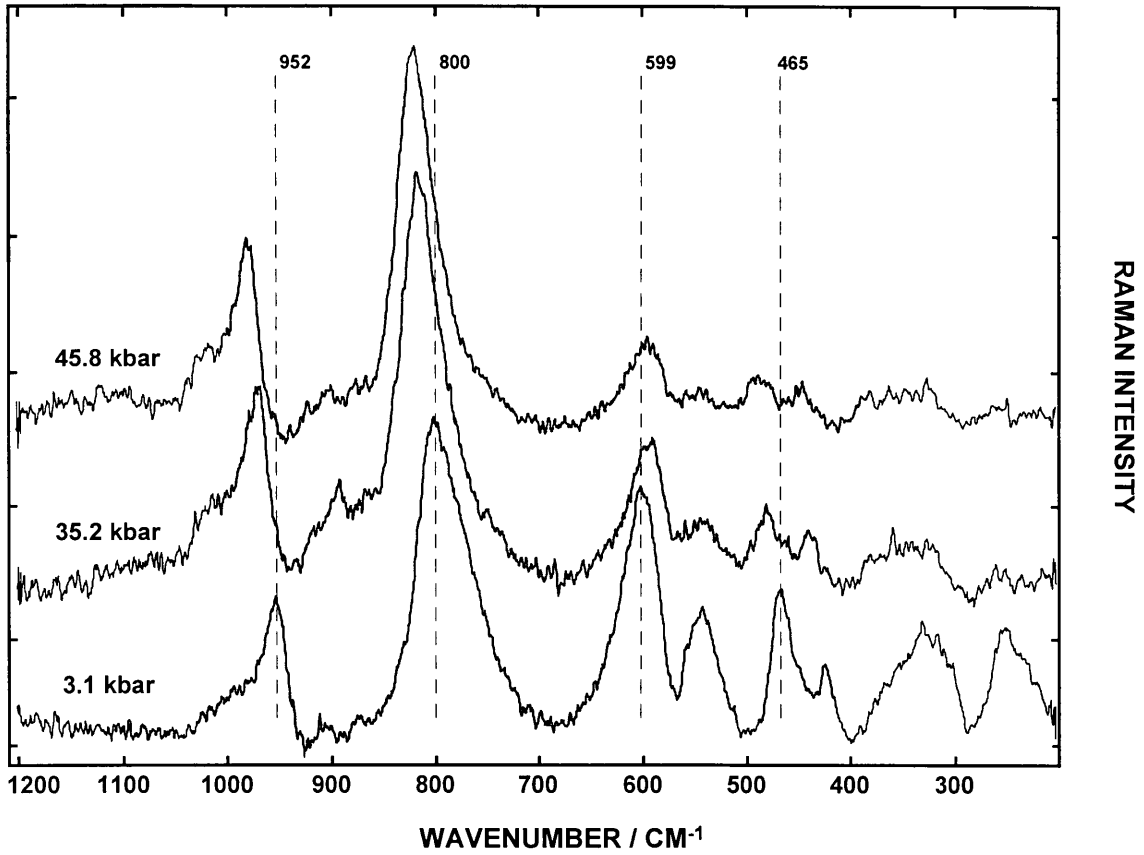

Figure I-3.4 Raman spectrum of chromium doped $CaTiOSiO_4$ at 3.1, 35.2 and 45.8 kbar (Macro - 0.5%Cr).

I-3.2 Electronic Spectra of Chromium Doped Titanite

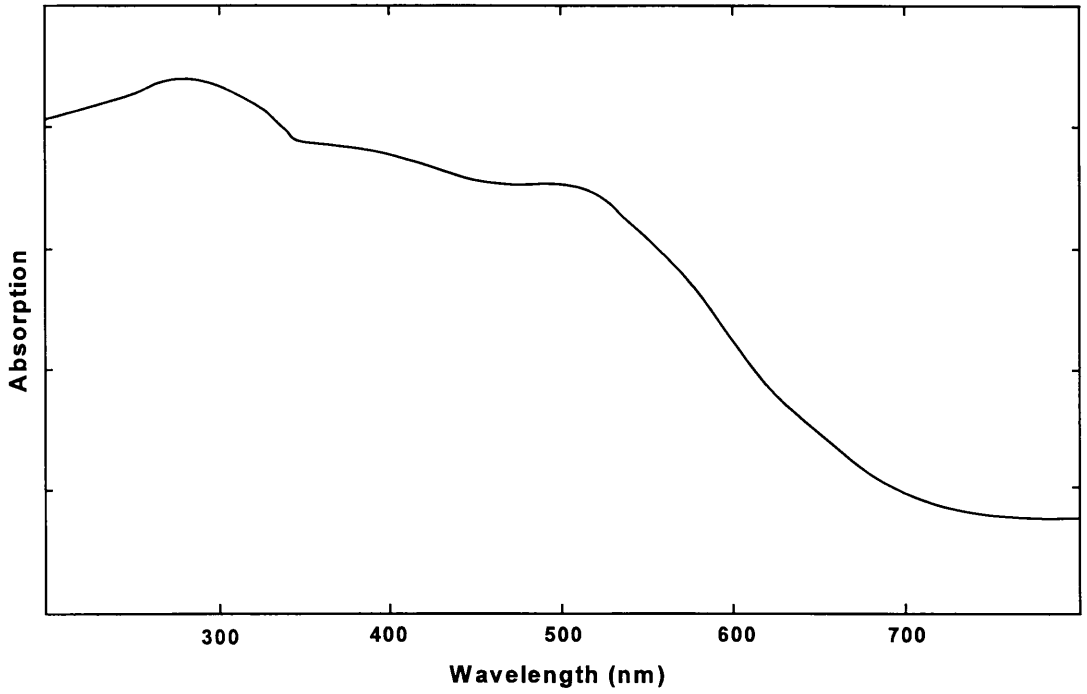

Figure I-3.5 Diffuse reflectance electronic spectrum of chromium doped $CaTiOSiO_4$.

I-4 VIBRATIONAL AND ELECTRONIC SPECTRA OF CHAPTER 4

I-4.1 Raman Spectra of Undoped and Calcium and Vanadium Co-Doped $Y_2Sn_2O_7$ and $Y_2Ti_2O_7$

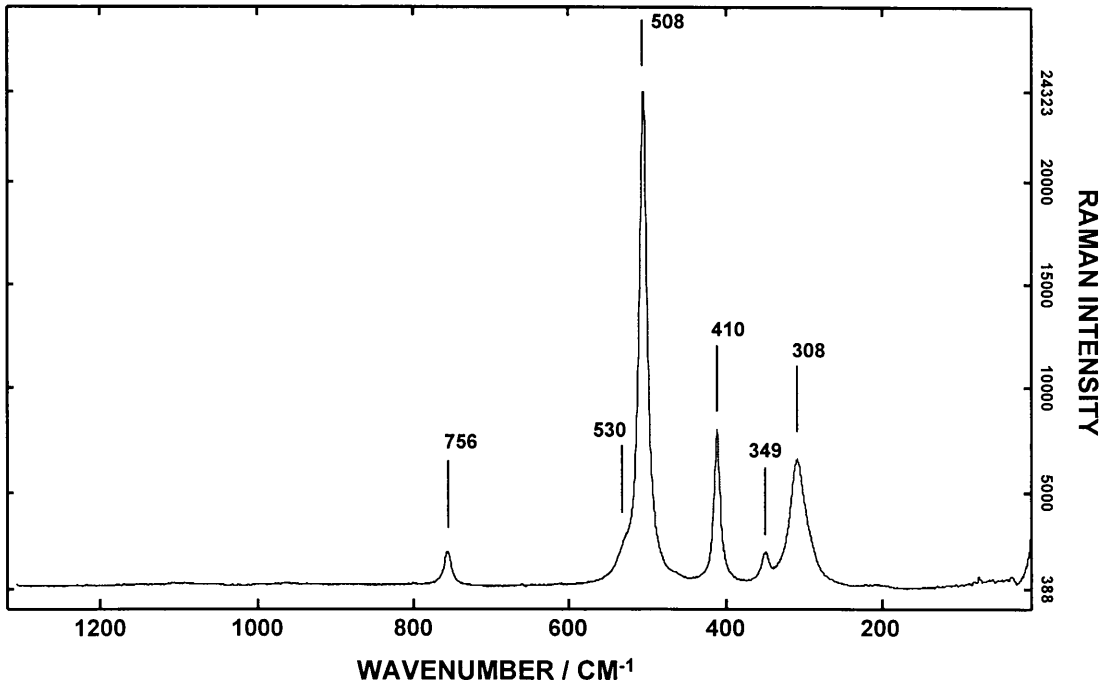

Figure I-4.1 Raman spectrum of undoped $Y_2Sn_2O_7$ (micro).

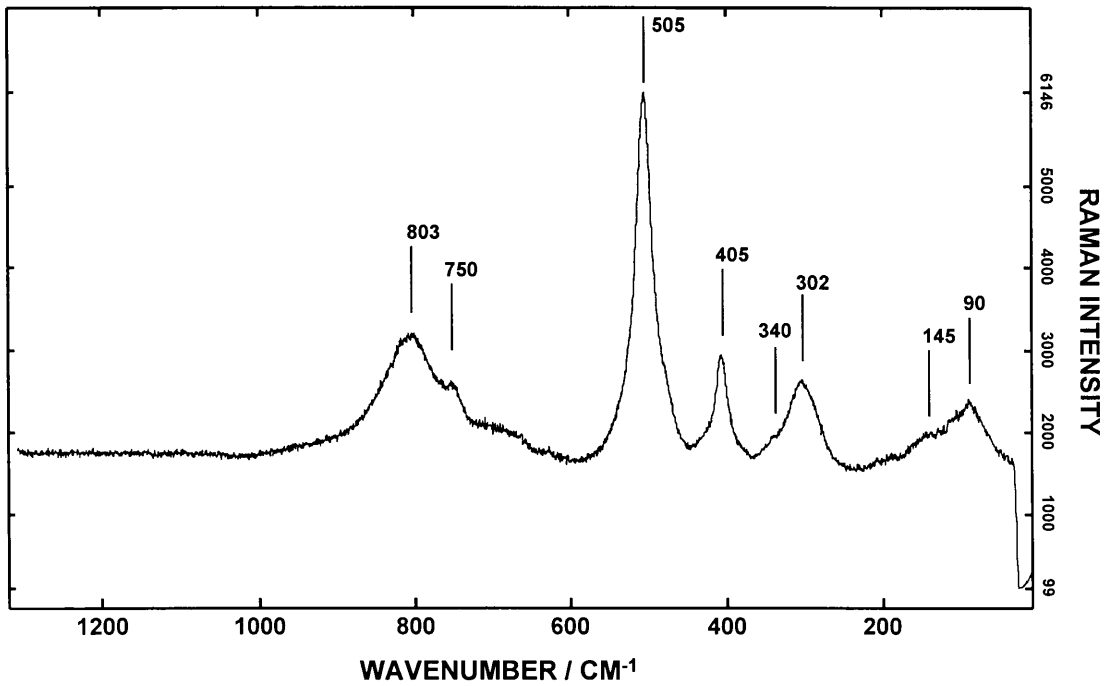

Figure I-4.2 Raman spectrum of calcium and vanadium co-doped $Y_2Sn_2O_7$ (micro - 2 atom% Ca & V).

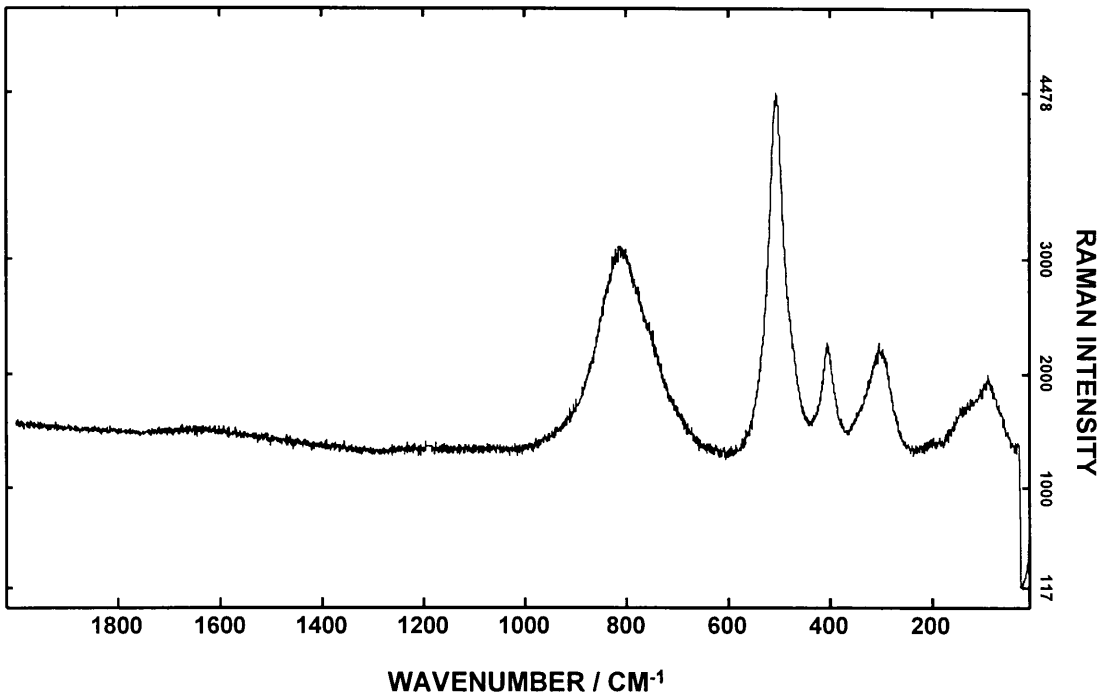

Figure I-4.3 Raman spectrum of calcium and vanadium co-doped $Y_2Sn_2O_7$ (Macro - 4 atom % Ca&V).

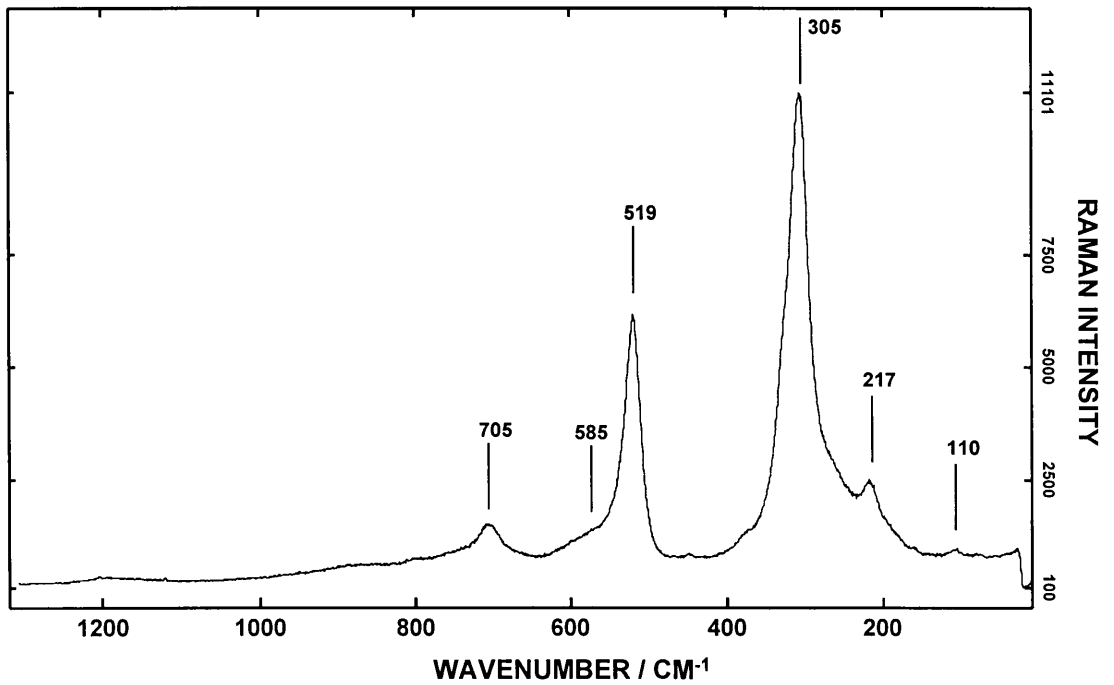

Figure I-4.4 Raman spectrum of undoped $Y_2Ti_2O_7$ (micro).

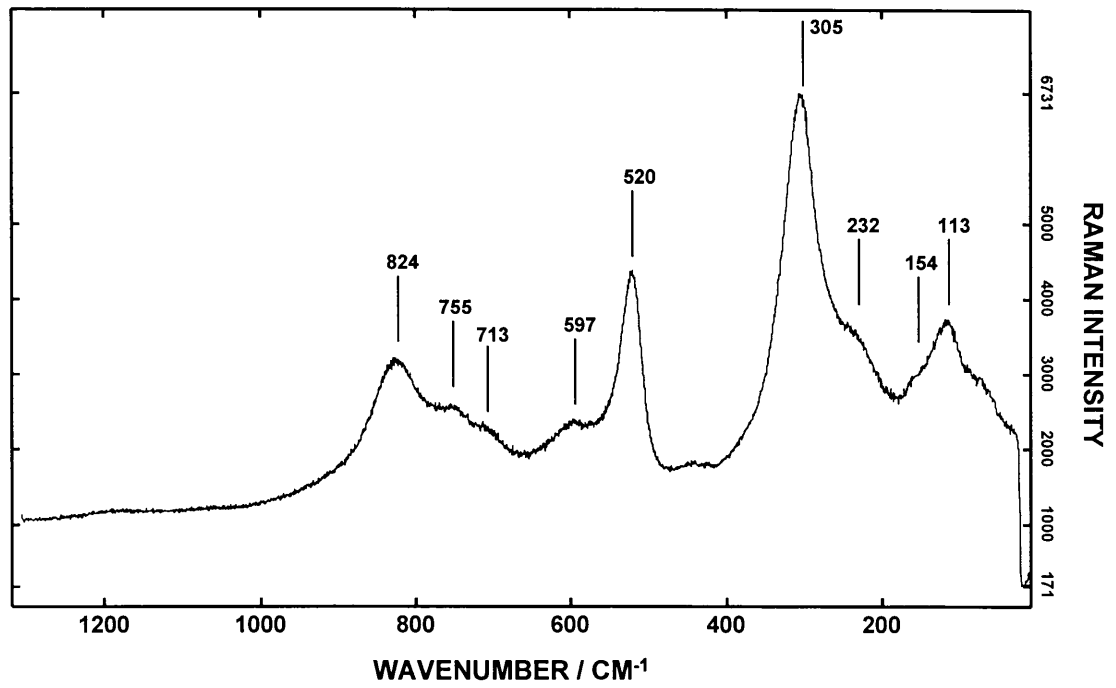

Figure I-4.5 Raman spectrum of calcium and vanadium co-doped $Y_2Ti_2O_7$ (micro - 2 atom% Ca & V).

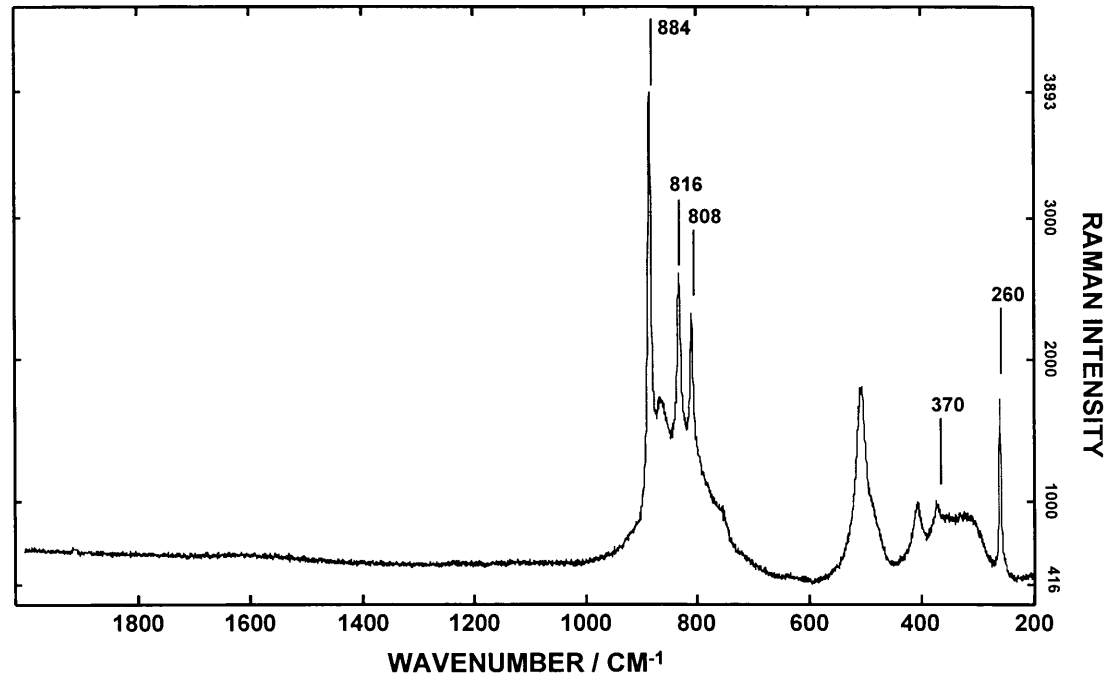

Figure I-4.6 Raman spectrum of $Y_2Sn_2O_7$ and YVO_4 (Macro).

I-4.2 Electronic Spectra of Calcium and Vanadium Co-Doped $Y_2Sn_2O_7$ and $Y_2Ti_2O_7$

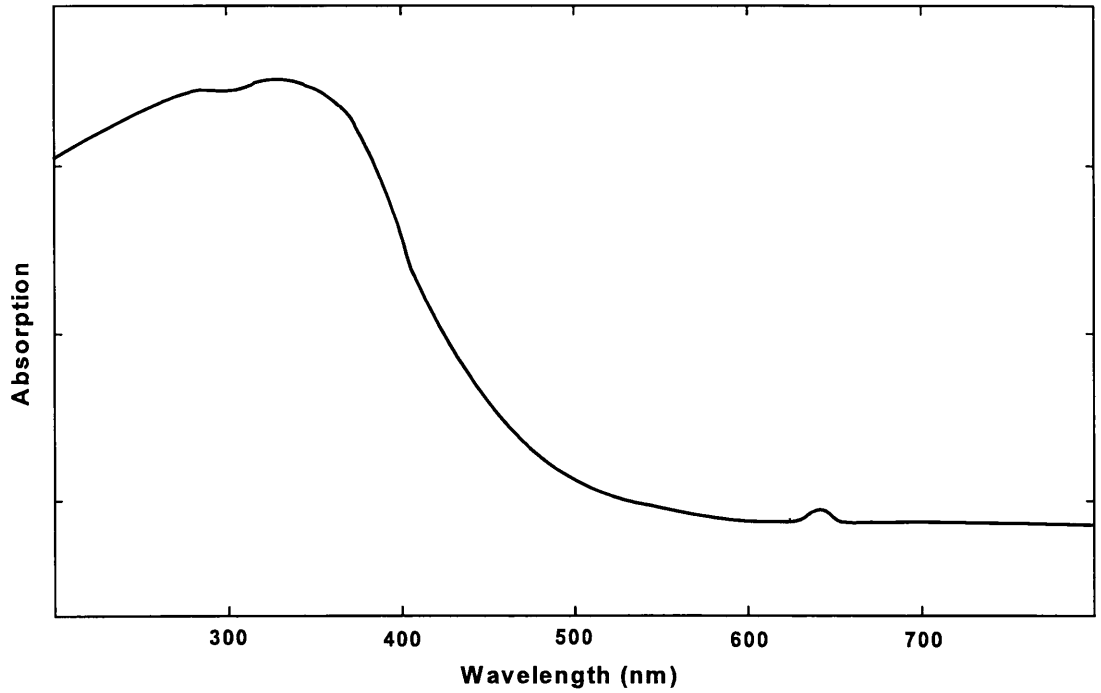

Figure I-4.7 Diffuse reflectance electronic spectrum of calcium and vanadium co-doped $Y_2Sn_2O_7$.

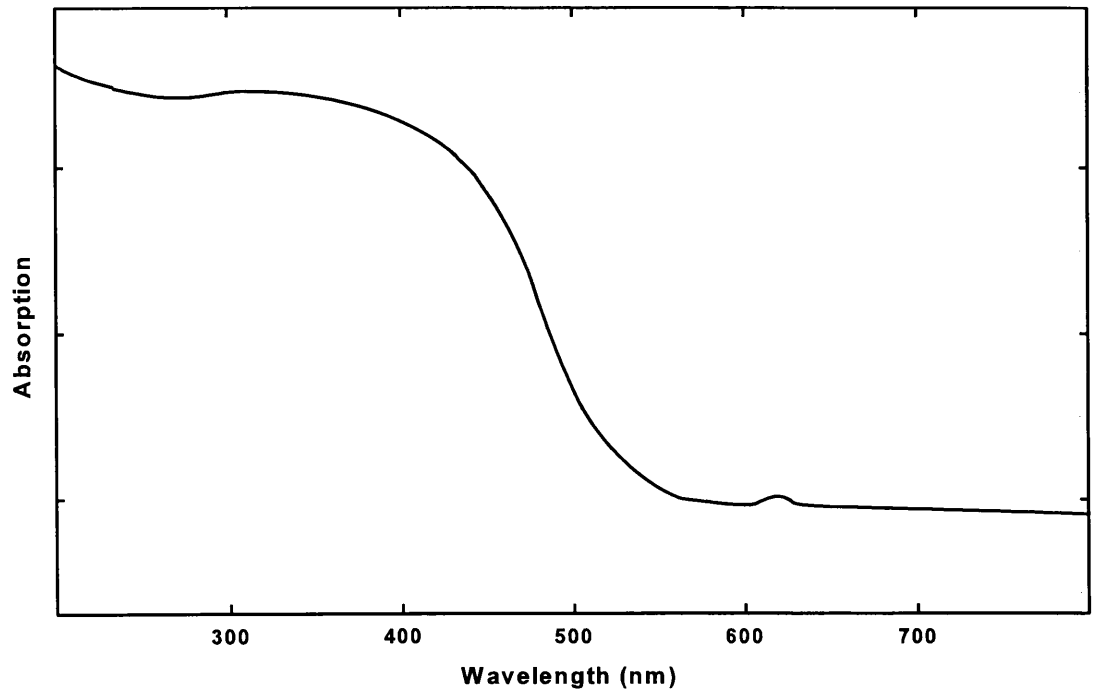

Figure I-4.8 Diffuse reflectance electronic spectrum of calcium and vanadium co-doped $Y_2Ti_2O_7$.

Appendix II

Instrumentation

II-1 SCANNING ELECTRON MICROSCOPY

All measurements were carried out on a Phillips 500 Scanning Electron Microscope coupled to a Tracor Northern/Noran eds System.

II-2 X-RAY POWDER DIFFRACTION

X-ray powder diffraction data was collected on an automated Siemens D501 diffractometer with a 40 position sample changer. Monochromated $Cu_{K\alpha}$ radiation was employed at 25 mA and 30 kV, at a scanning speed of 3° 2θ/min (step size = 0.05° 2θ, measuring time = 1 second) Patterns were recorded from 5 to 65° 2θ.

II-3 INFRARED SPECTROSCOPY

Infrared spectra were recorded on a Bruker ifs 113v spectrometer. Mid-infrared spectra were recorded with the samples in the form of KBr (potassium bromide) pellets. Far-infrared spectra were recorded with the samples in the form of polyethylene pellets.

II-4 RAMAN SPECTROSCOPY

The Raman spectra were recorded with a Dilor XY Raman Instrument using the 514.5 nm excitation line of an Ar^+-ion laser (Coherent Innova 90). All samples, unless otherwise stated, were recorded with a laser power of 50 mW at sample.

- Micro spectra were recorded with a micro probe under a 100x objective.
- Macro spectra were recorded with a 50 mm lens.
- High temperature spectra were recorded in the macro mode using a high temperature cell from Dilor.

High pressure measurements were made in the macro mode using a high pressure diamond anvil cell of the Merrill-Bassett type (model DXR-6) with brilliant cut diamonds of 0.09 carat each. The diamonds had a working face of 0.6 mm in diameter. A nickel-alloy (Inconel 718) gasket with a 1 cm diameter, a thickness of 0.25 mm and a hole of 0.3 mm, pre-indented to a depth of 0.15 mm was uses. Nujol was used as the pressure transmitting medium.

Appendix III

PUBLICATIONS AND CONFERENCE PROCEEDINGS

III-1 PUBLICATIONS RESULTING FROM THIS WORK

- AM Heyns and PM Harden, "A preliminary Raman study of the pyrochlores $Y_2B_2O_7$(B=Sn,Ti) co-doped with V^{5+} and Ca^{2+}", *Journal of Materials Science Letters*, **16**, 815-817, 1997.

- AM Heyns and PM Harden, "Resonance Raman scattering in chromium doped malayaite Cr^{4+}:$CaSnOSiO_4$", *Electrochemical Society Proceedings*, **97-39**, 1997.

- AM Heyns and PM Harden, "Evidence for the existence of Cr(IV) in chromium -doped malayaite Cr^{4+}:$CaSnOSiO_4$, a resonance Raman study", *Journal of Physics and Chemistry of Solids*, (in press), 1998.

- PM Harden and AM Heyns, "A Raman study of the phase transition in chromium-doped titanite $CaTiOSiO_4$", *Physics and Chemistry of Minerals*, (submitted for publication), 1998.

III-2 CONFERENCE PROCEEDINGS RESULTING FROM THIS WORK

I III-2.1 Papers Read

- PM Harden, "A structural approach to ceramic pigment synthesis", The South African Chemical Institutes Young Chemists Symposium (Southern Transvaal Section), Potchefstroom University for Christian Higher Education, Potchefstroom, October, SA 1994

- PM Harden, "A structural investigation of some tin- and titania- based pigments", The South African Chemical institutes Young Chemists Symposium (Southern Transvaal Section), Rand Afrikaans University, Johannesburg, SA, November 1995.

- AM Heyns,-Plenary lecture- "The Raman spectra of some ceramic pigments", XVth International Conference on Raman Spectroscopy, Pittsburgh, Pennsylvania, USA, August 1996.

- PM Harden and AM Heyns, "Resonance Raman scattering in chromium doped malayaite Cr^{4+}:$CaSnOSiO_4$", 4th International Symposium on Bioorganic Chemistry including the Carman National Physical Chemistry Conference, Cape Town, SA, April 1997

III-2.2 Papers Presented

- PM Harden, "A structural and spectroscopic investigation of some tin- and titania- based pigments", 33rd Convention of the South African Chemical Institute, Cape Town, SA, January 1996.

- AM Heyns and PM Harden, "Resonance Raman scattering in chromium doped Malayaite Cr^{4+}:$CaSnOSiO_4$", 9th International Conference on High Temperature Materials Chemistry, The Pennsylvania State University, Pennsylvania, USA, May 1997.

- PM Harden and AM Heyns, "Resonance Raman scattering and the antiferroelectric paraelectric phase transition of titanite", XVIth International Conference on Raman Spectroscopy, Cape Town, SA, September 1998.

- PM Harden and AM Heyns, "The Raman spectra of some tin and titania based ceramic pigments", XVIth International Conference on Raman Spectroscopy, Cape Town, SA, September 1998.

REFERENCES

1. TC Paton, "Pigment Handbook - Volume 2, Applications and Markets", John Wiley & Sons, 1973.

2. G Buxbaum, "Industrial Inorganic Pigments", VCH Verlagsgesellschaft mbH, 1993.

3. W Noll, R Holm and L Born, "Painting of Ancient Ceramics", *Angew. Chem. Int. Ed.*, **14**[9], 602-13, 1975.

4. F Hund, "Inorganic Pigments: Bases for Colored, Uncolored, and Transparent Products", *Angew. Chem. Int. Ed. Engl.*, **20**, 723-30, 1981.

5. PA Lewis, "Pigment Handbook - Volume 1, Properties and Economics", (second edition), John Wiley and Sons, 1987.

6. GR Streatfield, "Ceramic Colour", *Br. Ceram. Trans. J.*, **89**, 177-80, 1990.

7. A Burgyan and RA Eppler, "Classification of Mixed-Metal-Oxide Inorganic Pigments", *Am. Ceram. Soc. Bull.*, **62**[9], 1001-3, 1983.

8. S Takenouchi, "Hydrothermal Synthesis and Consideration of the Genesis of Malayaite", *Mineral. Deposita (Berl.)*, **6**, 335-47, 1971.

9. JB Higgins and FK Ross, "The Crystal Structure of Malayaite: $CaSnOSiO_4$ ", *Cryst. Struct. Comm.*, **6**, 179-82, 1977.

10. JB Higgins and PH Ribbe, "The Structure of Malayaite, $CaSnOSiO_4$, a Tin Analog of Titanite", *Am. Mineral.*, **62**, 710-20, 1977.

11. LA Groat, S Kek, U Bismayer, C Schmidt, HG Krane, H Meyer, L Nistor and G Van Tendeloo, "A Synchrotron radiation, HRTEM, X-ray powder diffraction, and Raman Spectroscopic Study of Malayaite, $CaSnSiO_5$", *Am. Mineral.*, **81**, 595-602, 1996.

12. RA Eppler, "Lattice Parameters of Tin Sphene", *J. Am. Ceram. Soc.*, **59** [9-10], 445, 1976.

13. DV Sanghani, GR Abrams and PJ Smith, "A Structural Investigation of Some Tin-Based Coloured Ceramic Pigments", *Trans. J. Br. Ceram. Soc.*, **80**, 210-4, 1981.

14. J Carda, P Escribano, G Monr□s, MD Rodrigo and J Alarcon, "Co-SnO_2-CaO-SiO_2 Based Ceramic Pigments", *Interceram.*, **39** [3], 22-4. 1990.

15. JR Ferraro and K Nakamoto, "Introductory Raman Spectroscopy", Academic Press, Inc., 1994.

16. PM Harden, "A Structural and Spectroscopic Investigation of Some Tin- and Titania- Based Pigments", MSc dissertation, University of Pretoria, 1995.

17. DM Adams and DC Newton, "Tables for Factor Group and Point Group Analysis", Beckman Instruments (UK).

18. DM Calistru, WB Wang, V Petričević and RR Alfano, "Resonance Raman Scattering in Cr^{4+}-Doped Forsterite", *Phys. Rev. B*, **51**(21), 14980-6, 1995.

19. HR Verdun, LM Thomas, DM Andrauskas, T McCollum and A Pinto, "Chromium-doped Forsterite Laser Pumped with 1.06μm Radiation", *Appl. Phys. Lett.*, **53**(23), 2593-5, 1988.

20. DM Calistru, SG Demos and RR Alfano, "Direct Observation of Second Neighbor Interactions for Cr^{4+} Doped Forsterite by Resonance Raman Scattering", *Appl. Phys. Lett.*, **68**(16), 2207-2209, 1996.

21. RD Shannon, "Revised Effective Ionic Radii and Systematic Studies of Interatomic Distances in Halides and Chalcogenides", *Acta Cryst.*, **A32**, 751-767, 1976.

22. H Eilers, U Hömmerich, SM Jacobsen, WM Yen, KR Hoffman and W Jia, "Spectroscopy and Dynamics of Cr^{4+}:$Y_3Al_5O_{12}$", *Phys. Rev. B*, **49**(22), 15505-13, 1994.

23. RJH Clark and B Stewart, "The Resonance Raman Effect. Review of the Theory and of Applications in Inorganic Chemistry", Struct. Bonding (Berlin), **36**, 1-80, 1979.

24. RJH Clark and TJ Dines, "Resonance Raman Spectroscopy, and Its Application to Inorganic Chemistry", *Angew. Chem. Int. Ed. Engl.*, **25**, 131-58, 1986.

25. BM Weckhuysen and IE Wachs, "Raman Spectroscopy of Supported Chromium Oxide Catalysts. Determination of Chromium-oxygen Bond Distances and Bond Orders", *J. Chem. Soc., Faraday Trans.*, **92**(11), 1969-73, 1996.

26. K Nag, SN Bose, "Chemistry of Tetra- and Pentavalent Chromium", Struct. Bonding (Berlin), **63**, 153-97, 1985.

27. KA Wilhelmi, "Crystal Structure of Sr Chromate (IV), Sr_2CrO_4", *Ark. Kemi.*, **26**[14-15], 157-65, 1966.

28. H-R Wenk and KN Raymond, "Four New Structure Refinements of Olivine", *Z. Kristallogr.*, **137**, S. 86-105, 1973.

29. JD Birle, GV Gibbs, PB Moore and JV Smith, "Crystal Structures of Natural Olivines", *Amer. Mineral.*, **53**, 807-24, 1968.

30. ID Brown and KK Wu, "Empirical Parameters for Calculating Cation-Oxygen Bond Valences", *Acta Cryst.*, **B32**, 1957-9, 1957.

31. G Herzberg, "Molecular Spectra and Molecular Structure. II. Infrared and Raman Spectra of Polyatomic Molecules", 3rd ed., D. Van Nostrand, New York, 1947.

32. K Iishi, "Lattice Dynamics of Forsterite", *Amer. Mineral.*, **63**, 1198-208, 1978.

33. AH Jubert, EL Varetti and EJ Baran, "The Resonance Raman Spectrum of Silver Permanganate", *J. Raman Spectrosc.*, **15**(2), 139-40, 1984.

34. JA Speer and GV Gibbs, "The Crystal Structure of Synthetic Titanite, $CaTiOSiO_4$, and the Domain Textures of Natural Titanites", *Am. Mineral.*, **61**, 238-247, 1976.

35. CR Robbins, "Synthetic $CaTiSiO_5$ and its Germanium Analogue ($CaGeSiO_5$)", *Mat. Res. Bull.*, **3**, 693-8, 1968.

36. JB Higgins and PH Ribbe, "The Crystal Chemistry and Space Groups of Natural and Synthetic Titanites", *Am. Mineral.*, **61**, 878-88, 1976.

37. M Taylor and GE Brown, "High-Temperature Structural Study of the $P2_1/a \rightleftharpoons A2/a$ Phase Transition in Synthetic Titanite, $CaTiSiO_5$", *Am. Mineral.*, **61**, 435-47, 1976.

38. S Kek, M Aroyo, U Bismayer, C Schmidt, K Eichhorn and HG Krane, "The Two-step Phase Transition of Titanite, $CaTiSiO_5$: a Synchrotron Radiation Study", *Z. Kristallogr.*, **212**, 9-19, 1997.

39. S Ghose, Y Ito and DM Hatch, "Paraelectric-Antiferroelectric Phase Transition in Titanite, $CaTiSiO_5$. I. A High Temperature X-Ray Diffraction Study of the Order Parameter and Transition Mechanism", *Phys. Chem. Minerals*, **17**, 591-603, 1991.

40. C Van Heurck, G Van Tendeloo, S Ghose and S Amelinckx, "Paraelectric-Antiferroelectric Phase Transition in Titanite, $CaTiSiO_5$. II. Electron Diffraction and Electron Microscopic Studies of the Transition Dynamics", *Phys. Chem. Minerals*, **17**, 604-10, 1991.

41. U Bismayer, W Schmahl, C Schmidt and LA Groat, "Linear Birefringence and X-Ray Diffraction Studies of the Structural Phase Transition in Titanite, $CaTiSiO_5$", *Phys. Chem. Minerals*, **19**, 260-6, 1992.

42. GL Catchen, RL Raseru, CA Randall, DK Smith and SK Kurtz, "Temperature Dependence of the Ti-Site Electric Field Gradient in Titanite, $CaTiSiO_5$", *Phys. Rev.B*, **45**(9), 5015-8, 1992.

43. E Salje, C Schmidt and U Bismayer, "Structural Phase Transition in Titanite, $CaTiSiO_5$: A Ramanspectroscopic Study", *Phys. Chem. Minerals*, **19**, 502-6, 1993.

44. M Zhang, EKH Salje, U Bismayer, H-G Unruh, B Wruck and C Schmidt, "Phase Transition(s) in Titanite $CaTiSiO_5$: An Infrared Spectroscopic, Dielectric Responce and Heat Capacity Study", *Phys. Chem. Minerals*, **22**, 41-9, 1995.

45. M Kunz, D Xirouchakis, D H Lindsley and D Häusermann, "High-pressure Phase Transition in Titanite ($CaTiOSiO_4$)", *Am. Mineral.*, **81**, 1527-30, 1996.

46. WP Griffith, "Raman Studies on Rock-forming Minerals. Part I. Orthosilicates and Cyclosilicates", *J. Chem. Soc.(A)*, 1372-7, 1969.

47. MJ Buerger, "Crystal-structure Aspects of Phase Transformations", *Trans. Am. Crystallogr. Assoc.*, **7**, 1-23, 1971.

48. CNR Rao and KJ Rao, "Phase Transitions in Solids. An Approach to the Study of the Chemistry and Physics of Solids", McGraw-Hill, 1978.

49. AR West, "Basis Solid State Chemistry", John Wiley and Sons, 1988.

50. U Bismayer, "Review. Hard Mode Raman Spectroscopy and Its Applications to Ferroelastic and Ferroelectric Phase Transitions", *Phase Transitions*, **27**, 211-67, 1990.

51. U Bismayer, "Hard Mode Raman Spectroscopy and Its Application to Ferroelastic and Ferroelectric Phase Transitions", *Phase Transitions*, **27**, 211-67, 1990.

52. EKH Salje, "Hard Mode Spectroscopy: Experimental Studies of Structural Phase Transitions", *Phase Transitions*, **37**, 83-110, 1992.

53. EKH Salje and U Bismayer, "Hard Mode Spectroscopy: The Concept and Applications", *Phase Transitions*, **63**, 1-75, 1997.

54. RWG Wyckoff, "Crystal Structures - Volume III" (Second Edition), Interscience Publishers (John Wiley & Sons) 1965.

55. McCauley, "Structural Characteristics of Pyrochlore Formation", *J. Appl. Phys.*, **51**(1), 290-4, 1980.

56. CG Whinfrey, DW Eckart and A Tauber, " Preparation and X-Ray Diffraction Data for Some Rare Earth Stannates", *J. Am. Soc.*, **82**, 2695-7, 1960.

57. MT Vandenborre and E Husson, "Comparison of the Force Field in Various Pyrochlore Families. I. The $A_2B_2O_7$ Oxides", *J. Solid State Chem.*, **50**, 362-71, 1983.

58. MT Vandenborre, E Husson and H Brusset, "Analyse en Coordonnées Normales des Composés $A_2^{III}B_2^{IV}O_7$ (A=La,Nd; B=Zr,Hf) de Structure Pyrochlore", *Spectrochimica Acta.*, **37A**, 113-8, 1981.

59. MT Vandenborre, E Husson, JP Chatry and D Michel, "Rare-earth Titanites and Stannates of Pyrochlore Structure; Vibrational Spectra and Force Fields", *J. Raman Spectroscopy*, **14** [2], 1983.

60. CG Whinfrey and A Tauber, "Rare Earth Stannates, $R_2Sn_2O_7$", *J. Am. Chem. Soc.*, **83**, 755-6, 1961.

61. MT Vandenborre, E Husson and JL Fourquet, "Spectres Vibrationnels et Champs de Force de Divers Composes de Formule $A_2B_2O_7$ et $A_2B_2O_6$ de Structure Pyrochlore", *Spectrochimica Acta.*, **38A** [9], 1982.

62. CP Grey, CM Dobson, AK Cheetham and RJB Jakeman, "Studies of Rare-Earth Stannates by ^{119}Sn MAS NMR. The use of Paramagnetic Shift Probes in the Solid State", *J. Am. Chem. Soc.*, **111**, 505-11, 1989.

63. GR Facer, CJ Howard and BJ Kennedy, "Structure Refinement and calculated X-Ray Powder Data for the Pyrochlore $Y_2Sn_2O_7$ derived from Powder Neutron Data", *Powder Diffr.*, **8**[4], 245-8, 1993.

64. AJH Macke and G Blasse, "Vibrational Spectra of Oxidic Stannates in Relation to Order-Disorder Phenomena", *J. Inorg. Nucl. Chem.*, **38**, 1407-9, 1976.

65. K Fujiyoshi, H Yokoyama, F Ren and S Ishida, "Chemical State of Vanadium in Tin-Based Yellow Pigment", *J. Am. Ceram. Soc.*, **76** [4], 981-86, 1993.

66. EH Ray, TD Carnahan and RM Sullivan, "Tin-Vanadium Yellows and Praseodymium Yellows", *Am. Ceram. Soc. Bull.*, **40** [1], 13-6, 1960.

67. S Ishida, F Ren and N Takeuchi, "New Yellow Ceramic Pigment Based on Codoping Pyrochlore-type $Y_2Ti_2O_7$ with V^{5+} and Ca^{2+}", *J. Am. Ceram. Soc.*, **76** [10], 2644-48, 1993.

68. FD Hardcastle and IE Wachs, "Determination of Vanadium-Oxygen Bond Distances and Bond Orders by Raman Spectroscopy", *J.Phys. Chem.*, **95**, 5031-41, 1991.

69. NC Webb, "The Crystal Structure of β-$Ca_2P_2O_7$", *Acta Cryst.*, **21**, 942-8, 1966.

70. JA Konnert and HT Evans Jr, "Calcium Divanadate Dihydrate", *Acta Cryst.*, **B31**, 2688-90, 1975.

71. ID Brown and C Calvo, "The Crystal Chemistry of Large Cation Dichromates, Pyrophosphates, and Related Compounds with Stoichiometry $X_2Y_2O_7$", *J. Solid State Chem.*, **1**, 173-9, 1970.

71. PKL Au and C Calvo, "Crystal Structure of $Cd_2V_2O_7$", *Can. J. Chem.*, **45**, 2297-302, 1966.

73. R Gopal and C Calvo, "Crystal Structure of Magnesium Divanadate, $Mg_2V_2O_7$", *Acta Cryst.*, **B30**, 2491-3, 1974.

74. JA Baglio and JN Dann, "The Crystal Structure of Beta Strontium Pyrovanadate", *J. Solid State Chem.*, **4**, 87-93, 1972.

75. JC Pedregosa, EJ Baran and PJ Aymonino, "Notiz zur Kristallstruktur von Magnesium-, Calcium- und Kupferdivanadat", *Z. Kristallogr.*, **137**, 221-4, 1973.

76. HA Willis, JH van der Maas and RGJ Miller, "Laboratory Methods in Vibrational Spectroscopy", John Wiley and Sons, 1987.

77. DJ Cherniak, "Sr and Nd Diffusion in Titanite", *Chem. Geol.*, **125**, 219-32, 1995.

78. Y Pan and ME Fleet, "Intrinsic and External Controls on the Incorporation of Rare-Earth Elements in Calc-Silicate Minerals", *Can. Mineral.*, **34**, 147-59, 1996.